SHM-BASED CONDITION ASSESSMENT OF IN-SERVICE BRIDGE STRUCTURES USING STRAIN MEASUREMENT

Hong-Wen XIA

Ph.D.

THE HONG KONG POLYTECHNIC UNIVERSITY

2012

The Hong Kong Polytechnic University

Department of Civil and Structural Engineering

SHM-BASED CONDITION ASSESSMENT OF IN-SERVICE BRIDGE STRUCTURES USING STRAIN MEASUREMENT

Hong-Wen XIA

A thesis submitted in partial fulfillment of the requirements for the degree of

Doctor of Philosophy

April 2011

To my parents and wife

CERTIFICATE OF ORIGINALITY

I hereby declare that this thesis is my own work and that, to the best of my knowledge and belief, it reproduces no material previously published or written, nor material that has been accepted for the award of any other degree or diploma, except where due acknowledgement has been made in the text.

_____ (Signed)

_____ Hong-Wen XIA _____ (Name of student)

ACKNOWLEDGEMENTS

The road towards my PhD degree is not easy. I fortunately have had a group of people supporting, encouraging and helping me on the way and herein would like to express my sincerest thanks to them upon the completion of this PhD thesis. First of all, I owe my deepest gratitude to my supervisor, Prof. Y. Q. Ni, for his enlightening guidance, generous patience, highly sense of responsibility, and critical comments throughout my PhD study and preparation of the thesis.

I would like to express my warmest appreciation to Dr. K. Y. Wong from the Highways Department of HKSAR (Hong Kong Special Administrative Region) Government for providing me invaluable structural health monitoring data. I am also grateful to all of my friends and colleagues in the Department of Civil and Structural Engineering, particularly Dr. X. W. Ye, Dr. Z. W. Chen, Dr. L. Hu, Mr. P. Zhang, and Mr. W. A. Shen for their very precious discussions and suggestions on the thesis.

My heartfelt acknowledgement must go to the Research Committee of The Hong Kong Polytechnic University for providing me such a golden opportunity to undertake this research project. And I am also indebted to the staff in the university library, research office, and finance office, for their kindly help and assistance during my stay at the university.

Last but not least, I wish to express my intense gratitude to my beloved parents and wife. Without their everlasting love, support and encouragement during the past years, I cannot insist on the way of pursuing my doctoral study.

ABSTRACT

In realistic scenarios, in-service bridge structures are at risk from structural degradation, service demands of increasing traffic flow and heavier truck loads, natural or man-made disasters, or deferred maintenance. Condition assessment of these public facilities for future serviceability and safety is a challenging task to their owners and engineers. A paradigm of integrating structural health monitoring (SHM) data into procedures of structural condition assessment is expected to achieve objective and quantitative condition assessment in practice. The work addressed in this dissertation has been dedicated to investigating condition assessment of existing bridge structures using strain measurement acquired under in-service environment by a long-term bridge health monitoring system (BHMS).

Under in-service circumstance, bridge structures are subject to temperature variation, traffic and wind effect, and material deterioration due to aging or aggressive environmental attack. Strain measurement acquired under operational environment by the SHM system is naturally a result of combination of these external loadings and environmental effects. Source separation of these effects from the raw measurement is a challenging job and it is pursued in this study. The proposed method takes the benefits of discrete wavelet transform (DWT) which satisfies the mathematical principle of multi-component separation quite well (less distortion and

cross-talking among components). Based on the wonderful decomposition platform of DWT, component extraction with physical meanings is realized by integrating physical mechanism of the desired structural behavior into the selection criterion of source separation. Specific application of the proposed method in component analysis of the measured strains from the Tsing Ma Bridge (TMB) deck exemplifies its effectiveness in source separation of multi-component strain monitoring signals. By interpreting separated strain components from the raw measurement, structural behaviors of the TMB deck under temperature effect, live load effect and traffic effect are identified for further condition assessment.

When using the strain response data caused by live load effect for reliability assessment, another problem arises in the inference of probability distribution from the observed data that strain response due to live load effect collected under in-service environment is still a result of multi-load effect such as traffic (highway, railway, or both of them) and wind (monsoon or typhoon), and it cannot be characterized by a standard probability distribution model adequately. Mixed distributions existing in the monitoring data are explored primarily by histogram analysis. Then hybrid mixture estimation including model selection and parameter estimation is evaluated and a structure of mixed Weibull model is proposed for the probability density function (PDF) estimation of peak-stress values counted from the derived stress-time histories. Different mixture models (e.g., normal mixtures, log-normal mixtures and Weibull mixtures) are compared in the process of model

selection by calculating Akaike's information criterion (AIC) values. Convergences of AIC value with a varying component number are addressed for the optimal determination of component numbers in mixture models. Based on the estimated PDFs, reliability based condition assessment of the performance of the TMB deck trusses is carried out for various load scenarios such as monsoon, typhoon, with and without railway traffic.

As another target pursued in this study, strain response data due to traffic effect are used to estimate the neutral-axis position of the monitored deck section for further application in damage detection. It is revealed by the monitoring data that under traffic effect the TMB deck performs as a flexural beam, i.e., the deck top compresses and the deck bottom tensions concurrently, or vice versa. Based on the relation between the neutral-axis position and strain responses at the top and bottom of a cross section, a Kalman filter (KF) estimator for locating the neutral-axis position from strain measurement is elaborately designed and in succession comes the validation of its stability to noise disturbance through numerical studies. Two levels of noise contamination (5% and 10%) in the sensor readings are considered in the simulation studies. Results of the numerical simulation show that the KF based estimation method can generate better results in comparison with a direct estimation approach. Moreover, application of the proposed KF estimator to the neutral-axis position estimation of the instrumented TMB deck sections demonstrates its efficiency in the real monitoring data.

To further testify the feasibility of neutral-axis position as a damage indicator, experiment and numerical simulation are conducted to demonstrate its sensitivity to damage and independence of traffic load patterns. In design of the experiment, a flexible steel beam subject to moving bogies is objectively used as the testing model to simulate the structural behavior of a bridge deck under the traffic effect and a cut on a selected cross section is to simulate damage incurred on the testing model. By establishing a multi-scale finite element method (FEM) model, numerical simulation for damage detection (using the neutral-axis position as an indicator) of the testing model is conducted for static and moving load cases respectively. Physical experiment on damage detection of the testing model follows and the previously designed KF estimator is used to locate the neutral-axis position from the noisy experiment data. Results of the numerical simulation and physical experiment show that the neutral-axis position can serve as a good indicator of damage and it can be conveniently achieved through strain monitoring in practice.

In summary, the research described in this dissertation chiefly contributes to the development of a systematic framework for condition assessment of existing bridge structures making use of long-term monitoring data of strain responses. This approach involves the multi-component analysis of strain monitoring signals, mixture distribution model based reliability assessment, Kalman filter based optimal estimation of neutral-axis position, and neutral-axis position based damage detection.

Following this approach, objective and quantitative condition assessment of in-service bridge structures can be achieved with the use of SHM data.

LIST OF PUBLICATIONS

Journal Articles

H. W. Xia, Y. Q. Ni, and J. M. Ko (2011), "Kalman filter based estimation of neutral-axis position of bridge deck under operational traffic loading environment", submitted to *Mechanical Systems and Signal Processing*, in review.

H. W. Xia, Y. Q. Ni, and J. M. Ko (2011), "Reliability-based condition assessment of in-service bridge deck using mixture distribution models", submitted to *Computers and Structures*, in review.

Y. Q. Ni, H. W. Xia, J. M. Ko, and K. Y. Wong (2011), "In-service condition assessment of bridge deck using long-term monitoring data of strain response", *Journal of Bridge Engineering*, ASCE, in press.

Y. Q. Ni, H. W. Xia, and J. M. Ko (2008), "Structural performance evaluation of Tsing Ma Bridge deck using long-term monitoring data", *Modern Physics Letter B*, Vol. 22, No. 11, 875–880.

Conference Papers

H. W. Xia, Y. Q. Ni, and X. W. Ye (2011), "Kalman filter based estimation of neutral-axis position of bridge deck under traffic loading", accepted to *The 14th Asia Pacific Vibration Conference on Dynamics for Sustainable Engineering*, 5-8 December 2011, Hong Kong SAR, China.

Y. Q. Ni, H. W. Xia, and J. M. Ko, and K. Y. Wong (2010), "Condition assessment of

bridge deck truss using in-service monitoring data of strain", *Proceedings of the 5th International Conference on Bridge Maintenance, Safety and Management*, 11-15 July 2010, Philadelphia, USA, 799–805.

H. W. Xia, Y. Q. Ni, J. M. Ko, and K. Y. Wong (2010), "Measurement fusion for component estimation of long-term monitoring signal of in-service strain", *Proceedings of the 5th European Workshop on Structural Health Monitoring*, 29 June - 4 July 2010, Sorrento, Naples, Italy, 566-571.

H. W. Xia, Y. Q. Ni, J. M. Ko, and K. Y. Wong (2010), "Wavelet-based multi-resolution decomposition of long-term monitoring signal of in-service strain", *Proceedings of the 2nd International Postgraduate Conference on Infrastructure and Environment*, 1-2 June 2010, Hong Kong SAR, China, Vol. 2, 278–285.

Y. Q. Ni, H. W. Xia, J. M. Ko, and K. Y. Wong (2009), "Probability-based structural assessment of Tsing Ma Brige deck sections using in-service monitoring data", *Proceedings of the 10th International Conference on Structural Safety and Reliability*, 13-17 September 2009, Osaka, Japan, 2568–2574 (CD-ROM).

TABLE OF CONTENTS

LIST OF FIGURES

LIST OF TABLES

LIST OF ABBREVIATIONS

Abbreviation	Description
AASHTO	American Association of State Highway and Transportation Officials
AIC	Akaike's information criterion
ASCE	American Society of Civil Engineers
BHMS	Bridge health monitoring system
BIC	Bayes information criterion
BMMS	Bridge management and maintenance system
BOFS	Brillouin optical fiber sensing
BSI	British Standards Institution
CDF	Cumulative distribution function
ECS	European Committee for Standardization
COMAC	Coordinate modal assurance criterion
DLV	Damage locating vectors
DWT	Discrete wavelet transform
EM	Expectation maximization
ESG	Electrical strain gauge
FEM	Finite element method
FHWA	Federal Highway Adminstration
FOSG	Fiber optical strain gauge
GPS	Global positioning system
HKSAR	Hong Kong Special Administrative Region
ICLC	Integrated classification likelihood criterion
ILT	Instrumented load testing

KF	Kalman filter
KSMB	Kap Shui Mun Bridge
LEC	Laplace-empirical criterion
MAC	Modal assurance criteria
MDLAC	Multiple damage location assurance criterion
MIRC	Minimum information ratio criterion
MLE	Maximum likelihood estimation
MOM	Method of moments
NDT	Nondestructive testing
NEC	Normalized entropy criterion
PDF	Probability density function
PR	Perfect reconstruction
PRFB	Perfect reconstruction filter bank
SB	Stonecutters Bridge
SFRF	Strain frequency response function
SHM	Structural health monitoring
STFT	Short-time Fourier transform
TFD	Time-frequency distribution
TKB	Ting Kau Bridge
TMB	Tsing Ma Bridge
UIL	Unit influence line
VWSG	Vibrating wire strain gauge
WASHMS	Wind And Structural Health Monitoring System
WCB	Western Corridor Bridge
WIM	Weigh-in-motion
WMRA	Wavelet multi-resolution analysis
WVD	Wigner-Ville distribution

LIST OF SYMBOLS

Symbol	Description
Chapter 2	
x_t	Input signal
y_t	Output signal
w_t	Filter coefficients
Chapter 3	
$\mathbf{s}(t)$	Source signals
$\mathbf{x}(t)$	Mixture signals
A	Mixing matrix
W	Separation matrix
$\Psi(t)$	Mother wavelet
$f(t)$	Signal function
a	Scale parameter
b	Time parameter
$W_{\psi f}(a,b)$	Wavelet transform
$r_i(t)$	Reference signal
$E(\cdot)$	Expected value
$D(\cdot)$	Variance
ε_t	Temperature-induced strain
Δl	Longitudinal displacement at expansion joint
l	Length of bridge deck

Chapter 4

$f(x\|\mathbf{\Theta})$	Mixture distribution function
$\mathbf{\Theta}$	Mixture distribution parameter vector
a_j	Component distribution weights
$\boldsymbol{\theta}_\mathbf{j}$	Component distribution parameter vector
$f_j(x\|\boldsymbol{\theta}_\mathbf{j})$	Component distribution function
$L_n(\mathbf{\Theta})$	Log-likelihood function
k	Number of free parameter
β	Shape parameter of Weibull distribution
θ	Scale parameter of Weibull distribution
$\mathbf{\Theta}^{(k)}$	k step parameter vector
$\mathbf{\Theta}^{(k+1)}$	k+1 step parameter vector
λ	Lagrange multiplier
R	Material resistance
S	Load effect
$g(\mathbf{X})$	Limit state function

Chapter 5

ρ	Curvature radius
M	Bending moment
I	Inertia moment
ε_t	Strain response at top location
ε_b	Strain response at bottom location
h	Height of beam cross section
y_n	Neutral-axis position in distance
r	Neutral-axis position in ratio
$\hat{r}$	Direct estimation

$\hat{r}_k$	Estimation state in Kalman filter
Φ_k	Propagation matrix
w_k	White noise process
H	Measurement matrix
z_k	Observation state
v_k	Measurement noise
$\tilde{r}$	Estimation error
K_k	Kalman filter gain
P_k	Covariance matrix of estimate error
Q_k	Covariance matrix of state process noise
R_k	Covariance matrix of measurement noise

CHAPTER 1

INTRODUCTION

1.1 Research Background

Bridges are defined as structures, which provide a connection or passage over a gap without blocking the opening or passageway beneath (Tonias and Zhao 2007). According to the specific landform of their location bridges can be over streams, canals and rivers; creeks and valleys; or roads and railways passing underneath. Bridges are even now being provided across ocean bodies and for linking a number of islands. With respect to the played role in their lifetime, bridges can be for passage or carriage of persons, cattle, vehicles, water or other material carried across in pipes or conveyors. As expected bridges are built for enhancing the quality of life of the society; the benefits of some major bridges can go to the people of an entire nation such as the bridges across Yangtse River or Yellow River in China (Feng 2009), the bridges across Ganga River in India (Ponnuswamy 2008), and the Honshu-Shikoku Connection across many islands in Japan (Wu *et al*. 2003). They can even benefit more than one country as in the case of the Oresund Link Crossing over the Baltic ocean (Matthiessen 2000). It is highly spoken by Ponnuswamy (2008) that no other

creation of a civil engineer has such a general appeal and fascination to the people.

Because of playing an important role in enhancing the life quality of the society, bridge structures are expected to function well for a long term. However, in realistic scenarios, bridges cannot last forever although desired to be. Whatever forms of construction are used and whatever materials adopted, sooner or later the effects of degradation will appear (Catbas and Aktan 2002). There are many contributory factors that affect the nature and degree of degradation of in-service bridge structures. They generally come from two categories: (1) the bridge structure itself; (2) the external working environment. Factors concerning the structure itself mainly include the adopted structural form, the quality of construction, design and detailing, construction material deterioration, inadequate maintenance, and structural damage from natural or man-made disasters. On the other hand, factors from the working environment consist of adverse atmospheric environment, weather, floods, earthquakes, etc. Structural degradation could make bridge components unserviceable and even finally might lead to the collapse of an entire bridge. Failures of some major bridges, arising from such as lack of inspection and maintenance, or natural and man-made disasters, have been widely addressed and acknowledged in the community of bridge engineering (Shepherd and Frost 1995; Wang *et al*. 2002). A notable example is the failure of Ashtabula Bridge in 1876 attributed to the passage of a high-speed train during severe storm. About eighty deaths were caused. Investigation showed that this failure resulted from buckling and fracture of critical

members due to lack of inspection and maintenance. By bitter experience people learnt that it is of vital importance to assess in-service bridge structures from time to time during their operation.

On purpose of possibly avoiding the tragic disasters, condition assessment of in-service bridge structures (Ratay 2006) arises as a fascinating and challenging task to the bridge engineers. Its fascination exists in an expectation that condition assessment of an existing bridge may be conducted to develop a bridge load rating, or confirm an existing load rating, or to determine whether the bridge must be posted in the interest of public safety when natural disasters are incoming. The challenge is that subjective and inaccurate condition assessment is easy to run into in practice. It is identified as the most critical technical barrier to effective management of highway bridges (AASHTO 1989; Aktan *et al*. 1996). As commonly used structural analysis based condition assessment is typically based on an idealized analytical model. In a sense, this approach may not permit an accurate evaluation of the bridge condition because it takes no consideration of the existing states and actual behavior of the as-built bridge structures. Inspection does find signs of damage (such as cracks, spalls, chemical deterioration, and corrosion) when they become visible. Nevertheless, the relation between visible damage signs and the bridge condition is often very difficult to establish and hence decision making on management has to be carried out by heuristic and experience (Aktan *et al*. 1997). Bridge engineering community has long been aware of the limitation of visual inspection (FHWA 2001),

and thereby turns to the objective measuring of bridge conditions.

Measurement based approaches to condition assessment of the existing bridges are generally divided into three classes: instrumented load testing (ILT), local nondestructive testing (NDT) and structural health monitoring (SHM). ILT is dedicated to investigating actual behavior of the instrumented bridge under controlled truck loadings. With the ability of considering as-built characteristics, ILT can provide an improved estimate of load-carrying capacity and may avoid unnecessary or ill-advised posting. Lousily, the expense of ILT may be magnified by traffic restriction or closure if the bridge is on a major traffic artery. The use of NDT technologies could provide invaluable information on bridge conditions without reducing the functional capability as opposed to the destructive testing. Common NDT methods include ultrasonic, magnetic-particle, liquid penetrant, radiographic, eddy-current testing, etc. (Stubbs and Farrar 1995). Nevertheless, the most significant challenge faced by any local NDT technology is that there are difficulties in directly relating the testing results to the global condition of bridges. With sensors densely distributed over bridge structures, SHM systems can offer rich information on bridge conditions in a localized or globalized way without the limitation of traffic restriction or closure.

On the promise that SHM can provide accurate and objective information on structural condition via various sensors, it has been practiced increasingly in bridge

engineering community around the world (Andersen and Pedersen 1994; Cheung *et al*. 1997; Barrish *et al*. 2000; Sumitro *et al*. 2001; Mufti 2002; Koh *et al*. 2003; Wang *et al*. 2003; Wong 2004; Ko and Ni 2005; Ou and Li 2005; Wang 2005). In the United States of American, a large research effort has been devoted to SHM-based bridge condition assessment (Aktan *et al*. 2000). Some collaborative projects on bridge health monitoring were organized at a national level in Europe (Grosso *et al*. 2002). In Japan, the need for monitoring is mainly driven by the concern of the effects of earthquakes on the integrity of bridge structures (Kashima 2000). In Hong Kong, several cable-supported bridges, such as Tsing Ma Bridge (TMB), Kap Shui Mun Bridge (KSMB), Ting Kau Bridge (TKB), Western Corridor Bridge (WCB) and Stonecutters Bridge (SB), were installed with a long-term structural health monitoring system (Wong 2004; Ko and Ni 2005; Wong and Ni 2009).

Although applications of SHM have gone far beyond the damage detection, detecting damage or deterioration as early as possible is still an important topic of an SHM system. In the past decades, vibration-based damage detection methods have obtained considerable research efforts; they are usually based on the fact that changes in physical properties (such as mass, stiffness and boundary conditions) give rise to changes in dynamic characteristics (such as modal frequency, modal shape, or their derivations). Although the underlying philosophy of vibration-based damage detection appears intuitive, assessing structural damage in large-scale bridges remains still a challenging task. The main pitfalls, limiting the practical applicability

of vibration-based damage detection methods, consist of the insensitivity of modal properties to local damage, uncertainty and incompleteness in measurement data, modal variability arising from varying operational and environmental conditions, as well as modeling errors in the analytical model. An experimental verification of vibration-based damage detection on a large-scale structure (Frishwell and Penny 1997) showed that modal characteristics are insensitive to the localized structural damage.

While vibration data remain valuable in bridge condition assessment, the measurements of strain response are receiving more and more attentions on the other hand. Strain data can be directly used to indicate the safety reserve of a bridge component (Bergmeister and Santa 2000; Koshiba 2001) or provide information on the load-carrying capacity of a whole bridge; and they may be better suited to characterize the local damage of the bridges than vibration data. In practice strain sensors can be intentionally placed at critical points of a bridge where high strains are expected to be developed that could approach or surpass the material resistance (Chakraborty and DeWolf 2005). Although the philosophy of strain measurement based condition assessment of in-service bridge structures appears intuitive, there are still some challenges. For example, the strain data acquired by an SHM system are a result of multi-source combination of external loadings and environmental effects. Processing them individually is practically desired, especially when each effect on structural behavior needs to be quantified. Another challenge arising in the strain

measurement based reliability assessment is that standard probability distribution models cannot be adequate to characterize the statistical properties of strain monitoring data collected by an SHM system. As to the problem of damage detection from the strain measurement, whether the strain-related indicators are sensitive to local damage and insensitive to the changing environment must be accounted for in the real application.

Stimulated by challenges and chances stated above, the aim of the present study is to explore structural condition assessment of in-service bridge structures using measured strains from an SHM system. This study starts with developing a multi-component separation method for the strain monitoring data analysis. Strain response due to temperature effect, live load effect and traffic effect will be extracted from the raw measurement data for further pertinent condition assessment. In recognizing that mixture distributions usually exist in the live-load effects, mixture distribution model based reliability assessment will be developed. A KF estimator will be specially designed to locate the neutral-axis position from the separated traffic-induced strains. To further testify the feasibility of the estimated neutral-axis position as a damage indicator of the bridge deck, an experimental verification will be conducted to demonstrate its sensitivity to damage and independence of traffic load patterns. Following these approaches, objective condition assessment of in-service bridge structures will benefit from the implemented SHM systems.

In Hong Kong, a sophisticated on-structure instrumentation system, called Wind And Structural Health Monitoring System (WASHMS), has been devised and deployed by the HKSAR Government Highways Department to monitor the five long-span cable-supported bridges, namely TMB, KSMB, TKB, WCB and SB (Wong 2004; Wong and Ni 2009). The on-line monitoring system for the five bridges consists of more than 3,000 sensors of different types permanently installed on the bridges, including accelerometers, strain gauges, displacement transducers, level sensors, anemometers, temperature sensors, corrosion sensors, weigh-in-motion (WIM) sensors and global positioning systems (GPS). Continuously acquired data by the WASHMS system provide research resources for this PhD project as well.

1.2 Research Objectives

The aim of this PhD study is to investigate condition assessment of in-service bridge structures using strain measurement data acquired by an SHM system. Related issues such as multi-component analysis of strain monitoring data, mixture distribution model based reliability analysis, as well as neutral-axis position based damage detection will be addressed in this study. The specific objectives of this research are:

(1) To develop a method for source separation of multi-component strain monitoring data according to physical meanings. Strain components due to temperature effect, live load effect and traffic effect will be separated from so that structural behaviors of the in-service bridge under each effect can be identified for further

pertinent structural condition assessment.

(2) To propose a systematic approach to reliability assessment of in-service bridge structures using strain monitoring data due to live load effect. Under in-service environment, bridge structures are subject to traffic (highway, railway, or both of them) and wind (monsoon or typhoon) effects. These external loadings cannot be controlled as people expect in a sense that their random combination produces the strain response data. In recognizing that the strain response data cannot be characterized by a standard probability distribution model adequately, mixture model based reliability assessment will be pursued in this PhD project.

(3) To develop an approach to optimal estimation of the neutral-axis position from the extracted traffic-induced strains. Under traffic effect, the bridge deck performs as a flexural beam, i.e., the top compressed and the bottom tensioned concurrently, or vice versa. Based on the relationship of strain responses at the top and bottom of a deck cross section, a KF estimator will be elaborately formulated. The stability of the proposed KF estimator to different extents of noise will be testified.

(4) To conduct an experimental verification of the neutral-axis position based damage detection. Utilization of the neutral-axis position as a damage indicator is based on the assumption that it will shift when damage occurs. Numerical simulation of damage detection using the neutral-axis position as an indicator will be conducted before the physical testing. Sensitivities of the neutral-axis

position to damage will be studied for both static and moving load cases.

1.3 Thesis Organization

There are seven chapters in this thesis, which are organized into three parts. Part I consists of Chapters 1 and 2. Research background and objectives are introduced in Chapter 1, and a literature review on the related research issues is provided in Chapter 2. Chapters 3 to 6 constitute Part II, as the main body of the thesis, which including multi-component analysis of strain monitoring data, mixture distribution model based reliability assessment, Kalman filter based optimal estimation of neutral-axis position, and experimental verification of the neutral-axis position based damage indicator. As the final part of this thesis, Chapter 7 gives conclusions obtained in this study as well as recommendations for future work. A brief description of these chapters is given as follows.

Chapter 1 introduces the background and research objectives of this PhD study, and the dissertation structure. The significance of bridge structures to the life quality of the society is demonstrated to fetch out the importance of bridge condition assessment under in-service environment.

Chapter 2 contains a literature review on the strain monitoring in SHM, source separation of multi-component monitoring data, mixture distribution model in reliability analysis, and damage detection using strain measurement. In general, the

literature review follows a clue that what the problem is and how it is to be solved. After a brief review of the practice of strain monitoring in SHM, the issue of source separation of strain monitoring data is introduced. Then, research efforts pertaining to source separation of multi-component signals from frequency filters to filter banks and wavelets are reviewed. When using extracted strain response data due to live load effect for reliability assessment, another issue arises in the monitoring data based reliability evaluation that the strain response due to live load effect collected under in-service environment is a result of multi-load effect. It cannot be characterized by a standard probability density function adequately. Hence the mixture distribution modeling methods in reliability analysis are reviewed. Literature review on damage detection using strain measurement is then conducted. As a result of the literature review, critical issues to be addressed in this PhD study will be discussed.

In Chapter 3, a wavelet based multi-component decomposition method is proposed to extract strain components of temperature effect, live load effect and traffic effect from the raw measurement data. Peculiarity of strain monitoring data collected by an SHM system is explained as a combination of live load and environmental effects. Principles for source separation of the multi-component data are then presented. By combining mathematical and physical principles elaborately, a method of component extraction according to the physical meanings is proposed and realized in the wavelet decomposition domain. Application of the proposed method to component analysis of the strain monitoring data from TMB is illustrated at the end of this chapter.

In Chapter 4, mixture distribution model based reliability analysis is proposed for the condition assessment of in-service bridge structures using strain response data due to live load effect (extracted from the raw measurement data). Inference of a probability distribution from the observed data is necessary in any reliability analysis. Often this inference is complicated by the presence of multiple engendering effects that may create a heterogeneous dataset, making standard distribution models inadequate. Mixture distributions existing in the strain data are first identified by the histogram analysis. Then mixture estimation including model selection and parameter estimation is addressed and a structure of mixed Weibull model is proposed for the PDF inference of peak-stress values counted from the derived stress-time histories. Further application of the mixed Weibull model for reliability assessment of the TMB deck is illustrated at the end of this chapter.

In Chapter 5, estimation of the neutral-axis position from the traffic-induced strain is explored and a KF estimator is proposed to perform the estimation with consideration of noise in the sensor readings. The neutral-axis position is provided as an indicator of damage because of its independence of traffic load patterns and its shift in the occurrence of damage. The design of the KF estimator is introduced firstly. In succession comes the validation of its stability to different levels of noise by numerical simulation. Application of the proposed KF estimator to the neutral-axis position estimation in TMB is provided at the end of this chapter.

In Chapter 6, an experimental verification of the neutral-axis position based damage

detection method is conducted. Experimental setup including design and fabrication of the test model, instrumentation, moving load and damage simulation is outlined first. By formulating a multi-scale FEM model, numerical simulation study on the damage detection of the test model (using neutral-axis position as an indicator) is then carried out for static and moving load cases, respectively. Physical experiment on damage detection of the test model is then conducted. The Sensitivity of the neutral-axis position to damage is discussed at the end of this chapter.

Chapter 7 summarizes contributions, findings and conclusions achieved in this PhD project through theoretical and experimental research. Recommendations for future work are also presented.

CHAPTER 2

LITERATURE REVIEW

A literature review was conducted before this research began. This literature review includes articles of strain monitoring in SHM, processing of multi-component monitoring data, mixture distribution models in reliability analysis, as well as damage detection using strain measurement. At the end of this chapter, a short summary of the previous studies as well as a number of key issues identified to be pursued in this PhD project will be provided.

2.1 Strain Monitoring in SHM

Accurate information on in-service bridge structures is an essential part of implementing a cost-effective and safety-conscious bridge management and maintenance system (BMMS). Expectedly SHM can provide more accurate information on the condition of in-service bridge structures that cannot be obtained by traditional visual surveys, and insights into actual behavior of bridges under in-service environment. In practice of bridge monitoring, most common measurement items include strain, displacement and acceleration responses of the

target bridge (Doebling *et al*. 1998; Chang 2001; Mufti and Bakht 2002). Particularly the capability of measuring strain response of a bridge during its operation is meaningful to bridge owners and engineers for a variety of reasons. Strain data can be directly used to indicate fatigue or yielding of the material, safety reserve or reliability of a structural component (Bergmeister and Santa 2000; Koshiba 2001), or provide information on the load-carrying capacity of a whole bridge. From another point of view, strain response data can be used to derive stresses or pressures. With careful design strain gauge arrays can be used to create very accurate transducers of acceleration, moment, and torque. Moreover these derived quantities can offer another perspective on the condition or status of in-service bridge structures. In a sense, as a typical local response, strain measurement may be better suited to characterize the local behavior or damage of the bridge structure than acceleration data, therefore strain sensors can be deployed at critical parts of a bridge where high strains are anticipated to be developed that could approach or surpass the material resistance (Chakraborty and DeWolf 2006).

The most common method of measuring strain is with an electrical strain gauge (ESG), a device whose electrical resistance varies in proportion to the amount of strain in the device. Resistive foil ESGs may set up in full-, half-, or quarter-bridge configuration with a voltage excitation source to measure the changes in electrical resistance. Usually the metallic strain gauge consists of a very fine wire or, more commonly, metallic foil arranged in a grid pattern bonded to a thin backing carrier,

which can be attached directly to the test specimen or real structures. Therefore, the strain experienced by the test specimen or real structures is transferred directly to the strain gauge. Another traditional method of measuring strain is the vibrating wire strain gauge (VWSG). This strain gauge operates on the principle that a tensioned wire, when plucked, vibrates at a frequency that is proportional to the strain in the wire. As to its configuration, the gauge is constructed such that a wire is held in tension between two mounting blocks that can be welded to the specimen or real structures. Loading on the targeted structure changes the distance between the two mounting blocks and results in a change in the tension of the wire. Then a controlled electromagnet is used to pluck the wire and measure the vibration frequency of the wire in tension. Strain is consequently calculated by applying calibration factors to the frequency measurement. VWSGs can be practically surface mounted or embedded into concrete structures. In comparison to ESGs, advantages of vibrating wire strain gauges are that the frequency output is immune to electrical noise, able to tolerate wet wiring, and capable of signal transmission of several kilometers without serious loss of the signal. However, as point sensors, ESG and VWSG have difficulties in enhancing their spatial resolution by sensor arrays densely distributed on the structure. In answer to the awkward problem, fiber optical strain gauges (FOSGs) have the ability to multiplex many sensors using only one optical fiber, providing a very low-cost mechanism for densely instrumenting large-scale structures. And optical fiber is comparatively smaller and much lighter than ESG and VWSG sensors so that extensive FOSG sensor installations can be made that were

hitherto impossible with ESG and VWSG sensors.

With rapid development of sensor technologies, the capabilities of strain monitoring in SHM have been vastly improved. Both short-term and long-term strain monitoring has been practiced according to different considerations of owners and engineers (Liu and Lin 1996; Shkarayev *et al*. 2001; Johnson *et al*. 2004). In short-term strain monitoring, interests are focused on short-term structural behaviors and monitoring systems can be configured for recording the strain responses under some specific load effects such as random truck passages, wind gusts, ice pack impacts, or some other extreme events. On the contrary, long-term continuous strain monitoring is to monitor and measure the structural behavior over an extended period of time (maybe more than weeks, months, years, or permanently). It is anticipated that the resulted database could provide high quality performance data to bridge engineers for better bridge management planning. In addition, on a continuous basis, long-term monitoring can offer a chance to track structure status dynamically and early warnings could be signaled before catastrophic failure happens. Related issues of short-term and long-term strain monitoring such as sensor selection and design, instrumentation system installation, data acquisition, data reduction, data interpretation and storage of the data were thoroughly investigated in the literature (Sartor *et al*. 1999; Chakraborty and DeWolf 2006).

2.1.1 Short-Term Monitoring

With respect to the process of human cognition, short-term strain monitoring was preliminarily practiced and expected to serve as a basis for the long-term strain monitoring in future. In the retrospection of the history of short-term strain monitoring program for evaluation of steel bridges done by the University of Connecticut (DeWolf *et al.* 1998), it was stated that the initial strain monitoring in bridge engineering began with a portable computer, which was originally developed for automobile testing. Adaption of this device for strain monitoring in bridge community involves extensive software development and in-house design of signal conditioning modules. These innovative technologies have greatly simplified such testing and hence provided an opportunity for full application in the field of bridge engineering.

As a useful tool in assessing condition of existing bridge structures, short-term strain monitoring was practiced on a variety of bridge structures of different types. Diaphragms of a typical composite multi-steel girder bridge (Bernard *et al*. 1997; DeWolf *et al*. 1998) were instrumented with a short-term strain monitoring system to determine the cause of cracking in diaphragms and provide information useful for making repairs. Short-term strain monitoring studies on critical components of several movable bridges (Sartor *et al*. 1999) were conducted to get answers to questions on condition assessment. DelGrego *et al*. (2004; 2008) conducted a field testing on a century-old railroad truss bridge to evaluate the structural behavior and the influence of aging. In this field testing, a data logger with 96 channels and a total

of 372 strain gauges were used to collect strain response data over a two-week period.

In view on applying strain measurement data to condition assessment, short-term strain monitoring was carried out by bridge engineers with different objectives. Nearly 20 years ago, Bernard *et al*. (1997) and DeWolf *et al*. (1998) conducted a field monitoring on a typical composite multi-steel girder bridge to demonstrate its feasibility of supplementing visual inspection and analytical studies in condition assessment of existing bridge structures. Kim and Nowak (1997) proposed that load distribution factors stipulated in AASHTO (American Association of State Highway and Transportation Officials) were definitely conservative to a series of steel multi-girder bridges. Chajes and Shenton (2005) involved use of strain measurement from controlled load tests to determine the actual load distribution, unintended composite action and contribution from nonstructural components. As to load ratings, special attention was paid to in-service monitoring of strain response from normal traffic environment by Bhattacharya *et al*. (2008). Barr *et al*. (2001) evaluated the flexural live load distribution factors for a three-span pre-stressed concrete girder bridge. Wang *et al*. (2005) studied the fatigue damage for typical multi-girder steel bridges through synthesizing traffic data collected by a WIM system. Yakel and Azizinamini (2005) proposed a method for the calculation of positive bending moment capacity of composite steel girders by using strain monitoring data.

2.1.2 Long-Term Monitoring

In recognizing that budget for the long-term monitoring effort is not very high, long-term strain monitoring in bridge engineering was practiced increasingly (Abe *et al*. 2000; Barrish *et al*. 2000; Feng and Kim 2001; Choi *et al*. 2004; DeWolf *et al*. 2006; Olund 2006). Increasing attentions from bridge owners and engineers are mainly due to an expectation that long-term continuous monitoring systems can provide ongoing information regarding the behavior and health of a bridge, fatigue performance, or general operational information over an extended period of time. Moreover, long-term monitoring data can be batched and fed back into the design process as well as can be integrated into the current procedure of condition assessment. Because the system need operate continuously at an unattended and often remote location, it is critical that high reliability and automaticity of the system should be guaranteed for the long-term running.

Regarding the nature of long-term monitoring, the long-term stability, accuracy and reliability of the sensing devices must be taken into account preliminarily. At the early stage, drifting phenomenon in sensor readings was identified in the practice of long-term strain monitoring. This is because there are no exactly the same coefficients of thermal expansion between two materials of sensor itself and substrate being monitored. Usually a temperature-compensated backing technology was utilized to eliminate much of the potential thermal effect (Smith *et al*. 1999). From

another way, Begueret *et al*. (1997) designed and tested two new converters of strain gauge transducers dedicated to long-term monitoring with minimum temperature effect as possible. An automatic offset cancellation capability is embodied in their circuitry design and hence this arrangement has a low drift characteristic and is well suited for the long-term monitoring. To testify the applicability of traditional and newly developed strain sensors in long-term monitoring, a notable program on instrumentation performance was conducted by Robertson *et al*. (2005) for ten years. Over 200 strain sensors were installed on a long-span box-girder viaduct on the island of Oahu and each of the instrumentation systems is evaluated for its performance in monitoring short-term and long-term structural behavior. Advantages and disadvantages of each type of strain sensors were summarized. Other research on the sensor durability, stability and reliability for the long-term strain monitoring can be found in the literature (Sohn *et al*. 2003). As a whole, in the current research of long-term strain monitoring, most of researchers focused on sensor devices, but less attention was paid on the peculiarity of long-term monitoring data analysis.

Generally the long-term monitoring system is designed with advanced automatic data collection algorithms, which record structural response under operational conditions in a real-time way. Rather than capturing triggered data of events, long-term continuous monitoring provides a unique perspective on structural response which allows detailed studies of long-term changes of structural properties, behavior and performance over time. Along with the advantage of automatic data collection,

challenges in the data analysis arise simultaneously. The peculiarity of long-term monitoring data is that it has a heterogeneous data structure engendered by the presence of multi-load and environmental effects, i.e., all different structural behaviors are mixed together. In the following, a literature review on source separation of monitoring signals will be carried out.

2.2 Source Separation of Multi-Component Signals

In view on the way of data acquisition, long-term SHM systems, on a continuous basis, acquire structural response data passively under operational conditions rather than measuring a specific structural behavior by actively controlling the load environment such as load testing. Therefore, SHM systems record information from various sources, such as external loading and environmental effects, sudden accident events, along with sensor noise, which might lead to a complicated multi-component data structure (Choi and Williams 1989; Cohen 1989). A logical way to efficiently interpolate the SHM measurement is to decompose the original measurement into mono-components such that distinct structural behaviors under different loading scenarios and environmental conditions can be revealed for the pertinent condition assessment or damage detection.

The recovery or separation of desired sources from an observed mixture is a classic but difficult problem in signal processing. Conventional approaches to signal

component separation originate in the discrete domain in the spirit of frequency filters (Weinstein *et al*. 1993). Although frequency filters does extract a component of exact frequency content, they simultaneously introduce modifications of the original source signal such as ringing effects and spurious oscillations (Abarbanel 1996; Kantz and Schreiber 1997). As another disadvantage, conventional frequency filters do not provide an extension beyond the two-mixture case, i.e., three or more signals mixed together cannot be separated in this manner. Aiming to the multi-component separation problem, filter banks are arranged as an array of frequency filters that separate the input signal into multiple components, each one carrying a single frequency content of the signal. Particularly, with a tree structure of a series of low-pass and high-pass filters, discrete wavelet filter banks have certain advantages in decomposition of a multi-component signal, such as parsimonious representation, energy decomposition, effective de-correlation and perfect reconstruction (PR). In regard to the main stream of research in this field, literature review on the source separation of multi-component signal was carried out from frequency filters, filter banks, to wavelets.

2.2.1 Frequency Filters

In signal processing, frequency filter is a device or operator that removes from a signal some unwanted component or feature in order to suppress interfering signals and reduce background noise. More often, this operator takes a filter function in the

Fourier domain and correspondingly the filtering process is implemented in the Fourier domain by multiplication. Since the multiplication in the Fourier domain is identical to convolution in the time domain, all frequency filters can in theory be realized in the time domain. As interpreted in the time domain, a linear filter simply converts a signal x_t into another signal y_t by a linear transformation. The output y_t of the linear filter is a result of the convolution of the input x_t with a coefficient vector w_t. The elements of the vector $w_t = (\ldots, w_{-2}, w_{-1}, w_0, w_1, w_2, \ldots)$ are called filter coefficients. The convolution of the input vector x_t with the coefficient vector w_t may be expressed as

$$y_t = \sum_{i=-\infty}^{\infty} w_i x_{t-i} \tag{2.1}$$

where the future values of x_t are required to obtain the filter output at time t. This may not be feasible in certain applications. As a result, some restrictions are imposed on a filter such that the output of the filter is not allowed to exist before the realization of the input, i.e.,

$$y_t = \sum_{i=0}^{\infty} w_i x_{t-i} \tag{2.2}$$

where only the past and present values of input are utilized. A filter with this property is called a causal filter or a physically realizable filter. The form of the filter function determines the effects of the operator. There are basically three different kinds of filters: low-pass, high-pass and band-pass filters.

- **Low-pass:** a low-pass filter attenuates high frequencies and retains low frequencies unchanged. The result in the time domain is equivalent to that of a smoothing filter. This filter is defined by two corner frequencies: low pass and low cut;
- **High-pass:** a high-pass filter, on the other hand, passes without attenuation frequencies above some cutoff frequency and attenuates all lower frequencies. This filter is defined by two corner frequencies: high cut and high pass;
- **Band-pass:** a band-pass filter is a trapezoidal filter defined by the four corner frequencies: high cut, high pass, low pass, and low cut. It is used to attenuate both low-frequency and high-frequency noise. Frequencies that fall within the bandwidth (from the high pass to low pass points) pass without any attenuation. Frequencies that fall on the slopes of the filter are increasingly attenuated away from the central bandwidth.

2.2.2 Filter Banks

Filter banks are arrangements of low-pass, band-pass, and high-pass filters used for the spectral decomposition of signals. They play an important role in many modern signal processing applications such as audio and image coding. The reason for their popularity is the fact that they easily allow simultaneous extraction of several spectral components of a signal at one implementation and, with two complementary analysis and synthesis filter banks, perfect reconstruction of the input signal can be

achieved. Perfect reconstruction means that the output signal is a copy of the input signal with no further distortion than a time shift and amplitude scaling. It is a rigorous requirement in the theory of signal decomposition but cannot be achieved by a low-pass, band-pass, or high-pass filter alone.

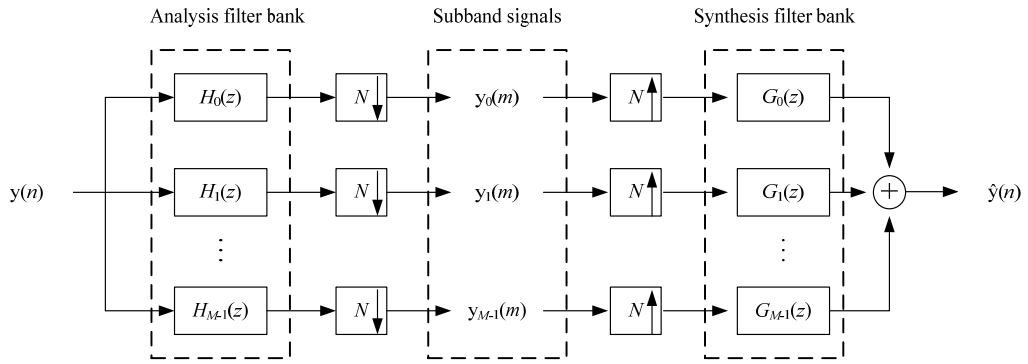

Figure 2.1 *M*-channel filter banks

Figure 2.1 shows an *M*-channel filter banks for an example. The input signal is decomposed into *M* sub-band signals by applying *M* analysis filters with different pass-bands. Thus each of the sub-band signals carries information of the input signal in a particular frequency band. The blocks with arrows pointing downwards in **Figure 2.1** indicate down-sampling (subsampling) by factor *N*, and the blocks with arrow pointing upwards indicate up-sampling by *N*. Subsampling by *N* means that only every *N*th sample is taken. This operation serves to reduce or eliminate redundancies in the *M* sub-band signals. Up-sampling by *N* means the insertion of (*N*-1) consecutive zeros between the samples. This allows us to recover the original

sampling rate. The up-samplers are followed by filters which replace the inserted zeros with meaningful values. Therefore, perfect reconstruction of the input signal can be achieved by delicately designing analysis and synthesis filter banks.

2.2.3 Wavelets

As reviewed in the previous section, an important issue in the filter bank theory is how to design perfect reconstruction filter banks. An easy way to construct multichannel filter banks is to cascade two-channel banks appropriately. One case can be seen in **Figure 2.2(a)**, where frequency analysis is obtained by simply iterating a two-channel division on the previous low-pass channel. This results in a tree with 2^J leaves, each corresponding to $(1/2^J)$th of the original bandwidth, with a down-sampling by 2^J. Considering the filter bank given in **Figure 2.2**, it shows that the signal is split first via a two-channel filter bank, then the low-pass version is split again using the same filter bank, and so on. This structure implements a discrete time biorthogonal wavelet series on the condition that the two-channel filter banks are perfect reconstruction. If the two-channel filter bank is orthonormal, then it implements an orthonormal discrete-time wavelet series. With orthonormal perfect reconstruction filter banks, Daubechies (1988) constructed compactly supported orthonormal wavelets and orthonormal scaling functions. Vetterli and Herly (1992) showed that biorthogonal perfect reconstruction filter banks could generate biorthogonal wavelets and biorthogonal scaling functions.

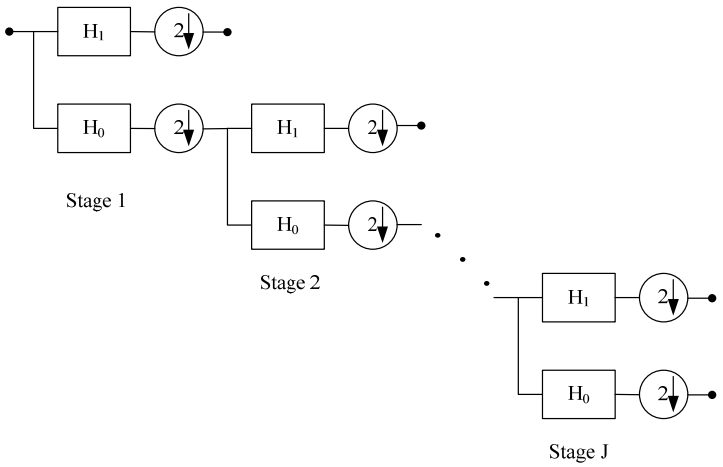

(a) Analysis part

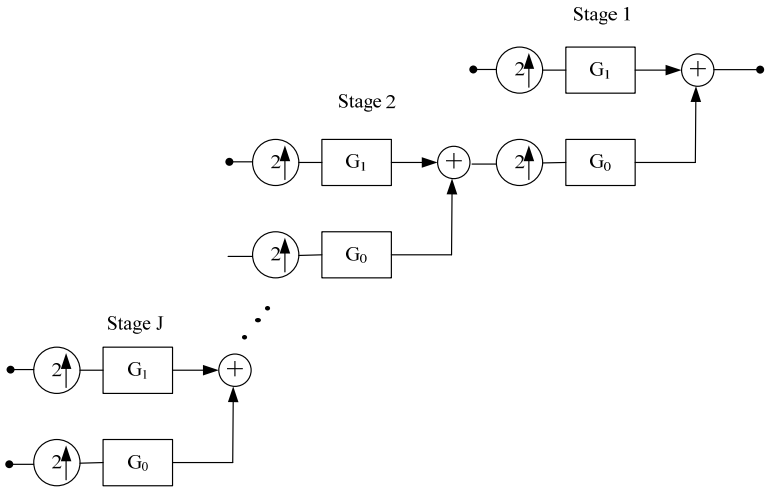

(b) Synthesis part

Figure 2.2 Implementation of an orthogonal discrete-time wavelet series

2.3 Mixture Distribution Models for Reliability Analysis

Condition assessment of in-service bridge structures becomes an increasingly active field driven in part by the need for efficient management of these public assets.

Available data in conventional practice of structural condition assessment generally come from visual inspections which have been proved to be limited and subjective. In addition to the inspection methods, a strategy of integrating structural condition assessment with the SHM system is expected to become a valuable practice in this field. Methods of integrating SHM data with procedures of reliability assessment have received much attention because reliability is an important performance measure of structural condition (Lark and Flaig 2005) and reliability based approaches have the capability of accommodating uncertainties in measurement data (Bhattacharya *et al*. 2008; Catbas *et al*. 2008). Messervey and Frangopol (2008) proposed a scheme of SHM based condition assessment in which reliability algorithms can be fed with SHM data. In their method, a standard density function was used for the reliability data modeling. However, in-service monitored response of bridge structures is a combination of multi-load effects such as traffic (highway, railway, or both of them) and wind (monsoon or typhoon), whose statistical properties may not be characterized by a single distribution function adequately.

2.3.1 Mixture Distribution in Reliability-Related Data Analysis

Finite mixture models made their first recorded appearance in a paper by Newcomb (1886) who used it in the context of modeling outliers. A few years later, Pearson (1894) used a mixture of two univariate Gaussian distributions to analyze a dataset containing ratios of forehead to body lengths for 1,000 crabs, and by the method of

moments (MOM) to estimate the parameters in the mixture model. More recently, mixtures of Poisson distributions have been used in the positron emission tomography to model emissions occurring in a line along each pair of electronically coupled photon-sensitive crystal detectors (Vardi *et al*. 1985). Poisson mixtures have also been used for document classification in the field of information retrieval (Li and Zha 2006). Other paramedic mixtures including the von Mises-Fisher distributions were proposed for the analysis of text and gene expressions (Banerjee *et al*. 2005). The mixture distribution in statistical analysis has long been aware of and, data modeling including model selection and parameter estimation has also been addressed.

2.3.2 Model Selection

Generally, a mixture distribution model is defined as a weighted sum of component distributions as

$$f(x|\mathbf{\Theta}) = \sum_{j=1}^{m} a_j f_j(x|\mathbf{\theta_j}) \tag{2.3}$$

where the overall parameter vector $\Theta = (a_1,\ldots, a_m; \theta_1,\ldots, \theta_m)$ and each component density function is parameterized by vector $\mathbf{\theta_j}$ (for $j = 1,\ldots, m$). The proportion a_j may be alternatively interpreted as the prior probability of observing a sample from class j. Furthermore, the prior probabilities a_j for each distribution must be nonnegative and sum-to-one, or

$$a_j \geq 0 \qquad for \quad j = 1, \cdots, m \tag{2.4}$$

and

$$\sum_{j=1}^{m} a_j = 1 \tag{2.5}$$

Correspondingly $f_j(x|\boldsymbol{\theta}_j)$ may be interpreted as the posterior probability distribution or conditional probability distribution. Through an appropriate choice of its components and weightings, a mixture model is expectedly able to model quite complex distributions. It is often in the case that what kind of mixture types and how many components in the model are not known at first and they must be estimated from the data. The task of finding the mixture type and optimal number of components is called model selection in a sense. In practice, it is usually assumed that the variables and the functional form of mixing densities are known. Therefore, model selection has typically referred to the problem of choosing the optimal number of components M.

In definition of a finite mixture, the most fundamental parameter, to some extent, is the number of components. Its importance results partially from technical considerations that without knowing the component number the process of mixture distribution estimation cannot go further. There is a vast literature devoted to the issue of choosing the optimal number of components. It can refer to McLachlan and Basford (1988) who provided a detailed review of different approaches available to

address this problem. Most common methods devoted to estimating M can broadly be divided into two categories both based on the log likelihood function. The first group of methods is information based while the second relies on the testing procedures. Information based approaches are usually used and they choose the component number by minimizing the negative log likelihood function. Various information based criteria such as Akaike Information Criterion (AIC) (Akaike 1973), Bayes Information Criterion (BIC) (Schwarz 1978) and their modifications such as quadratic AIC/BIC (Ray and Lindsay 2008), the Integrated Classification Likelihood Criterion (ICLC) (Biernacki *et al*. 2000), Normalized Entropy Criterion (NEC) (Biernacki *et al*. 1999), Minimum Information Ratio Criterion (MIRC) (Windham and Cutler 1992), and Laplace-Empirical Criterion (LEC) (McLachlan and Peel 2000), have been developed. Among the easily implemented methods, AIC has been repeatedly demonstrated good performance (Pan and Shen 2006), and is given as follows

$$AIC = -2L_n(\boldsymbol{\Theta}) + 2k \tag{2.6}$$

where $L_n(\boldsymbol{\Theta})$ is the log likelihood, and k is the number of free parameters in the mixture model. The model with a minimum AIC value is chosen to be the best model. Once the component number is specified, estimation of the mixture parameters can be conducted straightforward.

2.3.3 Parameter Estimation

The task of finding the mixture parameters is called parameter estimation and it was studied as early as 1890s by Pearson (1894). In his work, Pearson used the method of moments to extract model parameters for a mixture of two normal distributions. Solving for the parameters required finding a particular root of a ninth-order polynomial, a very difficult calculation in that time. Subsequently Cohen (1967) discovered an iterative method to solve the same problem that only requires solving cubic polynomials. However, the moment method does not guarantee any sort of optimality of the solution and was initially useful since MLE (Maximum Likelihood Estimation) methods were almost intractable before computers became commonly available. Fryer and Roberson (1972) and Tan and Chang (1972) showed that moment methods were inferior to MLE approaches in their problem of determining the parameters of a mixture of two normal distributions. With the availability of digital computers, MLE became practical tools for general mixture problems. EM (Expectation Maximization) algorithm was further developed by Dempster *et al*. (1977), which provides a general iterative procedure of computing the MLE solutions for mixture models. The EM algorithm has an important feature that the likelihood is non-decreasing in each iteration. Additionally, the maximization step can be done in closed-form for many distribution families (McLachlan and Basford 1988). In general, the EM algorithm is a simple and versatile procedure for the likelihood maximization in mixture estimation problems and thereby it has various applications in the real-world problems.

2.4 Measurement Based Damage Detection

As a primary part of SHM, damage detection has been extensively studied, producing a number of methods as summarized by Doebling *et al*. (1996) and Sohn *et al*. (2003). Generally, these methods were classified according to different standards such as destructive or non-destructive, static or dynamic, model-based or non-model-based, etc. Herein, they are particularly categorized as measurement based (signal based) or model based with respect to their dependence on the structural model (Lee *et al*. 2005). The model based approaches usually identify damage by correlating an analytical model, which is often established on the finite element procedure. On the contrary, measurement based damage detection does not require a detailed analytical structural model and can work by directly utilizing features extracted from recorded data. In this project, efforts mainly focus on the development of a strain measurement based approach to damage detection, therefore this section only reviews the damage detection methods using vibration and strain measurement data.

2.4.1 Vibration Based Approaches

As commonly used in SHM, vibration based damage detection methods have been extensively studied and a number of damage indices were proposed (Doebling *et al*. 1996; Sohn *et al*. 2003). Generally all of these indices are based on the assumption

that changes in physical properties (such as mass, stiffness and boundary conditions) will give rise to changes in dynamic characteristics (such as modal frequency, modal shape, or their derivations). Salawu (1997) outlined the damage characterization problem by using natural frequency changes identified from the acceleration data. But local damage in a structure may cause only very little changes of the natural frequency. The change of natural frequencies may not be sufficient for the damage location. Contrastively modal shape based methods have the ability of damage location. Two types of approaches based on the change of modal shapes and their derivatives were recently summarized by Gandomi *et al*. (2008). Pandey *et al*. (1991) demonstrated that the curvature of modal shape is more sensitive to damage than the mode shape itself. In their method, by plotting the difference of modal curvature between the intact and damage states, a peak at the damage element indicates the presence of a fault. A gapped smoothing method was presented by Hoerst and Ratcliffe (1997) and Ratcliffe and Bagaria (1998), which essentially improves the ability of extracting peaks. As a whole, vibration features applied for damage identification were summarized by Lee *et al*. (2002).

Although vibration based damage detection methods have some certain success in numerical simulations and laboratory experiments, their applicability needs further verification in real monitoring practices. Farrar and Jauregui (1998) presented a comparative study of damage identification algorithms, and found that standard modal properties, such as resonant frequencies and modal shapes, are poor damage

indicators. Actually changes in modal properties resulting from changes in environmental conditions can be as significant as the changes caused by damage (Abdel Wahab and De Roeck, 1997). Measurement noise can as well significantly affect the success of these detection techniques. For example, the curvature changes could be masked by the derivative operations when noise presenting in the modal shape data (Chance *et al*. 1994). On awareness of the limitation in vibration based damage detection methods, research attention nowadays goes to strain measurements.

2.4.2 Strain Based Approaches

Structural damage could be often discerned by the variation of strain response or its derivatives. But strain measurements always serve an auxiliary role in the damage detection, partially due to its locality that the influence of damage on strain response cannot be reflected effectively unless the area where the strain sensors deployed could cover the damaged region. Favorably the recent development of distributed Brillouin optical fiber sensing (BOFS) techniques improves the spatial resolution of strain measuring definitely. Therefore strain-related detection methods have received increasing efforts as described in the literature (Kahl and Sirkis 1996; Yam *et al*. 1996; Doebling *et al*. 1997; Oh and Jung 1998; Abdel Wahab and De Roeck 1999; Chen *et al*. 2000; Ray *et al*. 2000; Liang and Hwu 2001; Ndambi *et al*. 2002; Sahin and Shenoi 2003; Chen *et al*. 2004; Kang *et al*. 2006; Lee *et al*. 2006; Wu and Li

2007; Kesavan *et al*. 2008; Wildy *et al*. 2008; Cardini and DeWolf 2009; Katsikeros and Labeas 2009).

In general most of the proposed methods are based on the concepts of strain mode shape, flexibility matrix, damage locating vectors (DLV), and strain energy. Yao *et al*. (1992) presented a damage localization method by using the strain mode shape and strain frequency response function (SFRF). Stubbs *et al*. (1992) developed a modal strain energy method and demonstrated its applicability to various beam-like structures. Cornwell *et al*. (1999) further extended it to the plate-like structures. Zonta *et al*. (2003) proposed a strain-flexibility based approach and applied it to detect scattered cracks in a concrete beam. Adewuyi *et al*. (2009) summarized that damage detection techniques based on the distributed strain measurement are a more efficient choice than the traditional vibration approaches particularly when noises presenting in the sensor readings.

2.5 Key Issues Identified

The aim of this PhD study is to develop a systematic approach to condition assessment of in-service bridge structures using strain measurement acquired by an SHM system. Research interest includes the component analysis of strain monitoring data, reliability assessment using mixture distribution models, and neutral-axis position based damage detection along with experimental verification. As a result of

the literature review, critical issues to be solved in this PhD study are identified as follows:

(1) To develop a DWT based method for source separation of multi-component strain monitoring data according to physical meanings, such as temperature effect, live load effect, and traffic effect. Long-term SHM systems, on a continuous basis, acquire structural response data passively in a sense rather than measuring specific structural behavior by actively controlling the load environment. Therefore SHM systems record information from various sources, such as external loadings and environmental effects, sudden accident events, and along with the sensor noise, which will lead to a complicated multi-component data structure. A logical way to efficiently interpolate SHM measurement data is to decompose the original measurement data into mono-components such that distinct structural behaviors under different loading scenarios and environmental conditions can be revealed for pertinent condition assessment or damage detection. As reviewed in the literature, the recovery or separation of desired source signals from an observed mixture is a classic but difficult problem in signal processing. Although frequency filters can extract a component of exact frequency content, they simultaneously introduce modifications of the original source signal such as ringing effects and spurious oscillations. As another drawback, conventional frequency filters do not provide an extension beyond the two-mixture case, i.e., three or more signals mixed together cannot be separated in this manner. Filter banks are arranged as an array of frequency filters and can

decompose the input signal into multiple components, each one carrying a single frequency content of the input signal. Particularly with a specialized perfect reconstruction (PR) filter bank, the DWT decomposition method has advantages of parsimonious representation, energy decomposition, and effective de-correlation, which satisfy the mathematical principle of multi-component separation quite well (less distortion and cross-talking among components). Hence DWT techniques can offer a wonderful decomposition platform for component extraction according to physical meanings.

(2) To propose a mixture distribution based approach to reliability assessment of in-service bridge structures. Under in-service environment, bridge structures are subject to traffic (highway, railway, or both of them) and wind (monsoon or typhoon) effects. These external loadings cannot be controlled as people expect in a sense that their random combination produces the strain response data. It is recognized that strain measurement data due to the multi-load effect cannot be characterized by a standard probability density function adequately. Mixture model based reliability assessment of in-service bridge structures is thereby pursued in this PhD project. As reviewed, the Weibull family functions are the most commonly used distributions in the reliability-related data analysis because they have an excellent adaptability to different types of distributions. Hence they can be utilized as the base distribution of a finite mixture model. In contrasting with other parameter estimation methods, the EM algorithm is elegant, easy to implement, numerically stable, and its memory requirements are generally

reasonable even in very large-scale problems. Therefore mixed Weibull models with the EM algorithm for the parameter estimation will be explored in this study.

(3) To develop a strain-related condition index for bridge deck assessment which is estimated from the traffic-induced strain response data. With respect to its live load capacity, bridge deck is one of the most critical parts of a bridge system which directly carrying the traffic. Bridge decks are deteriorating at an ever-increasing number and pace according to the FHWA report (1977). Usually the obsolescence results from traffic or load increasing, harsh environment attacking, or other adverse changes in the use of the structure. Deterioration of bridge decks can cause public inconvenience, travel delay, economic impact, even life lost, giving rise to the most severe problem for the highway industry today. A cost-effective approach to preventing this problem is the use of monitoring technologies to collect data pertaining to the condition of in-service bridge decks. Such precautionary work can be done before more serious situation arises or catastrophe happens. In selecting condition indices for bridge deck monitoring, their sensitivity to damage and robustness with respect to random traffic load patterns should be taken into consideration. Although strain response at each measurement point of a bridge deck section evolves with time according to the incoming random traffic, their ratio of different locations on a same cross section, such as the top and bottom of the cross section, may be independent of the traffic loading. Theoretically, the neutral-axis position of the bridge deck section (in terms of the strain ratio at top and bottom locations) remains

unchanged under the varying traffic environment. And it has potential to have a high damage sensitivity because the neutral-axis position reflects the local cross-section property. In practice optimal estimation of the neutral-axis position from the strain measurement is a key issue of the proposed method. KF estimators have the anti-disturbance capability in noisy environment, and they will be pursued in this project for locating the neutral-axis position from the traffic-induced strain data.

(4) To conduct an experimental verification of the neutral-axis position based damage detection of beam-like bridge decks. Long-span bridge deck behaves as a flexural beam when traffic loads cause it to bend. Hence cracks are prone to happen in the beam-like decks under traffic loading environment. Crack damage can heavily affect the global safety and performance of the long-span bridge structures, and more severely, continual operation without noticing the damage accumulation would be disastrous. To testify the feasibility of the neutral-axis position as a damage indicator, experiment and numerical simulation will be conducted to demonstrate its sensitivity to crack damage and its independence of random traffic load patterns.

CHAPTER 3

WAVELET BASED MULTI-COMPONENT ANALYSIS OF STRAIN MONITORING DATA UNDER IN-SERVICE ENVIRONMENT

3.1 Introduction

In-service infrastructure systems are subject to age-related deterioration, leading to concerns regarding the safety and serviceability of these systems. Continuous awareness of the evolution of the structural condition of in-service infrastructure systems is of great value for their owners as it allows making informed decisions regarding the maintenance and management of the infrastructure assets (Ebeling 1997; Imai and Frangopol 2001; Ko and Ni 2005; Ratay 2006). Structural condition assessment via monitoring gains its popularity in recent years because it can provide engineers with plentiful information on structural condition by various sensors (DeWolf *et al*. 1998; Sartor *et al*. 1999; Sohn *et al*. 2000). Expectedly integrating the data from an on-line SHM system with structural condition assessment would be able to dynamically trace the health status of existing structures (Aktan *et al*. 1997; Wong 2004; Ko *et al*. 2009).

The most common measurements in structural monitoring are strain and acceleration responses (Doebling *et al*. 1998; Chang 2001; Mufti and Bakht 2002). In practice, in-service monitoring of strain response plays an important role in structural condition assessment via monitoring because strain measurement can, on one hand, be directly used to indicate fatigue or yielding of the material, on the other hand, offer derived information of stresses experienced by the structure during its operation. Generally, strain monitoring in the field can be classified into two categories: long-term monitoring and short-term testing (Sartor 1995; Bernard *et al*. 1997). During temporary field experiments such as traffic load testing, some long-term effect on strain response can be ignored since this kind of testing is usually completed in short time and purposed to record short-term structural behavior. Contrarily, long-term continuous monitoring, on a continuous basis, can capture real-time structural behavior not readily apparent from short-term testing, for instance, the daily and seasonal variations (Cardini and DeWolf 2009). More important, it can dynamically trace structural behavior and accumulate plentiful data for condition assessment. As a result, long-term continuous monitoring of real-time streaming of strain is emerging as a critical strategy in the assessment, inspection and decision making on maintenance/repair of bridges, buildings, and other civil engineering structures.

From a practical viewpoint, one main aim of in-service strain monitoring is to

acquire information about stresses experienced by the structure under operational environment. Stress is probably the most important data as it directly indicates the safety reserve of structural components (Bergmeister and Santa 2000; Koshiba *et al*. 2001) and stress response to external loadings is one of the main inputs into structural condition assessment procedures (Aktan *et al*. 1996; Ko and Ni 2005; Catbas *et al*. 2008; Frangopol *et al*. 2008). However, inferring stress based on the measured strain is not easy because strain not only arises from stress but also from temperature influences and from processes inside the material. Long-term strain data acquired under in-service conditions physically result from a combination of these effects leading to a multicomponent data structure. Strain components due to different effects play different roles in contribution to stress quantities. For example, the strain of bridge deck induced by temperature effect, although considerably large, contributes little to the stress as the majority of the temperature-caused strain will be released through expansion joints as expected in the design. Various effects mixed together also imply that the desired source signal in monitoring may be contaminated or distorted by other effects. An efficient way of interpolating multi-component strain monitoring signals is to decompose original measurement into mono-components such that distinct structural behaviors under different loading scenarios and environmental conditions can be revealed for pertinent condition assessment.

In this chapter, a wavelet based multi-component decomposition method is proposed to extract components (due to different loadings and environment effects) of

long-term monitoring strain data and is applied to the instrumented TMB to demonstrate the validity and efficiency of the proposed scheme. Peculiarity of strain monitoring data collected by an SHM system is explained as a combination of live load and environmental effects. Mathematical and physical principles for source separation of multi-component signals are then presented. Wavelet multi-resolution analysis (WMRA) satisfies the mathematical principle (less distortion and cross-talking among components) quite well with specialized perfect reconstruction (PR) filter banks. As a result, wavelet transform based decomposition offers a wonderful platform for component extraction according to physical meanings, which is the ultimate goal of signal separation. As to the real application, specific response properties of bridge structures under temperature effect, live load effect and traffic effect are utilized in the establishment of selection criteria to realize physical component separation of the strain monitoring data.

3.2 Principle of Signal Source Separation

A multi-component signal may contain a number of components that usually come from several different sources. In matrix form, the considered source separation model can be written as

$$\mathbf{x}(t) = A\mathbf{s}(t) \tag{3.1}$$

where $\mathbf{s}(t) = [s_1(t), \ldots, s_N(t)]^T$ represents the unknown sources, $\mathbf{x}(t) = [x_1(t), \ldots, x_N(t)]$

represents the mixtures, and A represents the N by N unknown mixing matrix. As depicted in **Figure 3.1**, source separation consists of recovering unmeasured source signals $\mathbf{s}(t)$ from observed mixtures $\mathbf{x}(t)$, by estimating a de-mixing or separation matrix W:

$$\hat{\mathbf{s}}(t) = W\mathbf{x}(t) \tag{3.2}$$

$$\hat{\mathbf{x}}(t) = \hat{A}\hat{\mathbf{s}}(t) \tag{3.3}$$

and

$$\hat{A} = W^{-1} \tag{3.4}$$

The superscript '^' denotes estimation and the superscript '-1' represents matrix inverse. Such problem arises in many real life applications such as mechanics, radar, sonar and wireless communication.

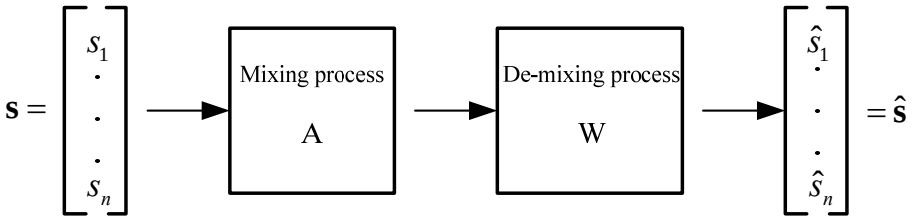

Figure 3.1 Principle of source separation

Without some a priori knowledge, it is not possible to uniquely estimate the original source signal because there is a basic indeterminacy that it is possible to construct

another solution satisfying the same condition. However, one can usually estimate them up to certain mathematical or physical principles. In a sense mathematical principles can be expressed as spatio-temporal de-correlation, statistical independence, sparseness, smoothness or lowest complexity. However, there is no guarantee that the estimated or extracted components according to the mathematical principles have exactly the same waveforms as the source signals, since these adopted mathematical principles for the separation may not match the physical mechanisms perfectly. Because physical mechanisms control the mixing process, the ultimate goal of signal decomposition is to estimate sources having true physical meanings or interpretations, not necessarily satisfying the mathematical requirements. In practice, the physical mechanism oriented separation is complicated by the fact that in real situations, many relevant characteristics, such as the exact frequency content of both the signal sources and the mixing media, are unknown.

Although source separation according to physical meaning is the ultimate goal, it is difficult to establish a mathematical principle satisfying all the physical mechanisms. In this study, a compromise way is designed consisting of two steps: (1) preliminary decomposition based on mathematical principles; (2) physical component extraction in the decomposition domain. Wavelet multi-resolution decomposition satisfies the mathematical principles (less distortion and cross-talking among components) quite well with perfect reconstruction (PR) filter banks. Hence wavelet transform based decomposition offers a wonderful platform for component extraction according to

physical meanings.

3.3 Wavelet Based Multi-Component Analysis

In signal processing, component separation methods are usually based on the understanding of signals themselves, such as parametric or non-parametric representations. Although parametric and semi-parametric methods have been available for this purpose (Fox and Taqqu 1986; Beran 1994), the performance of the parametric methods heavily depends on how well the parametric assumption (e.g., data structure model) fits measurement data. Alternatively, without the limitation of data structure model assumption, nonparametric approaches provide more flexibility and they are mainly enlightened by frequency or time-frequency representation of concerned signals.

3.3.1 Signal Representation and Wavelet

Before source separation methods could be designed pertinently, it is necessary to understand and describe signals in different forms. When a signal is measured with an oscilloscope, it is usually viewed in the time domain. For many signals, this is the most logical and intuitive way to view them. However, a time-domain graph can only show how a signal changes over time and cannot help our understanding of information contained in the frequency domain. Without the help of frequency

domain information, source separation based on time representations will become difficult in the case that components are overlapped in the time domain.

When the frequency content of a signal is of interest, it makes sense to view the signal graph in the frequency domain. The frequency representation shows how the energy of a signal is distributed over concerned frequency bands. The process of doing this is called Fourier Transform Analysis. Fourier theory says that any complex periodic waveform can be decomposed into a set of sinusoids with different amplitudes, frequencies and phases. Adding these sinusoids together again will reproduce exactly the original waveform. According to this principle, various frequency representation based band-pass filters have been developed, which can be used to isolate the component of a signal that lies within a particular band of frequencies. Nevertheless, the use of frequency filters for source separation will encounter difficulties when the signal components are overlapped in the frequency domain.

As described previously, component separation methods based on the time or frequency representation have their limitations in handling real life signals of complex data structures, e.g. overlaps in the time and frequency domains simultaneously. The time-frequency analysis technique (Li *et al*. 2004; Trung *et al*. 2005), among others, was proposed to deal with such problems. It is expected that, by the time-frequency representation, overlaps in the time or frequency domain can

be separated. The short-time Fourier transform (STFT) is one of the earliest methods used for time-frequency analysis. A moving window cuts out a slice of the signal, and Fourier transform of this slice gives the local properties of the signal. But the analysis result seriously depends on the choice of the window function, leading to a trade-off between time localization and frequency resolution (Cohen 1989). Another commonly used time-frequency distribution (TFD) is the Wigner-Ville distribution (WVD) (Classen and Mecklenbrauker 1980). Theoretically the WVD has an infinite resolution in time due to the absence of averaging over any finite time interval. With an infinite lag length, it has an infinite frequency resolution also. But the WVD, being quadratic in nature, will introduce cross terms in multi-component signal analysis. The generated cross terms may have significant amplitudes and can corrupt the separation method.

Wavelet based time-frequency representation relies on the introduction of an appropriate Hilbert space basis and spans the signal in it (Burrus *et al*. 1997). With various discrete scales acting on a mother wavelet, DWT resolves the fixed time-frequency resolution problems inherent in STFT. Besides, since a time-frequency representation of wavelet transform is linear by definition, DWT based methods do not have any cross term interference. Therefore, DWT based methods can decompose a multi-component signal into mono-components with significant reduction of distortions and cross talking.

3.3.2 Wavelet Multi-Resolution Decomposition

In the course of wavelet-based multi-resolution analysis, one at first chooses a particular function as the mother wavelet, and by scaling and shifting, defines a family of daughter wavelets which form a complete set of basis functions. Then map the signal into the transform space spanned by the derived basis functions. This elegant processing can decompose a signal into the meshed spaces of increasing frequency resolution without losing any part of the signal. From a practical point of view, DWT allows the decomposition of a signal into various resolution scales: the data with coarse resolution (approximations) contain the information about low-frequency components and the data with fine resolution (details) contain the information about high-frequency components (Burrus *et al*. 1997). The decomposition process is explained in detail as follows.

Using a selected mother wavelet function $\Psi(t)$, the continuous wavelet transform of a signal is defined as

$$W_{\Psi} f(a,b) = \left\langle f, \Psi_{a,b} \right\rangle = \frac{1}{|a|^{1/2}} \int_{-\infty}^{\infty} f(t) \overline{\Psi}(\frac{t-b}{a}) dt, a > 0 \tag{3.5}$$

where $\Psi(t)$ is so-called ‘mother wavelet’; a is scale parameter; and b is time parameter. The superscript ‘–’ denotes complex conjugation. It is known that the function $f(t)$ can be reconstructed from $W_{\Psi}f(a,b)$ by the double integral representation as defined by

$$f(t) = \frac{1}{C_\Psi} \int_{-\infty}^{\infty} \int_{-\infty}^{\infty} W_\Psi f(a,b) \Psi(\frac{t-b}{a}) \frac{1}{a^2} dadb \tag{3.6}$$

In practical signal processing, a discrete version of the continuous wavelet transform is often employed by discretizing the scale parameter *a* and the time parameter *b*. In general, the procedure becomes much more efficient if dyadic values of *a* and *b* are used, i.e.,

$$a = 2^j \quad ; \quad b = 2^j k \quad ; \quad j,k \in Z \tag{3.7}$$

where Z is a set of positive integers. With some special choices of $\Psi(t)$, the corresponding discretized wavelets $\{\Psi_{j,k}\}$ in the expression of

$$\Psi_{j,k}(t) = 2^{j/2} \Psi(2^j t - k) \tag{3.8}$$

constitute an orthonormal basis for $L^2(R)$. Using this orthonormal basis, the wavelet expansion of a function $f(t)$ can be obtained as

$$f(t) = \sum_j \sum_k \alpha_{j,k} \Psi_{j,k}(t) \tag{3.9}$$

where

$$\alpha_{j,k} = \int_{-\infty}^{\infty} f(t) \Psi_{j,k}(t) dt \tag{3.10}$$

In the discrete wavelet analysis, a signal can be represented by its approximations and details. The detail at level j is defined as

$$D_j = \sum_{k \in Z} \alpha_{j,k} \Psi_{j,k}(t) \tag{3.11}$$

and the approximation at level J is defined as

$$A_J = \sum_{j>J} D_j \tag{3.12}$$

It follows that

$$f(t) = A_J + \sum_{j \le J} D_j \tag{3.13}$$

Equation (3.13) provides a tree-structure decomposition of a signal (as shown in **Figure 3.2**) and a reconstruction procedure as well. By selecting different dyadic scales, a signal can be broken down into many frequency components.

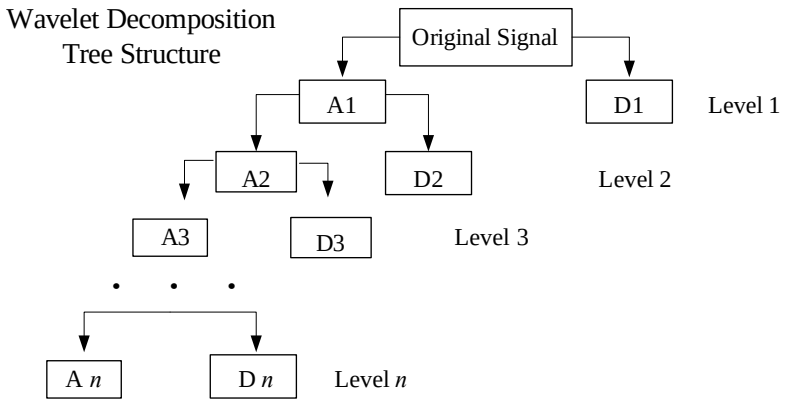

Figure 3.2 Tree structure of wavelet decomposition

3.3.3 Proposed Method for Component Extraction in Wavelet Decomposition Domain

As discussed before, the separated narrow-band components by DWT transform

satisfy the mathematical requirement only but have no physical interpretations. And the source signal (produced by a physical mechanism) may disperse on different levels of DWT decomposition. To restore the desired source signal, component extraction need be conducted in the wavelet decomposition domain. The proposed method for source separation of a signal according to physical meanings is illustrated in **Figure 3.3**. A multi-component signal $x(t)$ is firstly decomposed into multiple components using DWT. Then, they are set as the multiple inputs of the selection module, which use a pre-set criterion to select the wanted physical component.

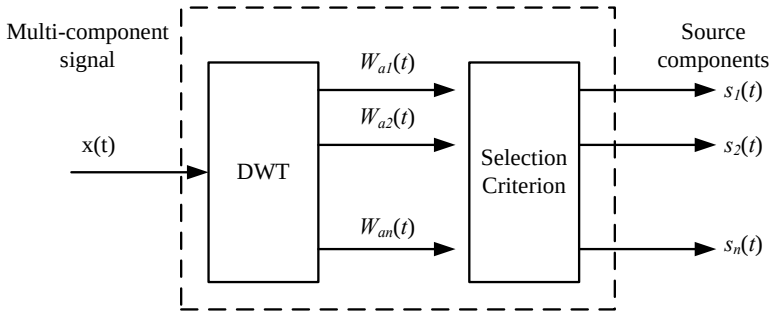

Figure 3.3 Wavelet decomposition based component extraction

Although the proposed method appears straightforward, there are still two unsolved issues. One is how to select wavelet scales to keep enough resolutions in the decomposition. The other is how to establish the selection criterion for physical source extraction. These two problems can be resolved by introducing correlation coefficients of the source component with a reference signal (produced by the same mechanism). Convergence of the correlation coefficient can be used to determine the

decomposition resolution. Then strong or weak correlation can be used to differentiate the level-component in the wavelet decomposition domain. Mathematically, for two datasets $s_i(t)$ and $r_i(t)$, their correlation is formulated as:

$$\mu_i = \left| \frac{E\left\{\left[s_i - E(s_i)\right]\left[r_i - E(r_i)\right]\right\}}{\sqrt{D(s_i)}\sqrt{D(r_i)}} \right| \tag{3.14}$$

where $E(\bullet)$ represents the mean and $D(\bullet)$ represents the variance; $s_i(t)$ denotes the desired source signal; and $r_i(t)$ denotes the reference signal from other channels. By calculating the correlation coefficient, the physical component can be extracted in the wavelet domain.

3.4 Application to Component Analysis of Strain Monitoring Data from TMB

3.4.1 TMB and Its SHM System

The TMB with a main span of 1,377 m is a suspension bridge carrying both highway and railway traffic. It forms a key part of the most essential transportation network linking the Hong Kong International Airport to the urban areas. After completing construction in 1997, the bridge was instrumented with a sophisticated long-term SHM system by the Highways Department of the HKSAR Government to monitor and evaluate the structural health and performance (Wong 2004). As part of the monitoring system, 110 strain gauges were installed to measure dynamic strain

response at three bridge-deck sections denoted by CH23488.00, CH23623.00 and CH24662.50 (chain mileages of the deck sections of TMB) as shown in **Figure 3.4**. The deployment locations of strain gauges include the chord members of the longitudinal trusses, cross-frame chord members, bracing members, deck trough and rocker bearings at one tower.

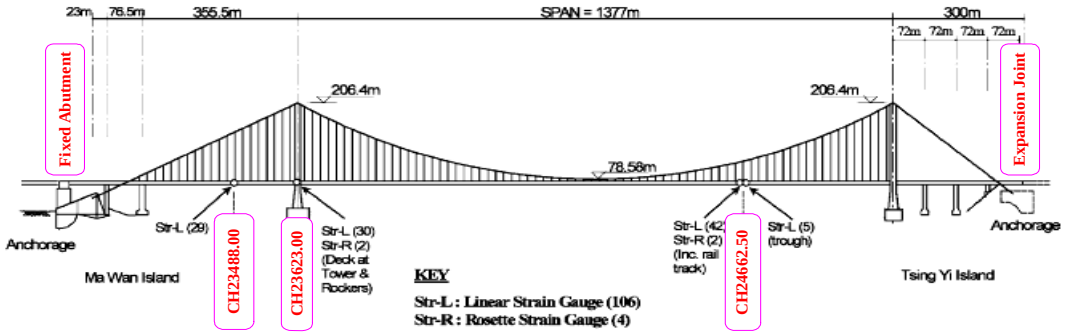

Figure 3.4 TMB and deck sections instrumented with strain gauges

Before interpreting readings from these strain gauges, it would be helpful to explain the structural configuration of the TMB deck. In the longitudinal direction, the bridge deck continuously expands from the Ma Wan abutment to the Tsing Yi abutment. On the Ma Wan abutment, the bridge deck is supported on hinge bearings as illustrated in **Figure 3.5(a)**, which allow the rotation of bridge deck other than the displacement; whereas an expansion joint is provided on the Tsing Yi abutment as shown in **Figure 3.5(b)**, which is designed to accommodate the longitudinal displacement of the deck due to temperature effect. The constraint condition of the bridge deck on the internal piers and towers allows free movement of the deck in the longitudinal direction.

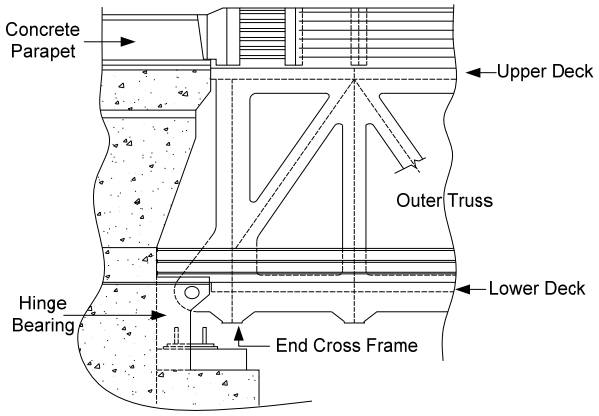

(a) Ma Wan abutment

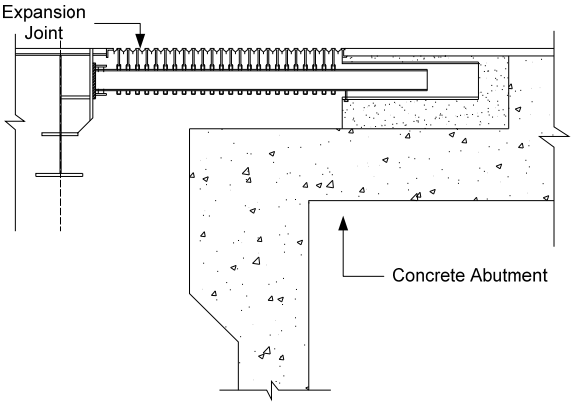

(b) Tsing Yi abutment

Figure 3.5 Support conditions of TMB deck at two abutments

As shown in **Figure 3.6**, the deck of TMB is a double-deck box with truss stiffening and non-structural edge fairing. The longitudinal diagonally braced trusses on the north and south sides of the cross-section consist of top chords, diagonal struts and bottom chords. All truss components on the selected cross-sections have been instrumented with strain gauges (single, pair and rosette strain sensors) as illustrated in **Figure 3.7**. The strain data were acquired at sampling rates of 25.6 Hz and 51.2

Hz, respectively. Strain responses of the deck trusses are monitored and recorded continuously.

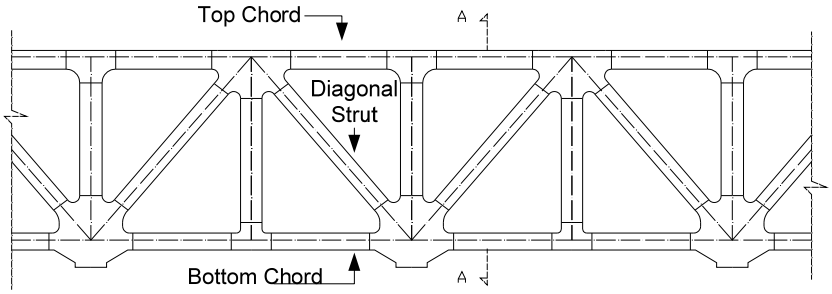

(a) Elevation view

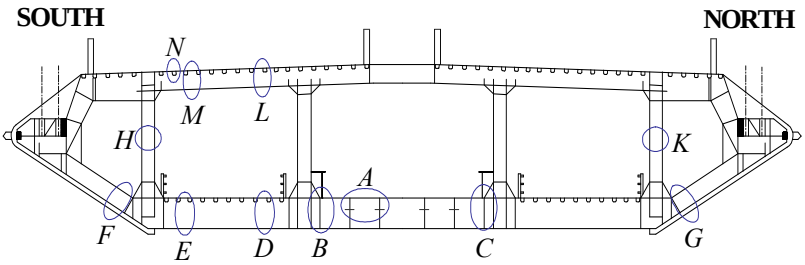

(b) Cross-section view

Figure 3.6 Truss deck of TMB

3.4.2 Strain Monitoring Data of Bridge Deck

In TMB, the in-service monitoring data of strain acquired from the deck trusses stem mainly from four effects: highway traffic, railway traffic, wind, and temperature (the static strain due to initial dead loads is unable to obtain as the strain gauges were installed after the completion of construction). Strain components due to different

effects play different roles in contribution to stress quantities. For example, the temperature-caused strain, although considerably large, contributes little to the stress as the majority of it is released since the movement of the bridge deck is accommodated at expansion joints and bearings (shown in **Figure 3.5**).

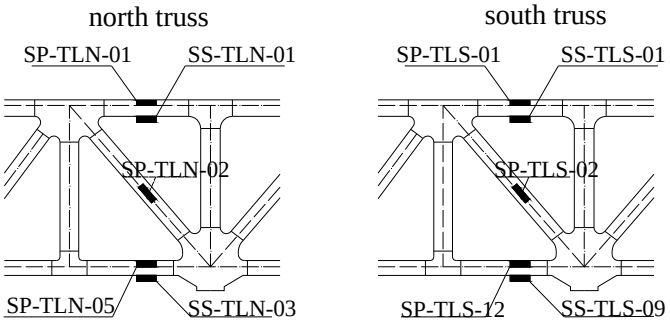

(a) Elevation view

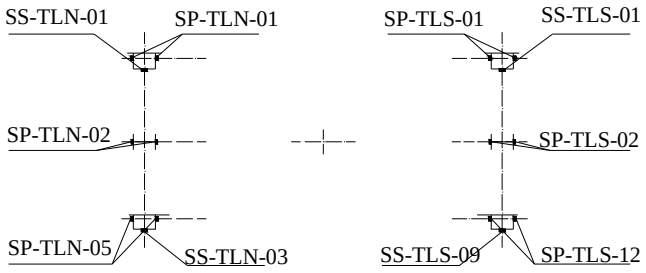

(b) Cross-section view

Figure 3.7 Strain gauges on deck section CH24662.50

The strain responses of truss members on the three cross-sections CH23488.00, CH23623.00 and CH24662.50 have been acquired simultaneously and continuously under operational conditions. **Figure 3.8** illustrates the measured in-service strain

data in one-day period (bottom chords on the north side of the three cross-sections). As shown in **Figure 3.8**, for all three cross-sections, the magnitude of the strain responses acquired at 2:00 to 5:00 am is relatively small since railway traffic ceases to operate during that period. It is also observed that there are trend ingredients (low-frequency components) in all three strain time histories, which will be demonstrated to be the daily cycle effect of temperature variation. It is reasonable to infer that the bottom chords on the three cross-sections expand and contract almost concurrently under temperature effect.

As illustrated by the monitoring data, under temperature effect, the bridge deck mainly behaves as expanding or contracting along the longitudinal direction, and accordingly the expansion joint moves forward or backward. Contrarily, under traffic loading, the bridge deck performs as flexural bending: the top chords compress and the bottom chords extend concurrently, or vice versa. These two kinds of distinct responses are mixed in the monitoring data. It is desirable to present and process them separately when each effect on structural behavior needs to be quantified. The extraction of a specific effect is not easy when the measured signals are nonstationary and non-Gaussian noising in nature. Parametric, semi-parametric, and nonparametric methods have been available for this purpose (Fox and Taqqu 1986; Beran 1994; Mallat 1999). But the performance of parametric or semi-parametric methods depends on how well the model assumption fits the measurement data. As an example, Catbas *et al*. (2008) proposed a linear regression model with a sinusoidal

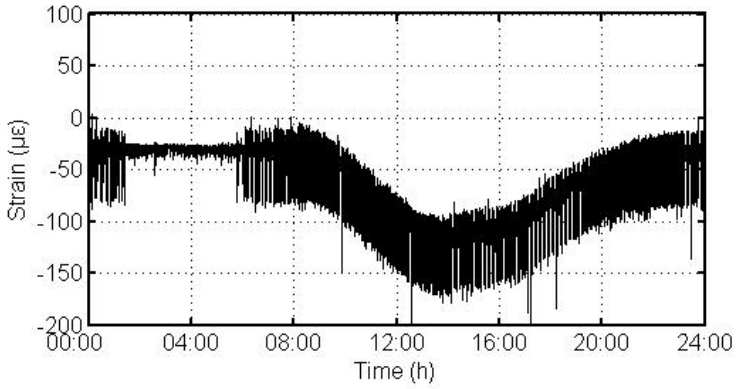

(a) CH23488.00

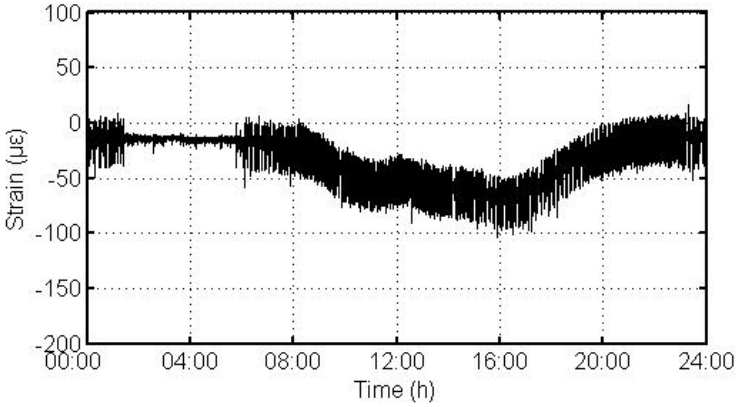

(b) CH23623.00

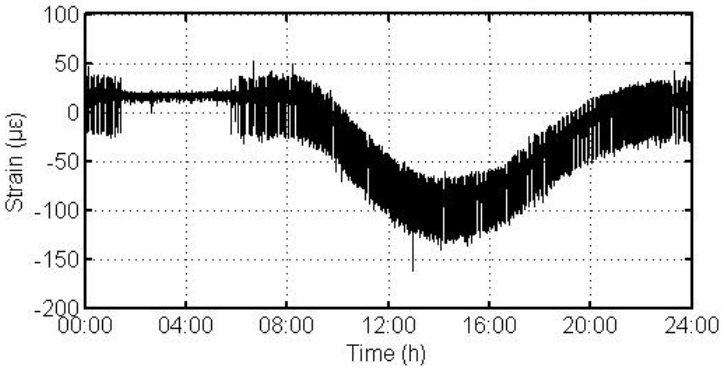

(c) CH24662.50

Figure 3.8 One-day monitoring data of strain (bottom chord on north truss side)

component to model temperature-induced strain and estimated the model parameters from monitoring data. They concluded that the temperature-induced strain was difficult to conceptualize and model with the use of conventional parametric methods. Alternatively, without the limitation of model assumption, nonparametric approaches provide more flexibility. The previously proposed method takes advantage of the nonparametric DWT decomposition delicately and will be applied to the component analysis of the strain monitoring data from TMB.

3.4.3 Component Extraction of Strain Monitoring Data

Utilizing the DWT decomposition procedure, the strain monitoring data from TMB are firstly decomposed into approximations and details (i.e., high-frequency and low-frequency components) at various levels. For each level, the high-frequency part (details) separated and the remaining low-frequency part (approximations) is transferred into the next level of decomposition. Through the elegant decomposition, the strain component due to temperature effect is modeled as the lowest-frequency part in the wavelet domain. **Figure 3.9** shows the results of multi-level decomposition of the strain signal and the temperature-induced strain is modeled successfully through 12-level decomposition. To illustrate the low-pass and high-pass characteristics of DWT level decomposition, the magnitude spectra of the decomposed level-component at different scales are shown on the right side of **Figure 3.9**. It is observed that DWT separates the stain data into a set of narrow-band

components whose spectra occupy different segments of the frequency axis. Based on the DWT decomposition platform, physical component extraction of temperature effect, live load effect and traffic effect is carried out as follows.

3.4.3.1 Strain response due to temperature effect

In TMB, under temperature influence, the bridge deck behaves mainly as expanding and contracting along the longitudinal direction and the expansion joint moves forward and backward accordingly. It implies that there exists a strong correlation between the temperature-induced strain and the displacement at the expansion joint because they are all produced by the temperature effect (as shown in **Figure 3.11(a)**). The relationship between the temperature-induced strain and the longitudinal displacement at the expansion joint is approximately expressed by

$$\Delta l = \int_0^l \varepsilon_t dl \tag{3.15}$$

where Δl is the longitudinal displacement at the expansion joint; ε_t is the strain caused by temperature variation. On the assumption that the temperature-induced strain is uniformly distributed along the bridge deck, the temperature-induced strain can be approximately estimated from the displacement at the expansion joint as

$$\varepsilon_t = \frac{\Delta l}{l} \tag{3.16}$$

where l is the length of continuous bridge deck in the longitudinal direction.

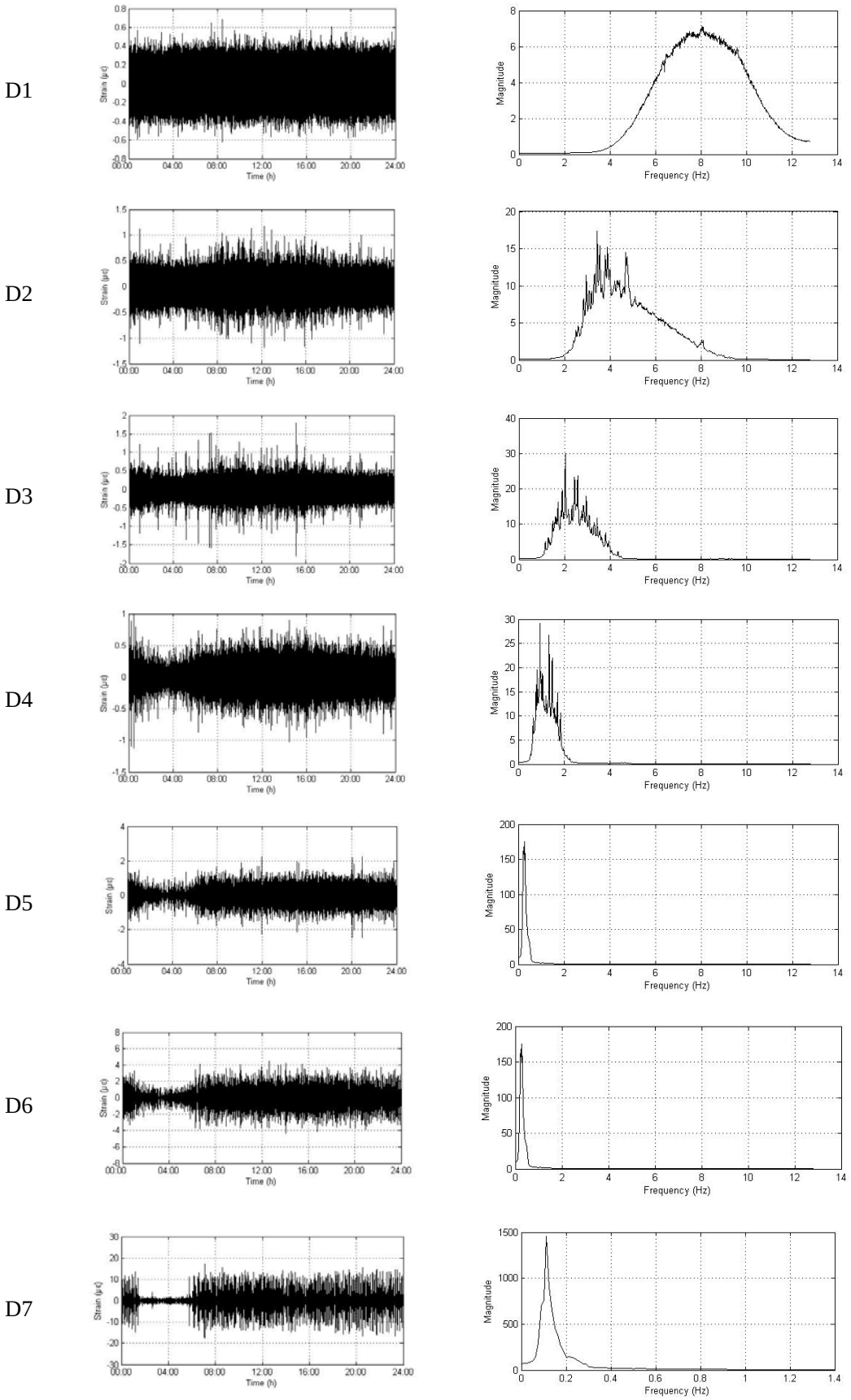

Figure 3.9 Multi-level wavelet decomposition (cont'd)

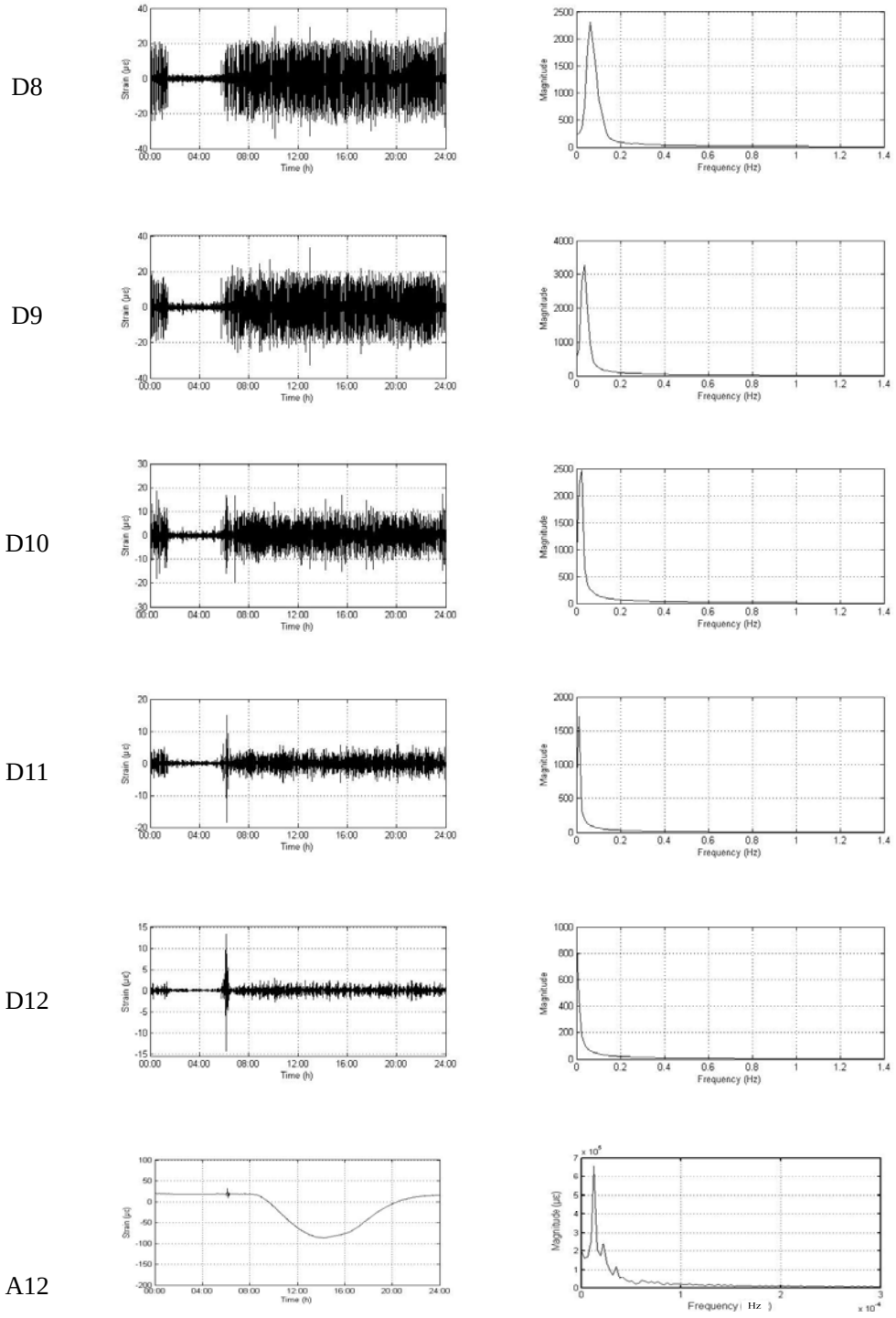

(a) Time domain (b) Frequency domain

Figure 3.9 Multi-level wavelet decomposition

In the present method, temperature-caused strain estimated from expansion joint displacement data is used as a reference signal. Its correlation with the lowest-frequency part separated by the DWT decomposition is further used for component matching. Separated low-frequency parts of A1~A12 for temperature effect modeling are shown in **Figure 3.10**. A quantitative evaluation of their quality is conducted by calculating the correlation coefficients. As shown in **Table 3.1**, the correlation coefficient from levels 9 to 12 almost does not change, implying that 12-level decomposition can ensure enough resolution for the temperature effect modeling. In the time domain, the extracted temperature-induced strain coincides favorably with its counterpart derived from the expansion joint displacement data as shown in **Figure 3.11(b)**. **Figure 3.11(a)** also illustrates atmospheric temperature variation and joint displacement.

3.4.3.2 Strain response due to live load effect

In the previous discussion, the in-service monitoring data of strain responses at TBM deck trusses are a combination of live load and temperature effects. The ingredient caused by the temperature effect, although considerably large, contributes little to the stress as the majority of temperature-caused strain is released by movement at the expansion joint. To obtain the strain response due to live load effect, the strain data are processed by eliminating the temperature-caused ingredient from the raw data. **Figure 3.12** illustrates a typical daily strain time history (of the top chord on the

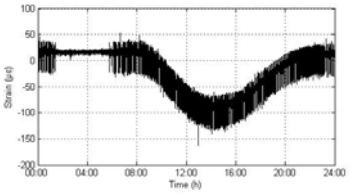

A1

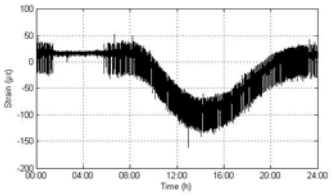

A2

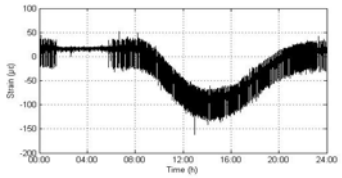

A3

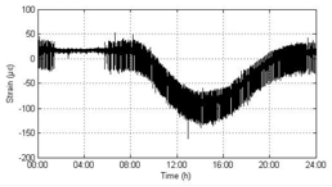

A4

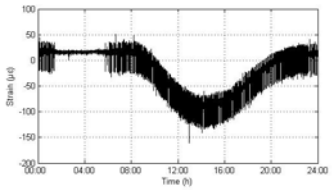

A5

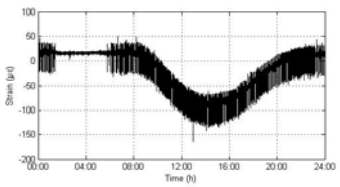

A6

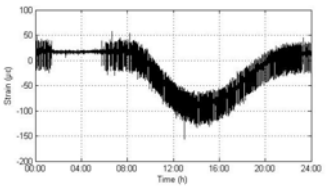

A7

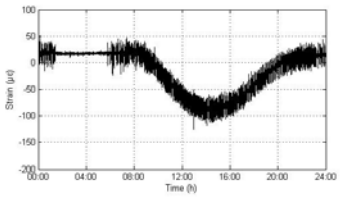

A8

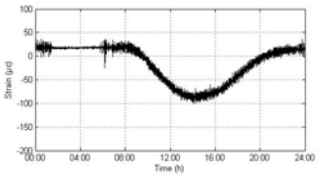

A9

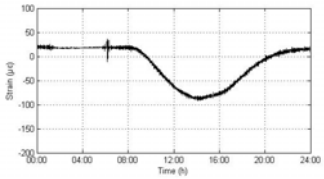

A10

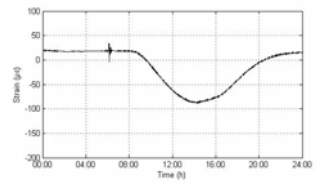

A11

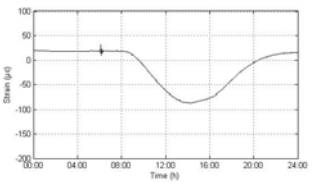

A12

Figure 3.10 12-level wavelet decomposition for approximations

Table 3.1 Correlation coefficients of approximations with displacement-derived strain due to temperature effect

Level	Time scale	Approximation	Correlation coefficient
0	2^0	A0	0.949531
1	2^1	A1	0.949542
2	2^2	A2	0.949569
3	2^3	A3	0.949799
4	2^4	A4	0.952326
5	2^5	A5	0.957979
6	2^6	A6	0.964319
7	2^7	A7	0.966266
8	2^8	A8	0.966879
9	2^9	A9	0.967101
10	2^{10}	A10	0.967145
11	2^{11}	A11	0.967150
12	2^{12}	A12	0.967153

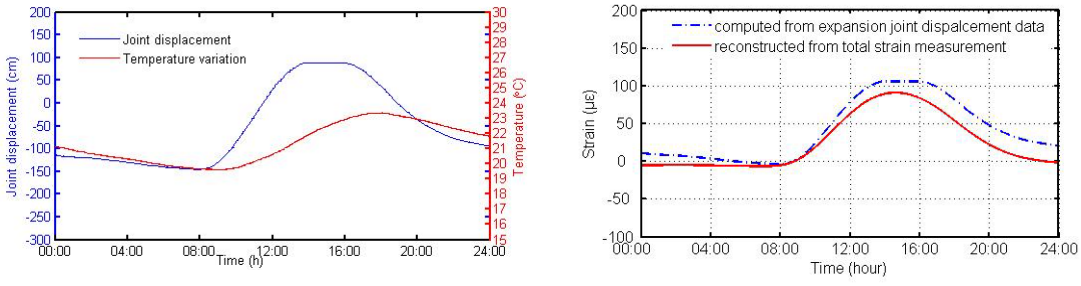

(a) Temperature variation and joint displacement (b) Temperature-induced strain

Figure 3.11 Extracted temperature-induced strain and displacement-derived strain

north truss side) under live load effect during operational traffic and normal wind conditions.

TMB is located at a region with typhoon wind climate. In 1999, totally five typhoons named “Leo”, “Maggie”, “Sam”, “York”, and “Dan” buffeted Hong Kong. **Table 3.2** lists the typhoon warning signals in 1999 issued by the Hong Kong Observatory. The strain response data during the typhoon attacks were recorded by the monitoring system. **Figure 3.13(a)** shows the recorded strain response of a bottom chord (on the north truss side of the monitored cross section CH24662.50) from August 20~23 under typhoon “Sam” attacking. The corresponding live load effect after eliminating the temperature-caused ingredient is illustrated in **Figure 3.13(b)**.

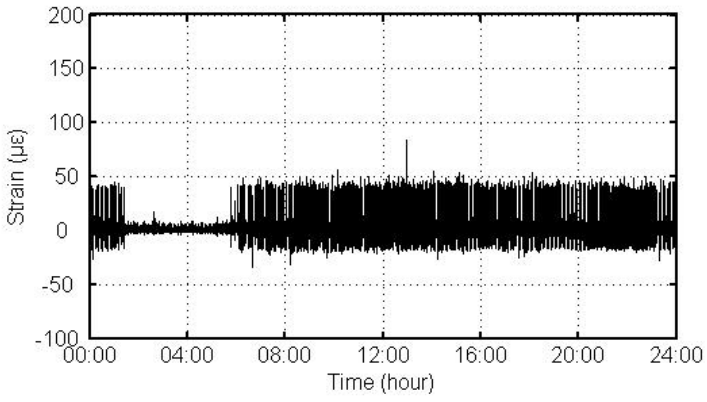

Figure 3.12 Typical daily strain time history under live load effect

Table 3.2 Typhoon warning signals in 1999 (Hong Kong Observatory)

Name	Signal	Issuing		Canceling	
		hh mm	dd/mon/yyyy	hh mm	dd/mon/yyyy
Leo	1	09:40	29/Apr/1999	16:15	30/Apr/1999
Leo	3	16:15	30/Apr/1999	13:30	02/May/1999
Leo	8 NE	13:30	02/May/1999	17:30	02/May/1999
Leo	3	17:30	02/May/1999	20:45	02/May/1999
Maggie	1	23:45	05/Jun/1999	14:15	06/Jun/1999
Maggie	3	14:15	06/Jun/1999	00:30	07/Jun/1999
Maggie	8 NW	00:30	07/Jun/1999	02:45	07/Jun/1999
Maggie	9	02:45	07/Jun/1999	05:45	07/Jun/1999
Maggie	8 NE	05:45	07/Jun/1999	10:30	07/Jun/1999
Maggie	3	10:30	07/Jun/1999	14:45	07/Jun/1999
Maggie	1	22:30	07/Jun/1999	00:45	08/Jun/1999
Maggie	3	00:45	08/Jun/1999	13:45	08/Jun/1999
Sam	1	16:15	20/Aug/1999	02:30	22/Aug/1999
Sam	3	02:30	22/Aug/1999	12:30	22/Aug/1999
Sam	8 NW	12:30	22/Aug/1999	20:10	22/Aug/1999
Sam	8 SW	20:10	22/Aug/1999	03:50	23/Aug/1999
Sam	3	03:50	23/Aug/1999	21:00	23/Aug/1999
York	1	10:45	13/Sep/1999	10:15	15/Sep/1999
York	3	10:15	15/Sep/1999	03:15	16/Sep/1999
York	8 NW	03:15	16/Sep/1999	05:20	16/Sep/1999
York	9	05:20	16/Sep/1999	06:45	16/Sep/1999
York	10	06:45	16/Sep/1999	17:45	16/Sep/1999
York	8 SW	17:45	16/Sep/1999	22:10	16/Sep/1999
York	3	22:10	16/Sep/1999	00:45	17/Sep/1999
Dan	1	20:45	05/Oct/1999	05:35	07/Oct/1999
Dan	3	05:35	07/Oct/1999	16:15	07/Oct/1999
Dan	1	16:15	07/Oct/1999	09:25	09/Oct/1999

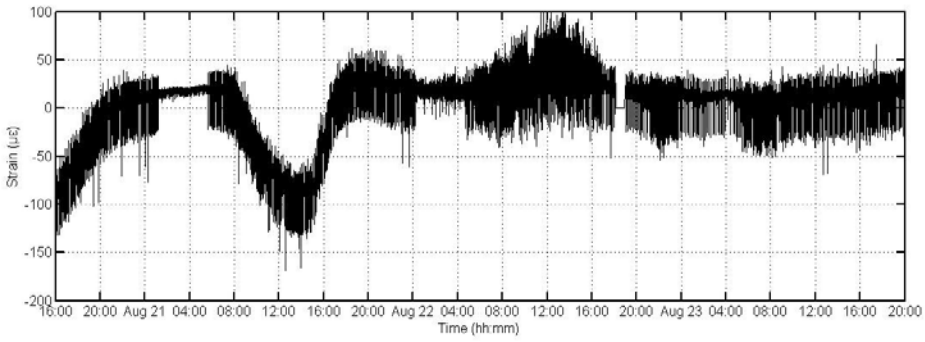

(a) Raw measurement data

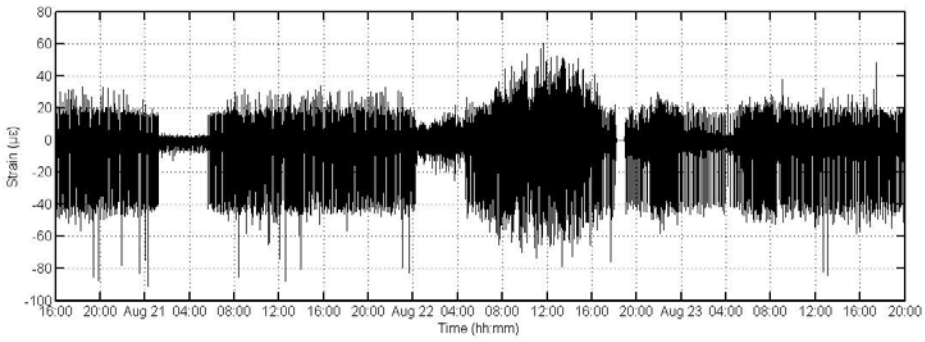

(b) Strain after eliminating temperature effect

Figure 3.13 Strain time history under live load effect during typhoon "Sam"

3.4.3.3 Strain response due to traffic effect

The proposed method also extracts the strain response due to traffic effect which is an outstanding live load effect in TMB. Under traffic loading, the truss stiffening bridge deck performs like a flexural beam, i.e., the top chords compress and the bottom chords extend concurrently, or vice versa. The dynamic strain data of the deck trusses on the same cross-section should reflect this behavior well if there is no temperature effect. As shown in **Figure 3.14**, the raw measurement data (total strain)

do not display the flexural behavior well owing to the presence of temperature effect. To restore the traffic-induced strain, DWT based 12-level decomposition of the strain data from top and bottom chords is conducted, and correlation coefficients of their level components are obtained in **Table 3.3**. Non-diagonal elements in **Table 3.3** are almost zero, which means that there is little correlation among them. However, coefficients on the diagonal show a certain correlation, varying between -1 and +1. There are only two of them positive that are 0.1555 and 0.9672 at D4 and A12 levels. With respect to the flexural behavior of the deck under traffic loading, correlation coefficients of the strain response at top and bottom chords should be non-positive. Therefore, in the extraction of traffic-induced strain, level components with positive correlation coefficients should be eliminated.

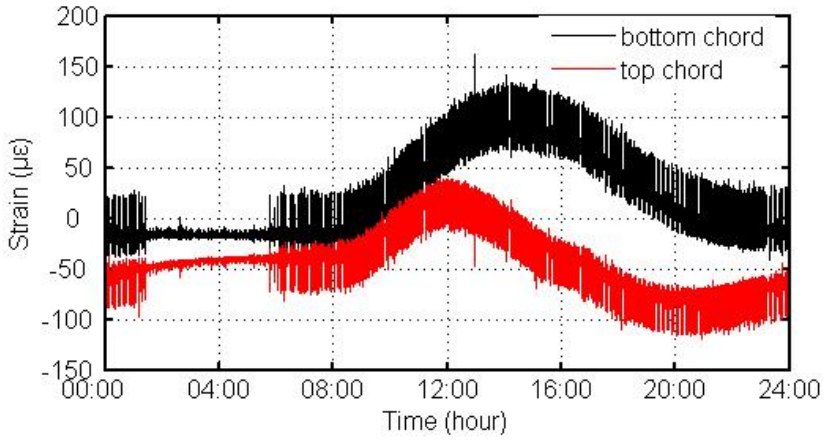

Figure 3.14 Total strain responses of top and bottom chords on deck cross section CH24662.50

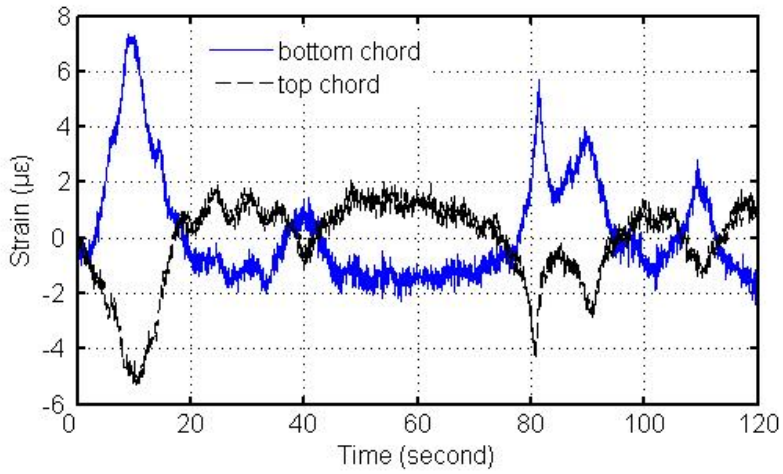

(a) Under highway traffic

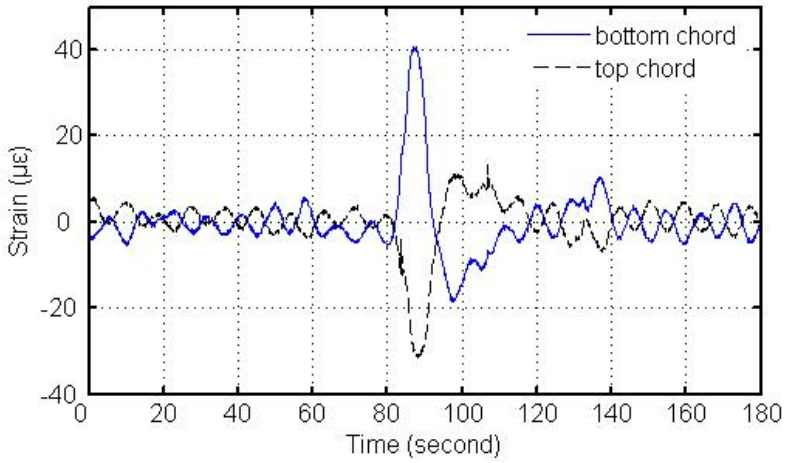

(b) Under railway traffic

Figure 3.15 Flexural behaviors of longitudinal trusses on deck cross section CH24662.50

The extracted traffic-induced strains restore the bending behavior favorably as shown in Figure 3.15. Figure 3.15(a) and 3.15(b) illustrate the traffic-induced strain time histories (experienced by a top chord and a bottom chord on deck section

CH24662.50) due to highway and railway traffic, respectively. It is observed that the strain at the top chord and the strain at the bottom chord evolve with time in almost same amplitudes but opposite directions. This observation verifies the quality of the extracted strain component.

Table 3.3 Correlation coefficients of 12-level decomposition components of strain data (top and bottom chords)

Top / Bottom	D1	D2	D3	D4	D5	D6	D7	D8	D9	D10	D11	D12	A12
D1	-0.0055	-1.5E-07	3.4E-08	-2.5E-08	9.6E-08	1.9E-07	6.7E-09	-1.2E-08	-1.3E-08	3.3E-09	4.0E-08	-3.0E-08	-4.5E-07
D2	-8.4E-07	-0.1149	8.7E-07	5.7E-07	1.1E-07	-1.8E-07	1.6E-07	1.6E-08	-2.5E-08	-2.5E-08	2.1E-08	-6.5E-08	1.4E-05
D3	-5.7E-07	4.5E-07	-0.1031	1.7E-06	5.5E-07	-2.8E-07	2.2E-07	-2.0E-08	-3.6E-08	-2.3E-08	2.2E-08	-5.7E-08	1.0E-05
D4	-4.2E-08	-2.0E-07	2.2E-06	0.1555	-3.9E-06	-6.5E-06	-4.2E-07	3.6E-07	4.4E-07	-5.4E-08	-1.3E-06	1.1E-06	-1.2E-05
D5	-2.1E-07	1.6E-07	1.6E-06	-2.3E-06	-0.1248	-3.0E-06	-1.2E-06	-6.7E-07	4.1E-07	3.6E-07	-1.1E-06	1.7E-06	-2.6E-04
D6	-6.4E-08	1.0E-07	-1.4E-07	1.0E-07	-1.2E-06	-0.6015	-8.7E-08	-3.2E-07	-1.4E-07	-5.0E-08	2.3E-07	-3.7E-07	5.6E-05
D7	-1.4E-07	1.2E-07	4.9E-07	-1.5E-06	-1.3E-06	-8.6E-07	-0.9216	-2.2E-06	-1.2E-06	8.2E-08	-6.2E-07	1.1E-06	-2.9E-04
D8	-1.2E-08	7.1E-09	-4.6E-09	-2.0E-07	-4.4E-07	3.9E-07	-3.0E-06	-0.9635	-5.9E-07	-6.4E-07	1.1E-06	-2.0E-06	3.3E-04
D9	2.5E-08	-2.8E-08	-7.7E-08	1.7E-07	1.9E-07	-4.2E-09	-1.4E-06	-6.6E-07	-0.9670	1.7E-07	6.8E-07	-1.3E-06	6.2E-04
D10	5.4E-08	-5.2E-08	-1.5E-07	5.0E-07	6.1E-07	-3.4E-07	6.0E-07	-1.3E-06	1.4E-07	-0.9458	-1.7E-06	6.9E-06	1.8E-03
D11	-1.0E-07	1.2E-07	2.2E-07	-7.1E-07	-1.3E-06	1.2E-06	-2.0E-06	2.7E-06	2.5E-06	-1.3E-06	-0.8598	-5.1E-05	-3.8E-03
D12	1.3E-07	-1.4E-07	-3.2E-07	1.1E-06	1.6E-06	1.3E-06	2.7E-06	-3.3E-06	-3.0E-06	3.2E-06	-4.2E-05	-0.8525	2.7E-02
A12	-1.3E-05	1.1E-05	4.3E-05	-1.6E-04	-1.6E-04	1.4E-04	-4.5E-04	2.3E-04	5.8E-04	9.1E-04	3.5E-06	8.6E-03	0.9672

3.5 Summary

On a continuous basis, long-term SHM systems acquire structural response data passively in a sense rather than measuring a specific structural behavior by actively controlling load environment. Therefore, SHM systems record information from various sources, leading to a complicated multi-component data structure. A logical way to efficiently interpolate the SHM data is to decompose original measurement data into mono-components so that distinct structural behaviors under different loadings and environmental conditions can be revealed for pertinent condition assessment or damage detection. With specialized perfect reconstruction (PR) filter banks, DWT based decomposition has advantage of parsimonious representation, energy decomposition, and effective de-correlation, which offers a wonderful decomposition platform for physical component extraction of the multi-component strain monitoring data.

To conduct the physical component extraction in the wavelet domain, correlation coefficients of the level components with a reference signal are calculated to establish a selection criterion. Based on the established selection criterion, physical source separation of the multi-component data is realized. With the application of the proposed method to TMB, the following observations have been made: (1) DWT can effectively separate a multi-component signal into a set of narrow band components

satisfying the mathematical requirement quite well; (2) the extracted temperature-induced strain component in along-bridge direction coincides well with the displacement time history measured at the expansion joint; (3) the extracted traffic-induced strains at the top chords and at the bottom chords of the same deck cross section evolve with time in almost same amplitudes but opposite directions, indicating flexural bending behavior of the deck cross section under traffic loading.

CHAPTER 4

RELIABILITY ASSESSMENT OF BRIDGE DECK USING STRAIN RESPONSE DUE TO LIVE LOAD EFFECT

4.1 Introduction

Condition assessment of in-service structures becomes an increasingly active field driven in part by the need for efficient management of these public assets (Ratay 2005). Of conventional way, structural condition assessment usually involves activities of visual observation, photographing, record keeping, documentation, report preparation and the like, which are still a standard practice today. However, the data from the traditional practice were proved to be limited and subjective (FHWA 2001). In addition to the existing inspection methods, a strategy of integrating structural condition assessment with SHM is expected to become a valuable practice in this field. The most challenging issue in implementing this strategy is how to develop an objective-oriented method to effectively process and interpret the monitoring data. Since reliability is an important performance measure of structural condition (Frangopol and Estes 1997), a reliability-oriented approach to processing SHM data for condition assessment naturally obtains its popularity. The

popularity is in a sense attributed to its capability in accommodating the uncertainties in response- and/or resistance-related parameters (Ellingwood 1996; Frangopol *et al*. 2001; Lark and Flaig 2005).

As well known, the elementary reliability indices can be approximated once probability distribution functions (PDFs) are determined from the observation data or investigations. Messervey and Frangopol (2008) proposed a scheme in which reliability algorithms can be fed by SHM data. As a further application, Catbas *et al*. (2008) conducted a reliability estimation study for main truss components of a long span truss bridge by using strain monitoring data. It was shown that temperature-induced strain had a significant effect on structural reliability and need to be considered for epistemic uncertainty. Usually temperature-caused strain in structure components is expected to be released through the movement of expansion joints. By using in-service monitoring strain data, Bhattacharya *et al*. (2008) proposed a reliability-based method to evaluate the safety of an existing bridge. A significant part of their effort involved statistical characterization of the live load effect based on a standard extreme distribution function. However, they inferred the probability distribution of peak strains on the assumption that they are caused by one traffic population whose characteristics do not evolve in the time. In reality, there will be more than one population of traffic passing through bridges during their service life time. It is reasonably presumed that the probability distribution of the response-related quantities may have a very complicated geometry due to multiple

load effects. They cannot be characterized by a standard distribution function adequately. Mixture distribution models shall be more adequate and provide more flexibility for this purpose.

In this chapter, mixture distribution model based reliability analysis will be developed and applied for condition assessment of the TMB deck. The in-service monitoring data of strain responses at the deck trusses of TMB stem mainly from four effects: highway traffic, railway traffic, wind, and temperature (the static strain due to initial dead loads is unable to obtain as the strain gauges were installed after the completion of construction). Although considerably large, the temperature-caused strain contributes little to the stress as the majority of it is released since the movement of the bridge deck is accommodated at expansion joints and bearings. Because of their contribution to stresses, the strain responses caused by live loadings such as traffic and wind are intentionally extracted for stress based reliability assessment. Mixed distributions existing in the live-load effect data are explored preliminarily by histogram analysis. Then hybrid mixture estimation including model selection and parameter estimation is addressed. A structure of mixed Weibull model is proposed for the PDF (probability density function) inference of peak stresses counted from the derived stress time histories. In the process of model selection, different mixture models (such as normal mixtures, log-normal mixtures and Weibull mixtures) are compared by calculating their AIC (Akaike Information Criterion) values. In the parameter estimation, the EM algorithm is applied and its efficiency in

the estimation will be demonstrated in terms of the component parameter convergence. Based on the inferred PDFs from the monitoring data, reliability-based condition assessment of the TMB deck trusses is realized for different load scenarios such as monsoon, typhoon, with and without railway traffic.

4.2 Finite Weibull Mixture Models

4.2.1 Structure of Weibull Mixtures

Inference of a probability distribution from observed data is necessary in any reliability analysis. Often this inference is complicated by the presence of multiple engendering effects that may create a heterogeneous dataset, making standard distribution models inadequate. Finite mixture distributions are expected to be of considerable interest and importance in modeling measurement data like this. Some of the most important references that discussed different types of mixture distributions are a monograph by Everitt and Hand (1981) and two survey books by Tittringto *et al*. (1985) and McLachlan and Basford (1988).

Theoretically mixture distribution models consist of a weighted sum of standard distributions and therefore are a flexible tool in modeling measurement data with a heterogeneous population. For a random variable X, finite mixture distribution models decompose a probability density function $f(x|\mathbf{\Theta})$ into the sum of m class

probability density functions $f_j(x|\boldsymbol{\theta}_j)$ (for $j = 1,\ldots,m$), and the expression can be written as

$$f(x|\boldsymbol{\Theta}) = \sum_{j=1}^{m} a_j f_j(x|\boldsymbol{\theta}_j) \tag{4.1}$$

where $\Theta = (a_1,\ldots, a_m; \boldsymbol{\theta}_1,\ldots, \boldsymbol{\theta}_m)$ is the overall parameter vector and each component density function is parameterized by the vector $\boldsymbol{\theta}_j$ (for $j = 1,\ldots, m$). The proportion a_j can be interpreted as the prior probability of observing a sample from class j. Furthermore, the prior probability a_j for each class distribution must be nonnegative and sum-to-one, or

$$a_j \geq 0 \qquad for \quad j = 1,\cdots,m \tag{4.2}$$

and

$$\sum_{j=1}^{m} a_j = 1 \tag{4.3}$$

Correspondingly $f_j(x|\boldsymbol{\theta}_j)$ is interpreted as the posterior probability distribution or conditional probability distribution. Through an appropriate choice of its components and weightings, a mixture model is expectedly able to model quite complex distributions.

In selection of elementary distribution for the mixtures, a significant and practical simplification can be achieved if all components are of the same type. Although

simplified loathly, this approach can recuperate its rationality if the parametric structure of the component density could model a variety of shapes. Particularly, in finite mixture modeling, Weibull mixtures have been studied frequently because Weibull family has a capability of extensive adaptation in modeling complicated shapes (Bučar and Nagode 2004). The two-parameter Weibull distributions are one of the most commonly used types and they can attain many shapes through various values of parameters β (shape) and θ (scale) in the expression

$$f_j(x|\mathbf{\theta_j}) = \frac{\beta_j}{\theta_j}\left(\frac{x}{\theta_j}\right)^{\beta_j - 1} \exp\left\{-\left(\frac{x}{\theta_j}\right)^{\beta_j}\right\}, \tag{4.4}$$

where the parameters β_j and θ_j stand for Weibull shape and scale of the component densities $f_j(x|\mathbf{\theta_j})$ (for $j = 1,\ldots, m$). The adaptability of Weibull family to different shapes is demonstrated in **Figure 4.1**.

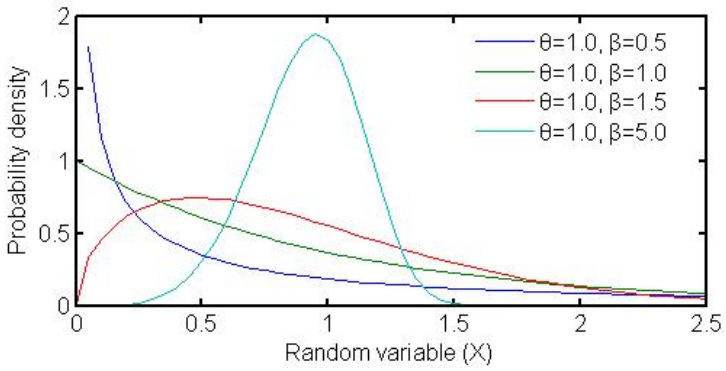

Figure 4.1 Adaptability of Weibull distribution families

4.2.2 Model Selection and Parameter Estimation

A mixture distribution model is generally defined as a weighted sum of component distributions. As shown in Equation (4.1), the overall parameter vector is $\boldsymbol{\Theta} = (a_1,\ldots, a_m; \boldsymbol{\theta}_1,\ldots, \boldsymbol{\theta}_m)$. Parameters a_j and parameter vectors $\boldsymbol{\theta}_j$ (for $j = 1,\ldots, m$) are unknown at first and must be estimated from observed data. How many components needed in the model are also not known and will be estimated from the data. In the process of model estimation, the task of finding the optimal number of components is called model selection while the task of estimating the parameters is called parameter estimation.

In a sense, the most fundamental parameter in definition of a finite mixture is the number of components. Its importance results partly from the technical consideration that without knowing the component number the process of mixture distribution estimation cannot go further. There is a vast literature devoted to this issue of choosing the optimal number of components, which can broadly be divided into two categories both based on the log likelihood function. The former selects the model by testing the significance of the component coefficients and the insignificant ones are deleted from the model. Whereas, the latter (information criterion based methods) chooses the model which minimizes a given risk function. The representative criteria are such as Akaike information criterion (AIC) by Akaike (1973), Bayesian information criterion (BIC) by Schwarz (1978), and their modifications. As widely

discussed, the AIC is given as follows:

$$AIC = -2L_n(\boldsymbol{\Theta}) + 2k \tag{4.5}$$

where $L_n(\boldsymbol{\Theta})$ is the log likelihood, and k is the number of free parameters in the mixture model. The model with a minimum AIC value is chosen to be the best model.

When the model is specified the parameter estimation is conducted straightforward. There is a remarkable variety of estimation methods that have been applied to finite mixture problems such as MOM, MLE and Bayesian approaches. With the availability of digital computers, MLE has been by far the most commonly used approach to the general mixture problems. The EM algorithm provides a general iterative procedure to obtain the MLE solution of a mixture model. In the EM algorithm some estimates for the parameters are fixed initially which can be arbitrary but their selection will affect the final result. The expectation of the log likelihood is then calculated and the resulting value of the expectation is maximized by selecting new parameter estimates according to the direction of the gradient. The expectation and maximization steps are iterated until a stopping criterion is met. Formulas of the EM algorithm for the mixed Weibull model will be derived in the following.

4.2.3 Reliability Estimation Using Finite Weibull Mixture Model

As discussed in the previous section, Weibull mixtures have advantages in modeling measurement data with multimodalities, and EM algorithm performs excellently in the parameter estimation. In recognizing this, EM algorithm based Weibull mixture modeling will be developed in this section. Theoretically the EM algorithm is a general method for finding the maximum-likelihood estimate of the parameters in underlying distributions for a given data set. And it can be implemented for mixture estimation by an iterative procedure in practice. Each iteration consists of two steps: estimation of the membership of the sample data by expectation (E-step); maximization of the updated likelihood given the estimate (M-step). In the E-step, the expected likelihood can be simplified as the so-called Q-function and formulated as follows (Bishop 1995)

$$\begin{aligned} Q(\boldsymbol{\Theta}, \boldsymbol{\Theta}^{(k)}) &= \sum_{i=1}^{n}\sum_{j=1}^{m} f(j \left| x_i, \boldsymbol{\Theta}^{(k)}\right.) \log\left\{ a_j f_j(x_i \left| \boldsymbol{\theta}_{\mathbf{j}}\right.)\right\} \\ &= \sum_{i=1}^{n}\sum_{j=1}^{m} f(j \left| x_i, \boldsymbol{\Theta}^{(k)}\right.) \log(a_j) \\ &\quad + \sum_{i=1}^{n}\sum_{j=1}^{m} f(j \left| x_i, \boldsymbol{\Theta}^{(k)}\right.) \log\left\{ f_j(x_i \left| \boldsymbol{\theta}_{\mathbf{j}}\right.)\right\} \end{aligned} \tag{4.6}$$

where the posterior probability $f(j|x_i,\boldsymbol{\Theta}^{(k)})$ can be expressed using the Bayes's rule as

$$f(j \left| x_i, \boldsymbol{\Theta}^{(k)}\right.) = \frac{a_j^{(k)} f_j(x_i \left| \boldsymbol{\theta}_j^{(k)}\right.)}{\sum_{j=1}^{m} a_j^{(k)} f_j(x_i \left| \boldsymbol{\theta}_j^{(k)}\right.)} \tag{4.7}$$

The evaluation of this expectation is called the E-step of the algorithm. The second step (M-step) of the EM algorithm is to maximize the expectation computed in the first step to obtain new parameter estimations $\boldsymbol{\Theta}^{(k+1)}$. As shown in Equation (4.6), the

term containing a_j and the term containing $\boldsymbol{\theta}_\mathbf{j}$ can be maximized independently since they are not related. To find the expression for a_j, the Lagrange multiplier λ with the constraint of Equation (4.3) is introduced and the derivatives of Equation (4.6) with respect to a_j are taken to be zero:

$$\frac{\partial}{\partial a_j}\left[\sum_{i=1}^{n}\sum_{j=1}^{m} f(j\left|x_i,\boldsymbol{\Theta}^{(k)}\right.)\log(a_j)+\lambda\left(\sum_{j=1}^{m}a_j-1\right)\right]=0 \tag{4.8}$$

or

$$\sum_{i=1}^{n}\frac{1}{a_j} f(j\left|x_i,\boldsymbol{\Theta}^{(k)}\right.)+\lambda=0 \tag{4.9}$$

Summing both sides over j and using $\sum_{j=1}^{m} f(j\left|x_i,\boldsymbol{\Theta}^{(k)}\right.)=1$, it is obtained that λ = -n resulting in:

$$a_j^{(k+1)}=\frac{1}{n}\sum_{i=1}^{n} f\left(j\left|x_i,\boldsymbol{\Theta}^{(k)}\right.\right) \tag{4.10}$$

For Weibull mixture models, analytical expressions for the parameters (β_j and θ_j) can be obtained as follows: Taking the natural logarithm of Equation (4.7) and substituting it into the right side of Equation (4.8), the term containing β_j and θ_j can be re-written as:

$$\begin{aligned}\sum_{i=1}^{n}\sum_{j=1}^{m} f(j\left|x_i,\boldsymbol{\Theta}^{(\mathbf{k})}\right.)\log\left\{f_j(x_i\left|\boldsymbol{\theta}_\mathbf{j}\right.)\right\}&=\sum_{i=1}^{n}\sum_{j=1}^{m} f(j\left|x_i,\boldsymbol{\Theta}^{(\mathbf{k})}\right.)\\ &\times\left\{\log(\beta_j)+(\beta_j-1)\log(x_i)-\beta_j\log(\theta_j)-\left(\frac{x_i}{\theta_j}\right)^{\beta_j}\right\}\end{aligned} \tag{4.11}$$

Taking the derivative of Equation (4.11) with respect to β_j and θ_j, after some algebra we get:

$$\frac{1}{\beta_j^{(k+1)}}+\frac{\sum_{i=1}^{n} f(j\left|x_i,\boldsymbol{\Theta}^{(k)}\right.)\log(x_i)}{\sum_{i=1}^{n} f(j\left|x_i,\boldsymbol{\Theta}^{(k)}\right.)}-\frac{\sum_{i=1}^{n} f(j\left|x_i,\boldsymbol{\Theta}^{(k)}\right.)x_i^{\beta_j^{(k+1)}}\log(x_i)}{\sum_{i=1}^{n} f(j\left|x_i,\boldsymbol{\Theta}^{(k)}\right.)x_i^{\beta_j^{(k+1)}}}=0 \tag{4.12}$$

$$\theta_j^{(k+1)}=\left(\frac{\sum_{i=1}^{n} f\left(j\left|x_i,\boldsymbol{\Theta}^{(k)}\right.\right)x_i^{\beta_j^{(k+1)}}}{\sum_{i=1}^{n} f\left(j\left|x_i,\boldsymbol{\Theta}^{(k)}\right.\right)}\right)^{1/\beta_j^{(k+1)}} \tag{4.13}$$

Then update Equations (4.10), (4.12) and (4.13) for the new estimation of the parameters $\boldsymbol{\Theta}^{(k+1)}$ in terms of the old parameters $\boldsymbol{\Theta}^{(k)}$. The algorithm proceeds by using the newly derived parameters as the guess for the next iteration until the algorithm converges. Once mixture models are inferred from observation data, it is straightforward to conduct reliability analysis for a defined failure criterion. For example, the cumulative distribution function (CDF) of a mixed Weibull model can be obtained as follows:

$$\begin{aligned} F(x\left|\Theta\right.) &= \sum_{j=1}^{m} a_j F_j(x\left|\theta_j\right.) \\ &= \sum_{j=1}^{m} a_j\left(1-\exp\left(-\left(x/\theta_j\right)^{\beta_j}\right)\right) \end{aligned} \tag{4.14}$$

4.3 Statistical Analysis of Stress Data from TMB

4.3.1 Stress Time Histories from Extracted Strain Data

For the TMB deck, traffic, wind and temperature effects mixed together to produce the strain measurement data. The temperature-caused strain, although considerably large, contributes little to the stress as the majority of them are released by the movement and rotation of the bridge deck at expansion joints and bearings. Contrarily, the strain components caused by live loadings (such as traffic and wind) develop into stresses. As described in Chapter 3, the DWT based component extraction method has successfully separated live-load effects from the raw measurement data. On the monitored deck cross sections, strain response data from truss chords and diagonal struts were obtained. **Figure 4.2** shows the measured strains from a top chord on the deck cross section CH24662.50. **Figure 4.2(a)** illustrates the sensor deployment on the chord section and recorded strain responses at the top and bottom locations are illustrated in **Figure 4.2(b)**. It is observed that the strains at the opposite sides of the chord section evolve with time almost in same amplitudes. Similar observations are obtained in other truss members. It reasonably infers that the truss members perform like axial bars and the stress distribution on the truss section is uniform. Hence stress based safety assessment is viable for the TMB deck trusses. The stress time histories undergoing in the truss members are obtained by multiplying the extracted strain data of live-load effect with elastic modulus E of the steel material, in recognizing the fact that the bridge is almost in elastic stage under in-service conditions. A typical daily stress time history experienced by a bottom chord is illustrated in **Figure 4.3**.

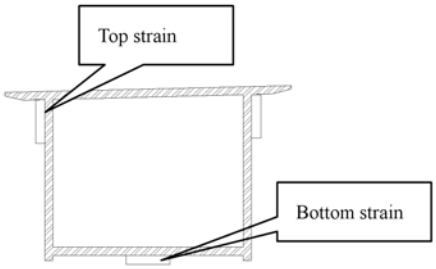

(a) Sensor distribution

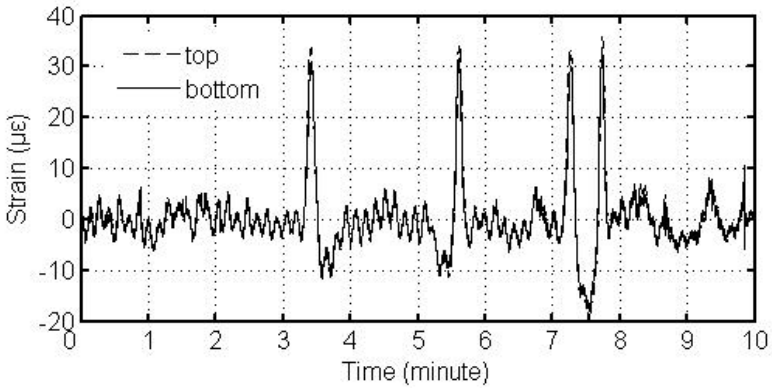

(b) Strain measurements

Figure 4.2 Strain responses at top and bottom locations of a top chord cross section

4.3.2 Statistical Counting of Peak Stresses

The stress time histories undergoing in the deck truss members are random processes in nature. Some methods such as the sampling method, threshold method, level crossing methods were proposed for the statistical counting of peak stresses (Frýba 1996). Illustrated in **Figure 4.4** are the peak values counted from the stress time histories (the threshold level is set as 0.1 MPa). In this study, one-year stress history data have been processed to explore

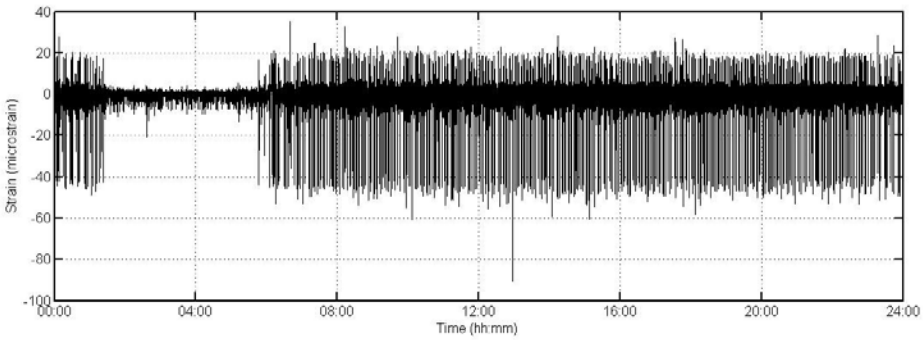

(a) Extracted strain data sequence

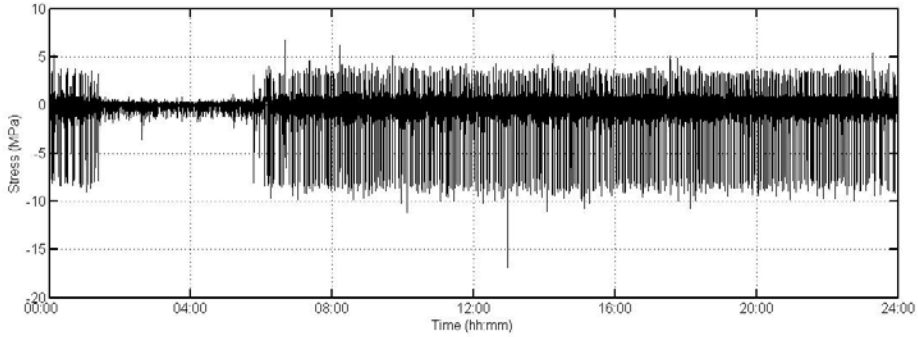

(b) Derived stress time history

Figure 4.3 Typical daily stress time history derived from extracted strain data (bottom chord on north truss side)

their probability distribution. All the obtained peak stresses are classified into three groups according to different load scenarios: HL + NW (highway traffic + normal wind); HL + RL + NW (highway traffic + railway traffic + normal wind); and HL + RL + TW (highway traffic + railway traffic + typhoon).

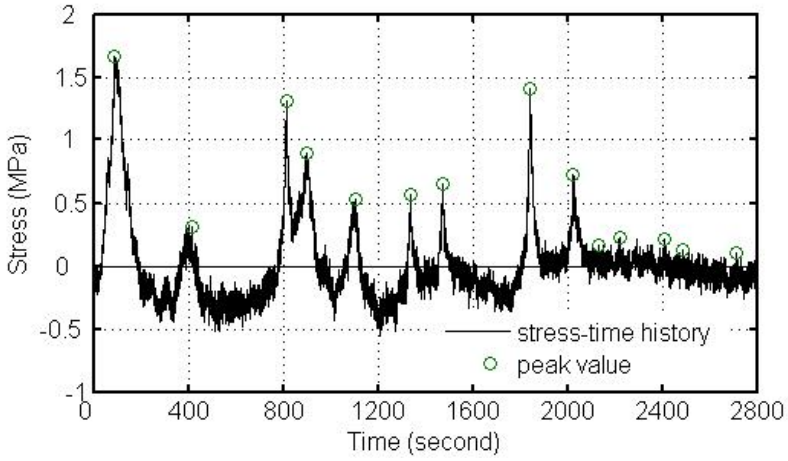

(a) Under highway traffic

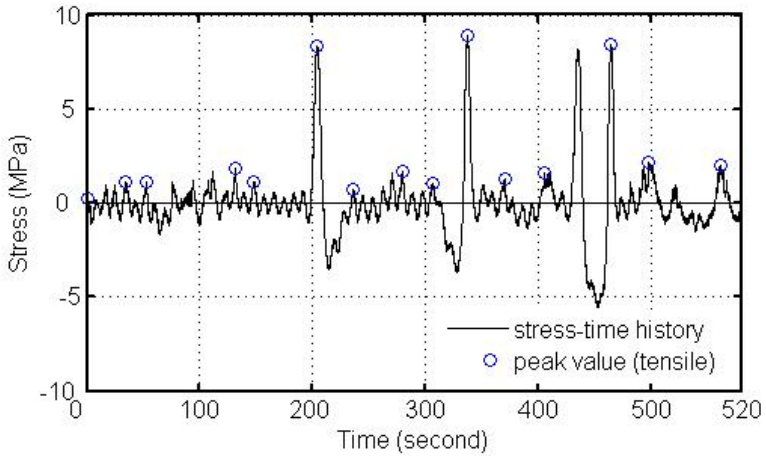

(b) Under railway traffic

Figure 4.4 Peak counting of stress time histories

As shown in **Figure 4.5**, the obtained peak stresses are randomly dispersed. In the case of HL + NW, most of the stress peaks are less than 2 MPa, whilst for the each of the other two cases of HL + RL + NW and HL + RL + TW, there are two clustering centers around 1 MPa and 10 MPa respectively. Different from the case of HL + RL + NW, it is observed that in the case of HL + RL + TW there are more in-between values as shown in **Figure 4.5(c)**, which may due to the typhoon effect.

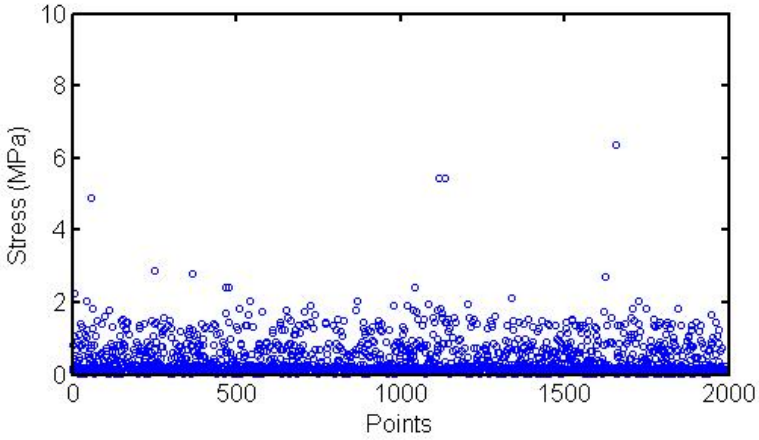

(a) HL + NW

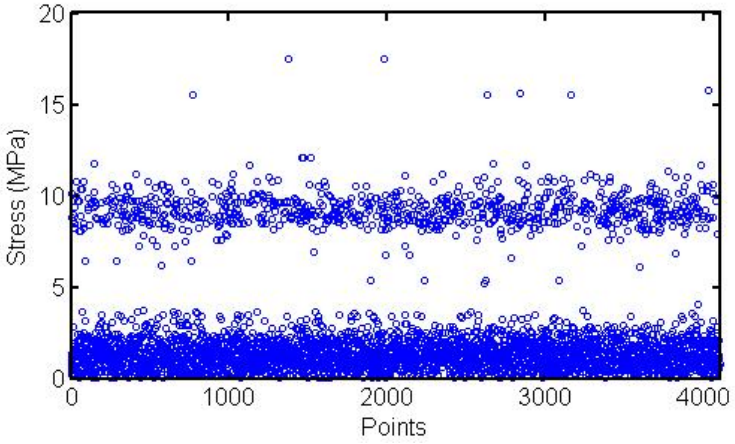

(b) HL + RL + NW

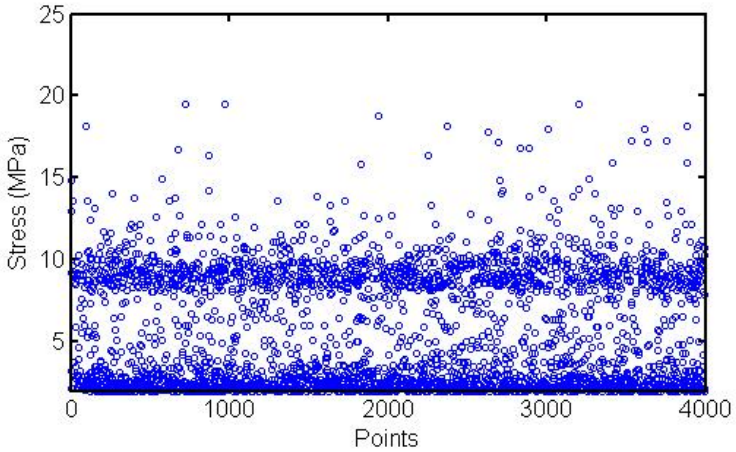

(c) HL + RL + TW

Figure 4.5 Counted peak stresses under three load conditions

4.3.3 Histograms of Peak Stresses

As a non-parametric approach histograms can offer preliminary information about the probability distribution. Histograms of peak stresses are shown in **Figure 4.6** for a bottom chord on the deck cross section CH24662.50. Mixture distributions are clearly displayed in **Figures 4.6(b)** and **4.6(c)**, which represent a combination of different load effects. Even for the simplest load condition of HL + NW as shown in **Figure 4.6(a)**, it is difficult to specify the probability distribution satisfactorily by using a standard distribution function. This is because there are some hetero populations in the highway traffic with distinct statistical characteristics. Histogram analysis results show that the PDF inference is complicated by the presence of multiple engendering effects that create a heterogeneous dataset, making standard distribution models inadequate. Previously formulated Weibull mixture models will be adopted in the peak-stress data modeling.

4.4 Weibull Mixture Based Reliability Assessment of TMB Deck

4.4.1 PDF Estimation of Peak Stress Distribution

As discussed before, a key issue to finite Weibull mixture modeling is to find the optimal number of components. Once the component number is specified, estimation of its parameters is straightforward by applying the EM algorithm. Figure 4.7 shows

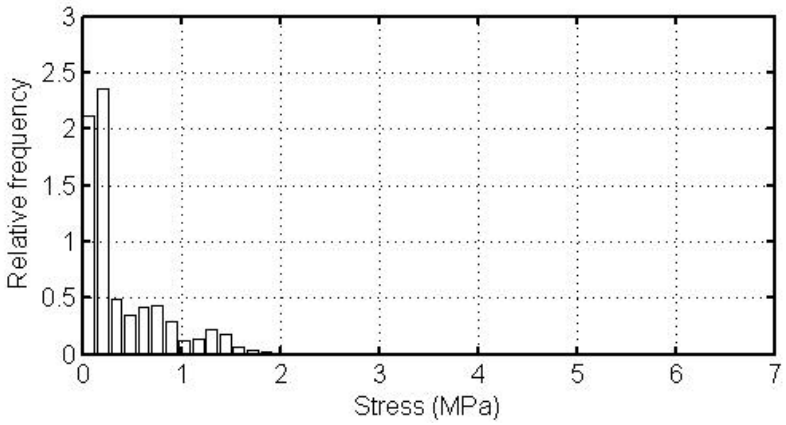

(a) HL + NW

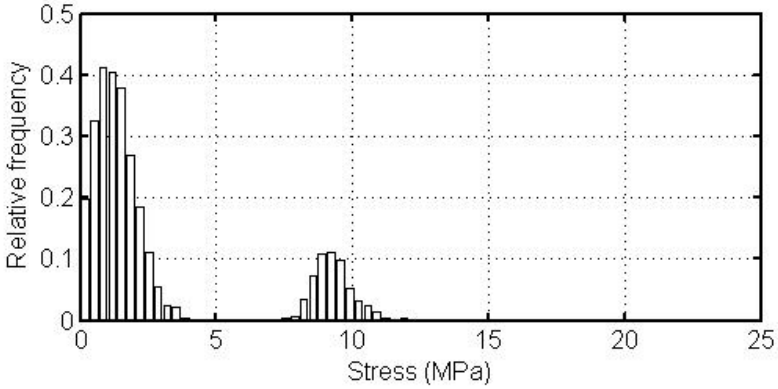

(b) HL + RL + NW

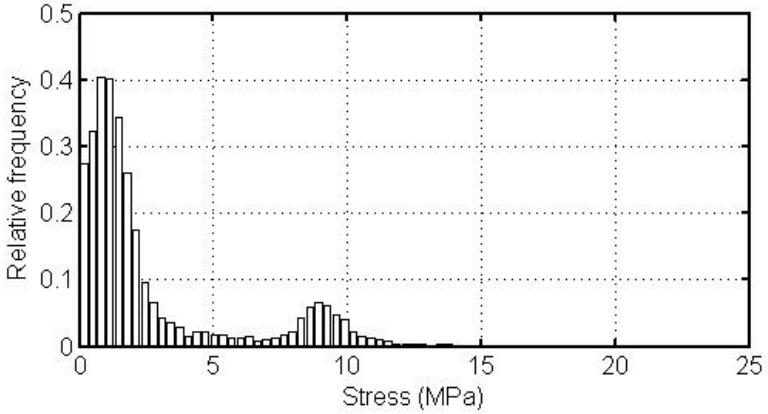

(c) HL + RL + TW

Figure 4.6 Histograms for three load conditions (truss element: bottom chord at north side)

the calculated AIC values for a varying component number in the case of HL + RL + TW. It shows that the Weibull mixture model has advantages of less component number and lower AIC values in comparison with normal and log-normal mixture models. The optimal component number (i.e. where the AIC value is the lowest) for this case is determined as four.

When the EM algorithm is applied for parameter estimation, the calculated log likelihood goes stability nearly at -21000 after 20 iterations as shown in **Figure 4.8**. Euclidean norm of the mixture parameter vector is calculated and utilized as the convergence criterion of the EM algorithm. Its relative errors during the iteration are shown in **Figure 4.9**. After around 20 iterations it goes nearly zero, which indicating the process of parameter searching can stop at this iteration step.

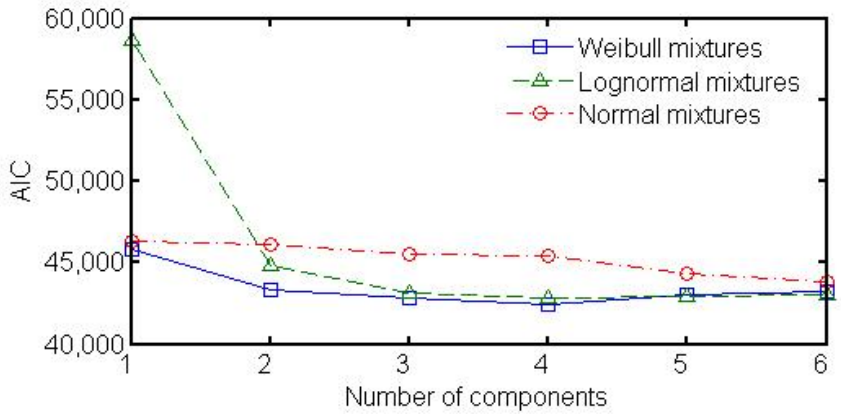

Figure 4.7 AIC values in the process of model selection

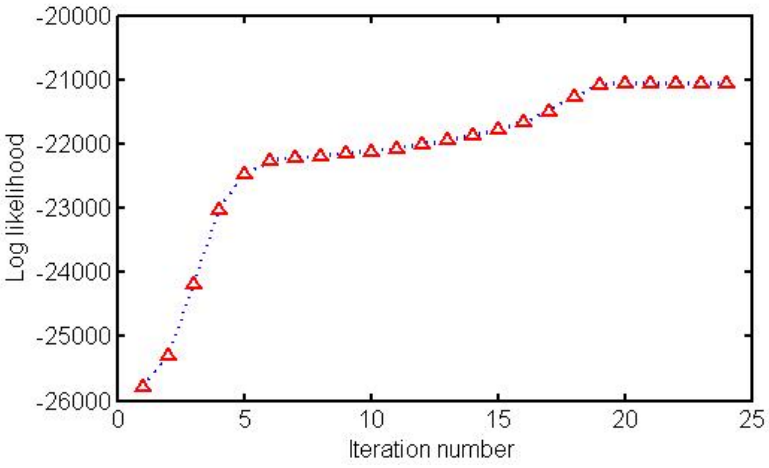

Figure 4.8 Log-likelihood in EM algorithm

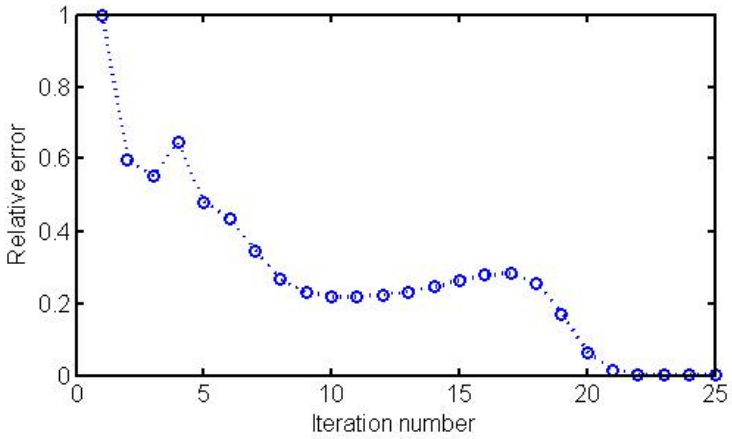

Figure 4.9 Convergence of Euclidean norm of parameter vector

Convergences for different component parameters are shown in **Figure 4.10**. Although there are some differences among them, all of the component parameters converge simultaneously after 20 iterations, demonstrating the efficiency of the EM algorithm for Weibull mixture estimation.

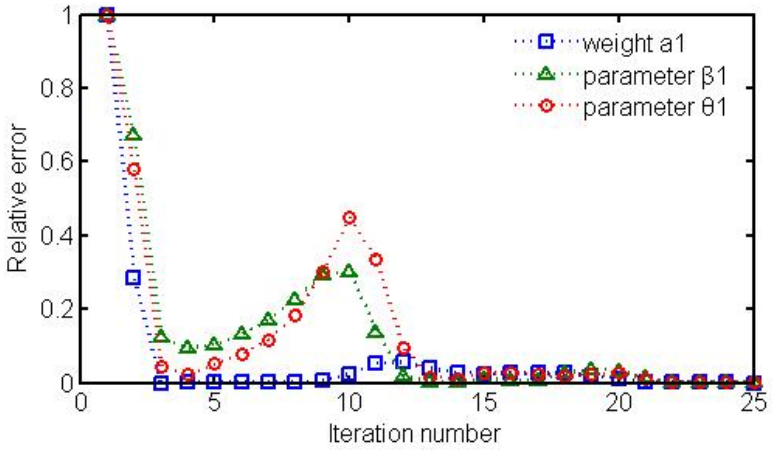

(a) Component 1

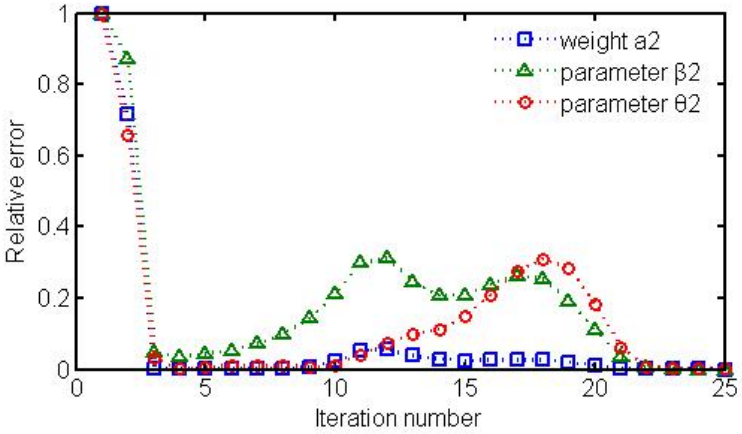

(b) Component 2

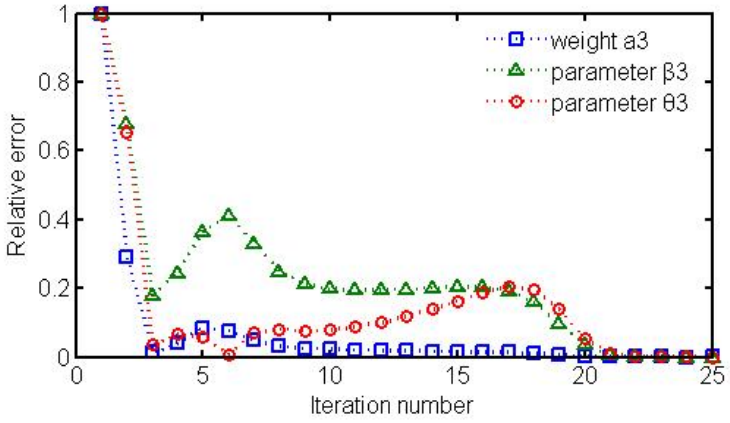

(c) Component 3

Figure 4.10 Convergence of component parameters in EM algorithm (cont'd)

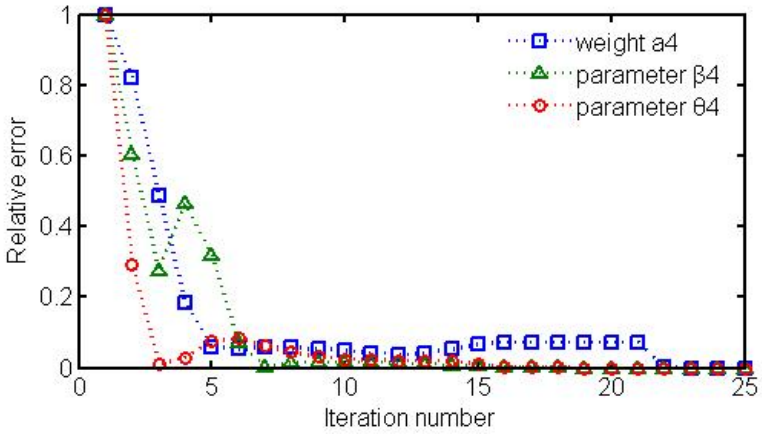

(d) Component 4

Figure 4.10 Convergence of component parameters in EM algorithm

The estimated mixture Weibull model and its component distributions are illustrated in **Figure 4.11**. Estimated parameters of the component distributions are listed in **Table 4.1**, where the parameters β_j and θ_j characterize each component of the Weibull mixture.

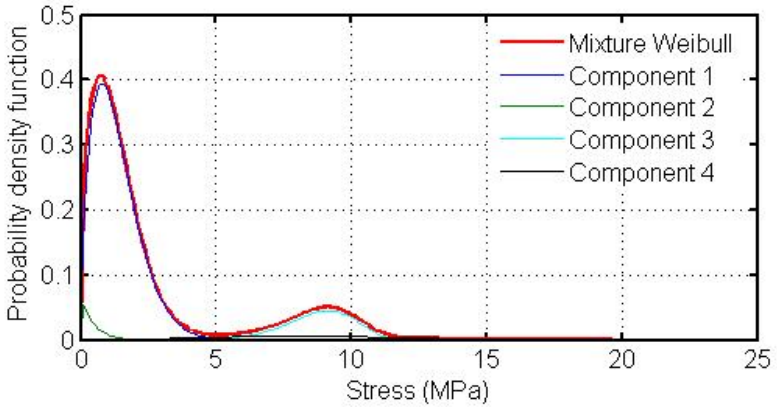

Figure 4.11 Estimated Weibull mixture and its component distributions

Table 4.1 Estimated parameters of Weibull mixture distribution (load condition: HL + RL + TW)

Component index	Component weight	Parametric family	Theta θ	Beta β
1	7.86E-01	Weibull	1.59E+00	1.58E+00
2	4.69E-02	Weibull	6.02E-01	1.60E+00
3	1.26E-01	Weibull	9.22E+00	7.84E+00
4	4.11E-02	Weibull	1.12E+01	4.18E+00

Figure 4.12 illustrates the formulated Weibull models for three load conditions (HL + NW, HL + RL + NW, and HL + RL + TW). It is observed that the proposed Weibull mixture model has an excellent performance in the PDF inference.

4.4.2 In-Service Condition Assessment Using Estimated PDFs

After obtaining the PDFs of peak stresses by finite Weibull mixture models, evaluation of the failure probability or reliability index can be conducted straightforward for a defined failure criterion. In this study, for the reliability method applied to sensor readings, limit state functions are defined in terms of sensor readings as proposed by Frangopol *et al*. (2008). It is required that the structural resistance R is greater than the monitored load effect S, i.e., $g(\mathbf{X}) = R - S > 0$ where

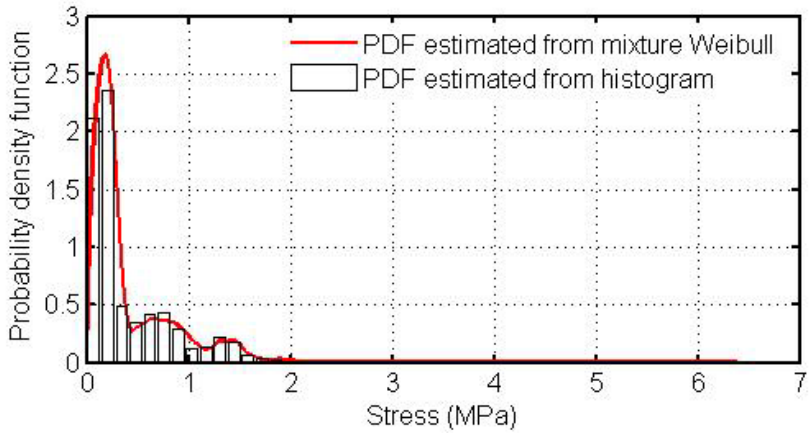

(a) HL + NW

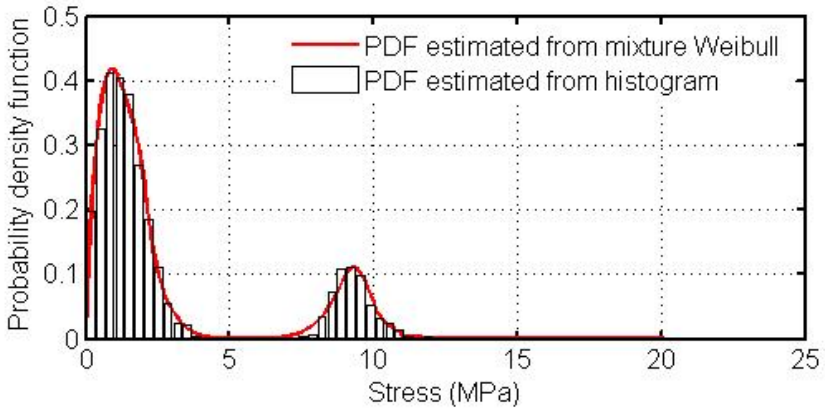

(b) HL + RL + NW

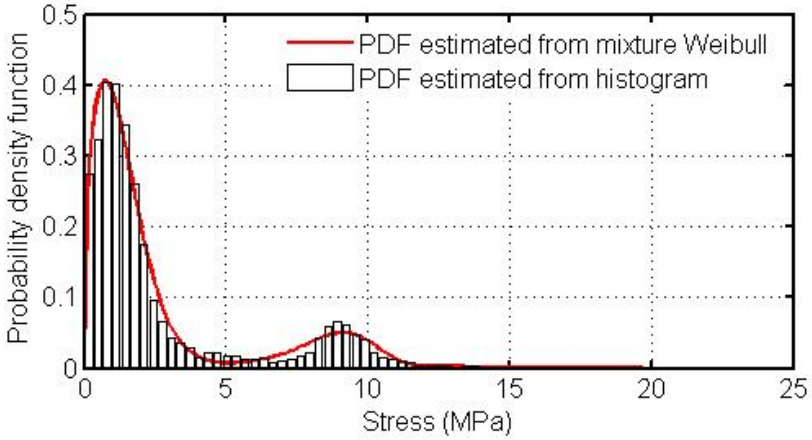

(c) HL + RL + TW

Figure 4.12 PDF inference in three load conditions (truss element: bottom chord on north truss side)

X is the parameter vector. In the design stage, the maximum allowable stress for live load effect was specified as 60 MPa (Wong 2007). Based on the estimated PDFs, the CDF for the case HL + RL + TW is calculated and illustrated in **Figure 4.13**.

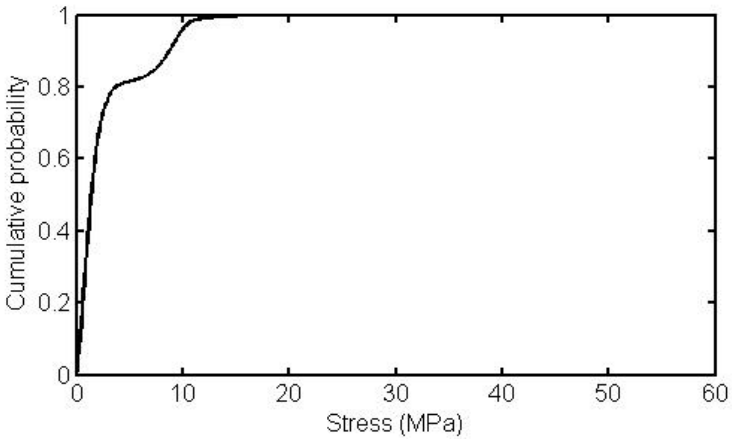

Figure 4.13 Cumulative probability based on estimated PDF (load condition: HL + RL + TW)

Table 4.2 Cumulative probability based on estimated PDF (load condition: HL + RL + TW)

Component index	Component weight	Parametric family	Cumulative probability
1	7.86E-01	Weibull	0.999999999995914
2	4.69E-02	Weibull	0.999999999949830
3	1.26E-01	Weibull	0.999999999991836
4	4.11E-02	Weibull	0.999999998502600
Mixture	probability 0.99999999993186 or reliability 6.42		

Table 4.2 provides the mixture CDF and its components, along with the

corresponding reliability index. Following the proposed approach, reliability indices of all the truss members on the deck cross section CH24662.50 are calculated and listed in **Table 4.3** for the three load conditions.

Table 4.3 Reliability indices of truss components for three load conditions (on deck cross section CH24662.50)

Location	Truss element	Load conditions		
		HL+NW	HL+RL+NW	HL+RL+TW
North Side	Top chord	9.76	8.11	6.84
	Diagonal strut	10.84	9.18	7.98
	Bottom chord	9.24	7.86	6.42
South Side	Top chord	9.72	8.20	6.80
	Diagonal strut	10.65	9.02	7.88
	Bottom chord	9.08	7.93	6.37

Note: HL – highway traffic; RL – railway traffic; NW – normal wind; TW - typhoon.

As shown in **Table 4.3**, the reliability indices of diagonal struts are higher than those of top and bottom chords for all the three load conditions, which means the safety condition of diagonal struts are better than the truss chords. Of all the three load conditions, the case of HL + RL + TW is the most dangerous. Bridge owner should pay more attention on guard when typhoon is coming. As shown in **Table 4.4**, the correspondence between the reliability index value and the required maintenance action has been established by Frangopol *et al*. (2001) and by Lark and Flaig (2005). By comparing **Table 4.3** and **Table 4.4**, it is concluded that all the deck truss

components are in a good safety condition, and hence no maintenance action is needed at present. With monitoring data continuously streaming in, the probability distribution model of the live load effect can be updated for future condition assessment.

Table 4.4 Relationship between safety state and maintenance action

Safety state	5	4	3	2	1
Reliability index	β>9.0	9.0>β>8.0	8.0>β>6.0	6.0>β>4.6	4.6>β
Attribute for safety	excellent	very good	good	fair	unacceptable
Maintenance action	No action	Preventive inspection	Detailed inspection	Possible strengthening	Rehabilitation

4.5 Summary

In TMB, the in-service monitoring data of strain responses at the deck trusses are a combination of live-load and environmental effects such as traffic, wind and temperature. Strain components due to different effects play different roles in contribution to stress quantities. As the majority of temperature-caused strain is released by the movement and rotation of the bridge deck at expansion joints and bearing, it contributes little to the stress although considerably large. Contrarily, the strain components caused by live loadings (such as traffic and wind) develop into

stresses and are extracted for the stress based reliability assessment.

When using strain response data due to live load effect for reliability assessment, a problem arises in the inference of probability distribution from observation data. Strain response due to live load effect collected under in-service environment is a result of multi-load effect such as traffic (highway, railway, or both of them) and wind (monsoon or typhoon). It cannot be characterized by a standard probability density function adequately. Weibull mixture models are developed and applied to characterize the statistical properties of peak-stress data. With the application of the proposed method to TMB, the following observations have been made: (1) the PDF of peak stresses has a very complicated shape due to multi-load effect; (2) Weibull mixtures have advantages of less component number and lower AIC values in comparison with normal and log-normal mixtures; (3) The EM algorithm is a suitable tool for the Weibull mixture parameter estimation with fast convergences and excellent stabilities; (4) Through reliability analysis, it is found that all the deck truss members are in a good safety condition and no maintenance action is needed; (5) Among the three load condition, the HL + RL + TW case is the most dangerous.

CHAPTER 5

KALMAN-FILTER BASED ESTIMATION OF NEUTRAL-AXIS POSITION OF BRIDGE DECK USING STRAIN RESPONSE DUE TO TRAFFIC EFFECT

5.1 Introduction

Long-span bridge deck can be considered to behave like a beam when its length exceeds its width by such an amount that its cross sections displace bodily and do not change shape when traffic loads cause it to bend. Cracks are prone to occur in beam-like bridge deck under traffic loading environment. Crack damage can heavily affect the global safety and performance of in-service bridges, and more severely, continual operation without noticing the damage accumulation will be disastrous. To understand the bridge deck failure, numerous studies of crack damage detections have been carried out on beam-like structures in laboratory (DeMerchant *et al*. 1999, 2000; Bao *et al*. 2001; Kim *et al*. 2002; Zeng *et al*. 2002; Bernini *et al*. 2006; Gao *et al*. 2006; Wu *et al*. 2006; Zhang *et al*. 2006). Kim (2003) conducted an experimental investigation of saw-cut damage on the 1/15 scale model of a suspension bridge deck. In his study, signal anomaly index was proposed as an indicator of damage. Park *et al*.

(2007) presented a strain flexibility based crack detection method for a steel beam. An experimental study was carried out by Lee *et al*. (2010) on a cracked cantilever beam to verify their proposed neural-network method for structural damage detection. Although the above methods achieved a certain success with simulation and laboratory data, they still have limitations in application to in-service monitoring data.

The use of structural response of a bridge deck under the operational traffic loading for structural condition assessment has received increasing attention in the past decade. Catbas and Aktan (2002) indicated that it is possible to extract the actual unit influence line (UIL) of a bridge deck for damage detection. Online evaluation of UIL under normal traffic environment is envisioned as long as the limitations of signal decomposition are clearly understood and mitigated. But UIL based damage detection methods may have the same problem of damage sensitivity as vibration based approaches have. Zhu and Law (2006) presented a wavelet-based method for crack detection under moving load condition. A dip of wavelet coefficients of one measurement signal was used as an indication of damage happening on a test beam. However, anomalies of the wavelet coefficient may be due to varying load patterns and they cannot be related to damage. In selection of damage indices for bridge deck assessment, their sensitivity to damage and robustness with respect to random traffic load patterns should be taken into consideration.

Theoretically the neutral-axis position of the bridge deck section remains unchanged under the varying traffic environment. On the other hand, it has potential in improving the sensitivity to damage because it reflects the local cross-section property. In this chapter, the neutral-axis position is proposed as an indicator of damage for deck condition assessment. A KF estimator is first formulated for locating the neutral-axis position from the local strain measurements. Numerical simulation is then conducted to verify its anti-disturbance in noise contaminations. Finally application of the proposed KF estimator to TMB for deck assessment is carried out.

5.2 Structural Behavior of Beam-Like Deck

Generally long-span bridge deck behaves like a bending beam because the cross section under eccentric loads has relatively little influence on the principal bending strain or stress responses. In the elastic theory of bending beams, it is assumed that the plane sections remain plane when deforming, and that the beam is composed of discrete linear fibers. From the assumption it can be shown that, at any point on a cross section, the longitudinal strain ε is proportional to the distance y of the point from the neutral axis, which passes through the centroid of the section. As illustrated in **Figure 5.1**, the flexural strain can be expressed as

$$\varepsilon = \lim_{\Delta s \to 0} \frac{\Delta s' - \Delta s}{\Delta s} = \lim_{\Delta s \to 0} \frac{(\rho - y)\Delta\theta - \rho\Delta\theta}{\rho\Delta\theta} = -\frac{y}{\rho} \tag{5.1}$$

where ρ is the curvature radius of the bending beam, y is the distance of the point from the neutral axis. According to force equilibrium, bending strain can also be formulated as

$$\varepsilon = -\frac{My}{EI} \tag{5.2}$$

where M is the total bending moment on section, I is the moment of inertia of cross section about the neutral axis. In a more complicated situation, if a beam is subjected to loads which are not normal to a principal axis of the section, then the loads can be resolved into components normal to the two respective principal axes. Bending analysis about each axis can be conducted separately.

5.3 Neutral-Axis Position Estimation

According to the Euler-Bernoulli assumption, the strain distribution is assumed to be linear over depth of the cross-section. Correspondingly strains at the bottom and top locations of the section are denoted by ε_b and ε_t respectively, as shown in **Figure 5.2**. Following the geometric relation, the ratio of ε_b and ε_t can be expressed as

$$\frac{\varepsilon_t}{\varepsilon_b} = \frac{y_t}{y_b} \tag{5.3}$$

or

$$\frac{\varepsilon_t}{\varepsilon_t + \varepsilon_b} = \frac{y_t}{y_t + y_b} \tag{5.4}$$

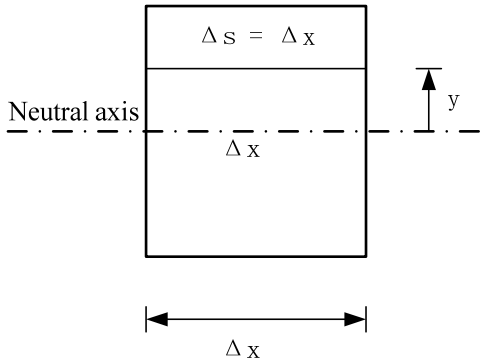

(a) Undeformed element

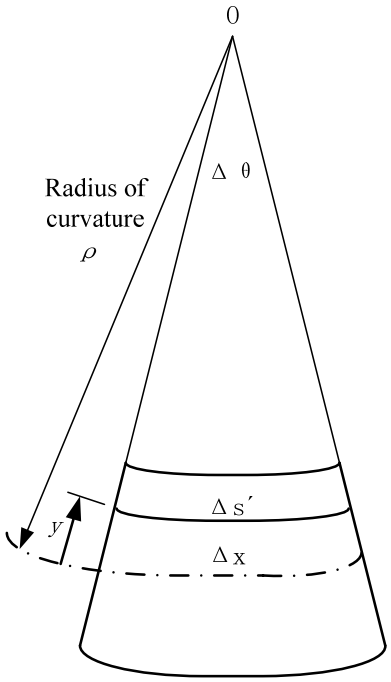

(b) Deformed element

Figure 5.1 Bending behavior of beam-like deck

where y_t is the distance between the top and the neutral axis, and y_b is the distance between the bottom and the neutral axis. The ratio in Equation (5.4) is equivalent to that of the neutral-axis location over the height of the cross section:

$$\frac{y_t}{y_t + y_b} = \frac{y_n}{h} = r \tag{5.5}$$

where y_n denotes the neutral axis location of the cross section, and h is the height of the cross section.

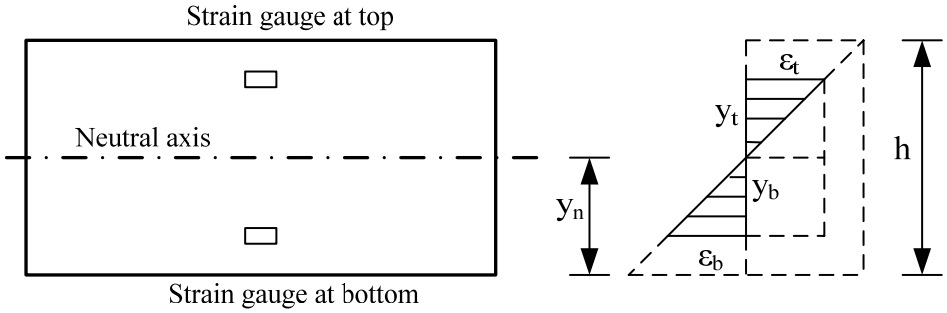

Figure 5.2 Flexural strain distribution over depth of cross section

5.3.1 Direct Estimation Method

Under traffic loadings, bending behavior dominates the response of beam-like bridge deck. The neutral-axis position can be estimated by

$$\hat{r} = \frac{\varepsilon_b}{\varepsilon_t + \varepsilon_b} \tag{5.6}$$

if the strain responses at top and bottom points are measured. But its efficiency can only be ensured on the condition that measurement data are without noise contamination.

5.3.2 KF Based Estimation Method

The Kalman filter is a mathematical method named after Kalman (1960). It is purposed to use measurements observed over time (containing noise and other inaccuracies) to produce values that tend to be closer to the true values of the measurements. Theoretically Kalman filter combines a system's dynamic model (i.e., physical laws of motion) and measurements (such as sensor readings) to form an estimate of the system's varying quantities (its state) that is better than the estimate obtained by measurement alone (Brown and Hwang 1992). It is similar in many respects to the least-square approach to estimation and, in a sense, Kalman filter can be regarded as a generalization of the least-square method (Sorenson 1970). A salient advantage of the Kalman filter is that the assumption of stationarity of the model coefficients can be relaxed.

In this study, the neutral-axis position in ratio ($r = y_n/h$) is taken as the state variable to be estimated. Because there is no deterministic disturbance or control scalar, the discrete model of the chosen state is given by

$$r_k = \Phi_k r_{k-1} + w_k \tag{5.7}$$

where Φ_k is the propagation scalar that propagates the state from one sampling instant to the next and w_k is the white process noise. And the measurement equation is given as

$$z_k = Hr_k + v_k \tag{5.8}$$

where H is the measurement scalar that relates the state to the observation z_k, and v_k is the measurement noise. In this special case the discrete Kalman filtering equation simplifies to

$$\hat{r}_k = \Phi_k \hat{r}_{k-1} + K_k(z_k - H\Phi_k \hat{r}_{k-1}) \tag{5.9}$$

From the preceding equations, the error in the estimate is

$$\tilde{r}_k = r_k - \hat{r}_k = r_k - \Phi_k \hat{r}_{k-1} - K_k(z_k - H\Phi_k \hat{r}_{k-1}) \tag{5.10}$$

Recognizing that the measurement can be expressed in terms of the state, Equation (5.10) can be formulated as

$$\tilde{r}_k = r_k - \hat{r}_k = r_k - \Phi_k \hat{r}_{k-1} - K_k(Hr_k + v_k - H\Phi_k \hat{r}_{k-1}) \tag{5.11}$$

Noting that the state at time k can be replaced by an alternate expression at time k-1, it is obtained that

$$\tilde{r}_k = r_k - \hat{r}_k = r_k - \Phi_k \hat{r}_{k-1} - K_k(H\Phi_k r_{k-1} + Hw_k + v_k - H\Phi_k \hat{r}_{k-1}) \tag{5.12}$$

Because

$$\tilde{r}_k = r_k - \hat{r}_k \tag{5.13}$$

it also says that

$$\tilde{r}_{k-1} = r_{k-1} - \hat{r}_{k-1} \tag{5.14}$$

Therefore, combining the similar terms in the error estimation equation yields

$$\tilde{r}_k = (1 - K_k H)\tilde{r}_{k-1}\Phi_k + (1 - K_k H)w_k - K_k v_k \tag{5.15}$$

If the covariance of estimate error is defined as

$$P_k = E(\tilde{r}_k^2) \tag{5.16}$$

and similarly

$$Q_k = E(w_k^2) \tag{5.17}$$

$$R_k = E(v_k^2) \tag{5.18}$$

then by squaring and taking expectations of both sides of Equation (5.15) yields

$$P_k = (1 - K_k H)^2 (P_{k-1}\Phi_k^2 + Q_k) + K_k^2 R_k \tag{5.19}$$

By defining

$$M_k = P_{k-1}\Phi_k^2 + Q_k \tag{5.20}$$

then the covariance equation becomes

$$P_k = (1 - K_k H)^2 M_k + K_k^2 R_k \tag{5.21}$$

The Kalman filter gain K_k that minimizes the variance of the error in the estimate can

be found by simply taking the derivative of the preceding expression with respect to the gain and setting the result equal to zero, that is,

$$\frac{\partial P_k}{\partial K_k} = 2(1 - K_k H)M_k(-H) + 2K_k R_k \tag{5.22}$$

Solving the preceding equation for the gain yields

$$K_k = \frac{M_k H}{H^2 M_k + R_k} = M_k H(H^2 M_k + R_k)^{-1} \tag{5.23}$$

Substitution of the optimal gain into the covariance equation yields

$$P_k = \frac{R_k M_k}{H^2 M_k + R_k} = \frac{R_k K_k}{H} \tag{5.24}$$

By inverting the optimal gain equation, it obtain

$$K_k R_k = M_k H - H^2 M_k K_k \tag{5.25}$$

Substituting the preceding equation back into the variance equation yields

$$P_k = \frac{R_k K_k}{H} = \frac{M_k H - H^2 M_k K_k}{H} = M_k - H M_k K_k \tag{5.26}$$

or, more simply,

$$P_k = (1 - K_k H)M_k \tag{5.27}$$

The above derivation shows that the gain of the Kalman filter is chosen to minimize

the variance of the error in the estimate. An iterative way of finding the optimal gain at each step is illustrated in Equations (5.20), (5.23) and (5.27).

5.3.3 Numerical Simulation

In the previous section, the KF estimator for neutral-axis position has been derived based on the relation between neutral-axis position and strain measurement. The validation of its stability to noise disturbance by numerical simulation comes in this section.

5.3.3.1 Case 1: Free of noise

Dynamic strain response data are first produced by FEM simulation of a flexural beam under moving load. Details of the FEM modeling and moving load simulation will be discussed in Chapter 6. The simulated strain responses at the top and bottom of a cross section are illustrated in **Figure 5.3**. It is shown that the strain responses at the top and bottom points evolve with time in almost same amplitudes but opposite directions, which favorably demonstrates the bending behavior.

In the Kalman filter method, improper filter initialization can degrade filter performance or cause the performance to collapse. Different initial values for the proposed KF estimator are first examined. **Figure 5.4** shows the

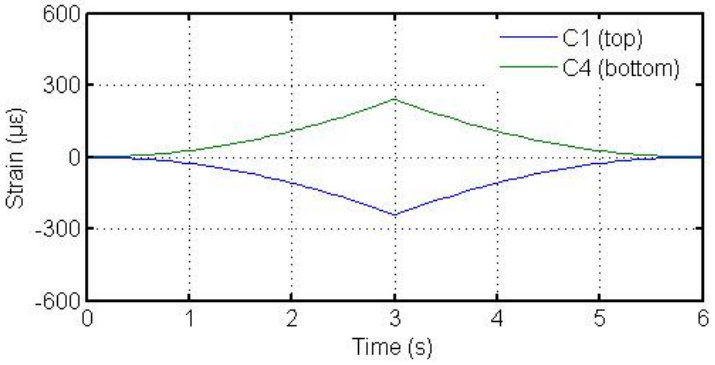

Figure 5.3 Simulated strain responses at top and bottom of section C

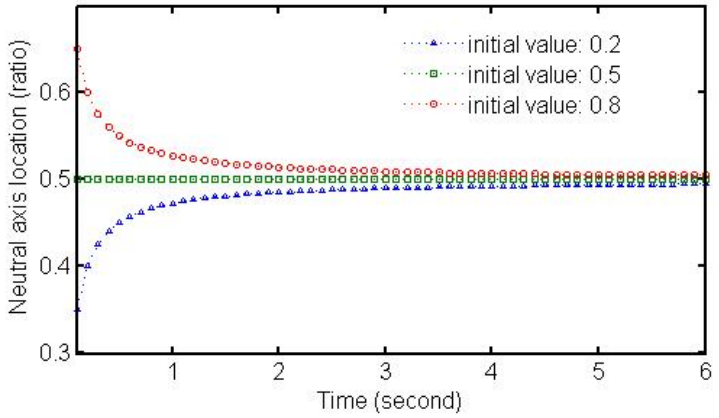

Figure 5.4 KF estimation of neutral-axis position (initial value: 0.2, 0.5, 0.8)

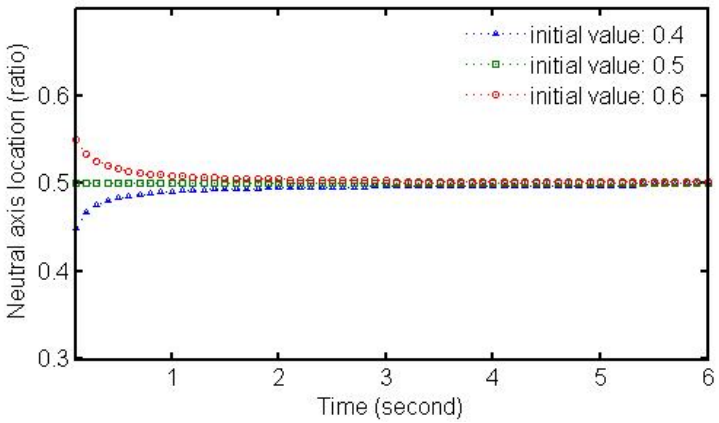

Figure 5.5 KF estimation of neutral-axis position (initial value: 0.4, 0.5, 0.6)

performance of the KF estimator when the initial values is chosen as 0.2, 0.5 and 0.8, respectively and **Figure 5.5** for another group when the initial value is 0.4, 0.5 and 0.6, respectively. The true value of the estimate is 0.5 where the structural model and the sensor location are symmetric. As shown in **Figure 5.4** and **Figure 5.5**, when the initial value is chosen to be the same as the true value, the proposed KF estimator has an excellent performance. In other cases, although the initial values have some deviation from the true value, the KF estimator can still converge to the true value. When the initial value is closer to the true value, the KF estimator has a faster convergence rate.

In the case of no additional noise contamination, the direct estimation method gives rise to satisfactory results which are further improved by the proposed KF estimator as shown in **Figure 5.6**. The direct estimation results vary between 0.4990~0.5010, and the KF estimation results (denoted by the line in **Figure 5.6**) fluctuate between 0.5000~0.5005, which are only 1/4 of those obtained by the direct estimation method. **Figure 5.7** illustrates the convergence of the Kalman gain in Case 1. It shows that the Kalman gain descends very fast at the first 10 steps of iteration. Then the descending speed decreases drastically, implying that the estimate is approaching to the true value.

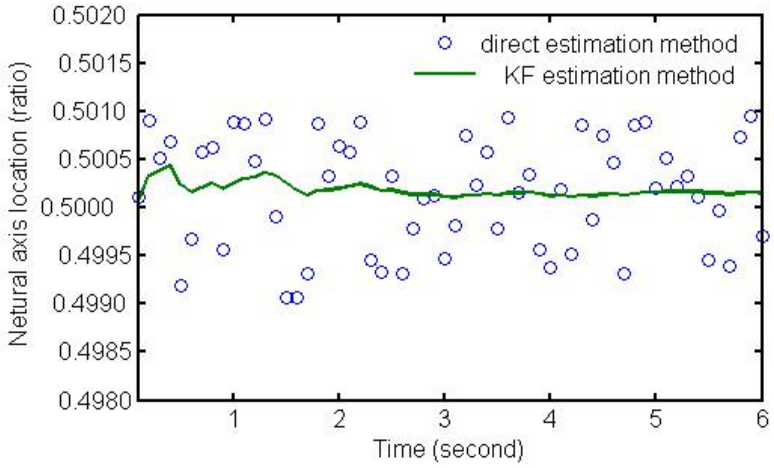

Figure 5.6 Comparison between direct and KF estimation methods in Case 1

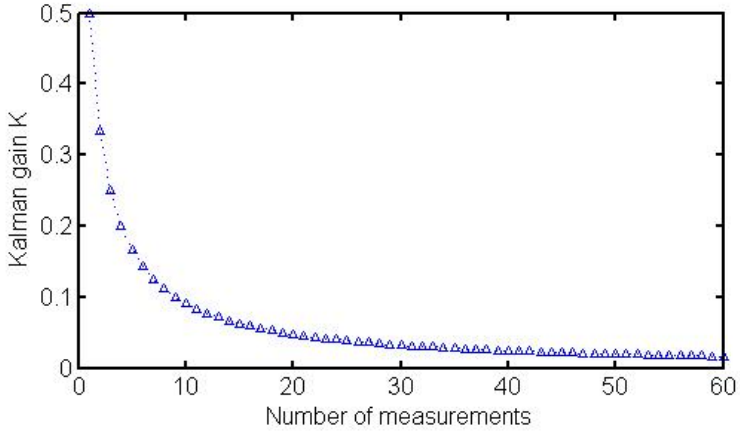

Figure 5.7 Kalman gain evolution in Case 1

5.3.3.2 Case 2: 5% noise contamination

As discussed before, the efficiency of the direct estimation method can only be ensured in the case of no noise corrupted in the data and the KF estimation method is superior in handling this kind of problems. In this and next sections, the anti-disturbance ability in noise contamination will be testified. In this case, 5%

Gaussian white noise process is added to the strain response data adopted in Case 1. **Figure 5.8** shows the generated data sequence with 5% Gaussian white noise. The Q-Q plot ("Q" stands for quantile) is used to verify the similarity of the generated sample data versus the standard normal distribution.

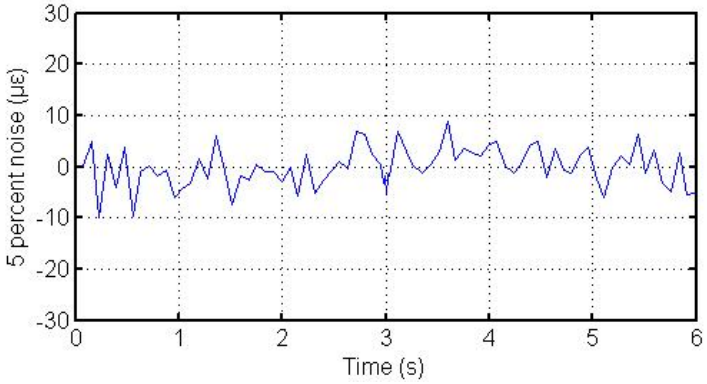

Figure 5.8 Generated Gaussian white noise sequence (5% noise)

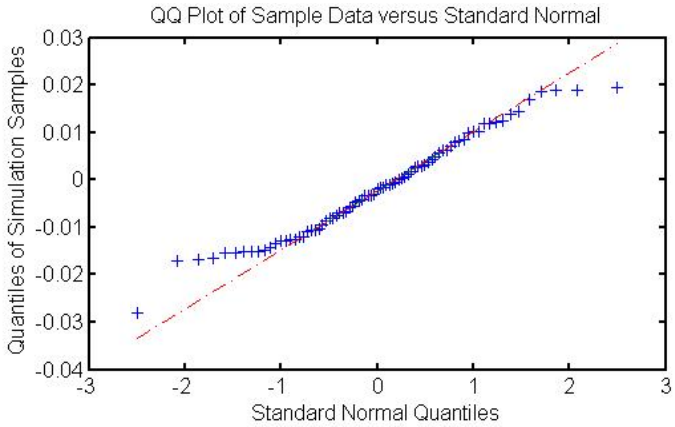

Figure 5.9 Q-Q plot of sample data versus standard normal distribution (5% noise)

As shown in **Figure 5.9**, the sample data are linearly related to the standard normal distribution, meaning that the sample data sets favorably conform to the pre-set standard Gaussian white noise generator. Data sequences of strain responses with 5% noise are illustrated in **Figure 5.10**. Compared with **Figure 5.3** of Case 1, the strain responses with 5% noise are not smooth.

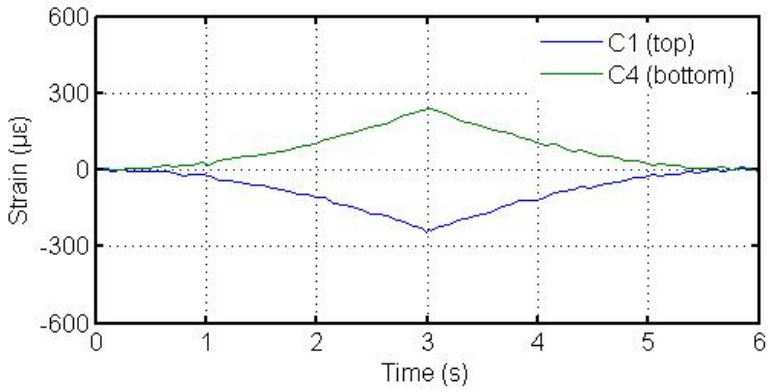

Figure 5.10 Simulated strain responses at top and bottom of section C (5% noise)

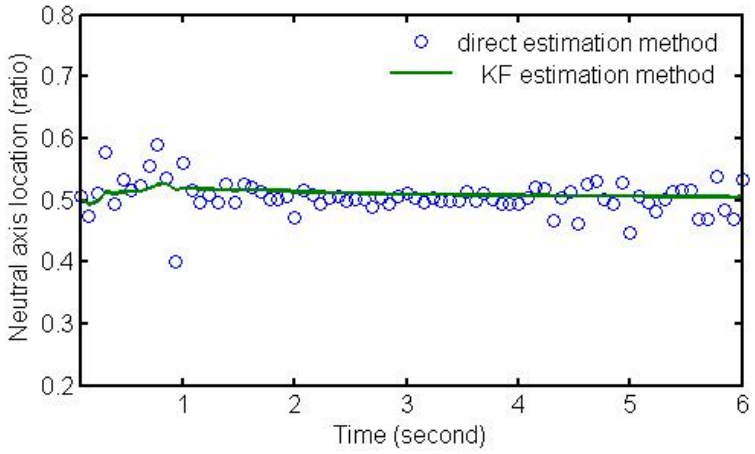

Figure 5.11 Comparison between direct and KF estimation methods (5% noise)

Although the 5% noise disturbances are not very remarkable in strain response data, the estimation results of neutral-axis position by the direct method fluctuate noticeably and the variation ranges between 0.4 and 0.6 as shown in **Figure 5.11**. Particularly the direct method has a worse performance at the beginning and ending of the data sequence as opposed to the middle part. Due to the low signal-noise ratio, the direct estimation results are unacceptable. In contrast, the KF method achieves a better estimation and particularly has an excellent performance when the signal-noise ratio is low. As shown in **Figure 5.12**, the Kalman gain converges after 10 steps of iteration. Residual errors of the KF estimator are illustrated in **Figure 5.13** which shows that the residual errors are randomly distributed around zero. The Q-Q plot, as illustrated in **Figure 5.14**, displays a strong linearity of the residual errors against the standard normal distribution. The residual errors follow a normal distribution, demonstrating again the validity of the proposed KF approach for neutral-axis position estimation.

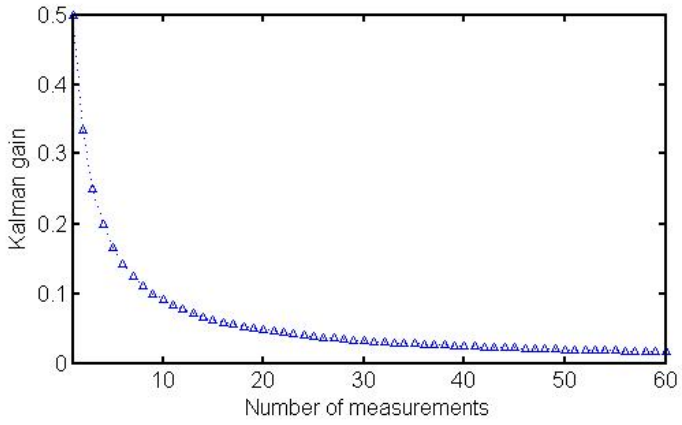

Figure 5.12 Kalman gain evolution in Case 2 (5% noise)

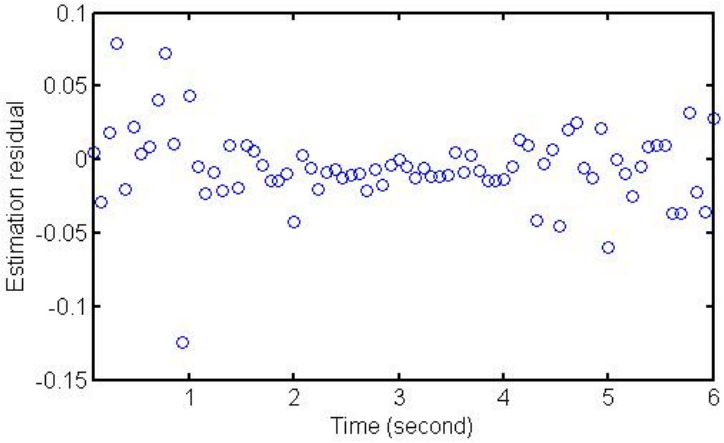

Figure 5.13 Residual errors (5% noise)

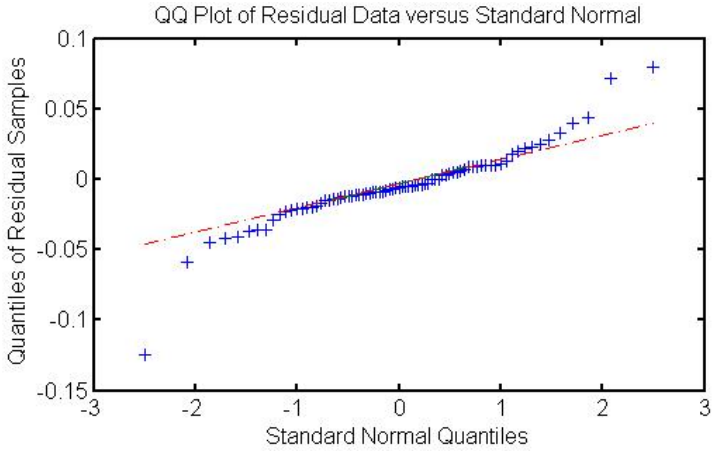

Figure 5.14 Q-Q plot of residual errors versus standard normal distribution (5% noise)

5.3.3.3 Case 3: 10% noise contamination

To simulate strain response data with 10% noise contamination, the random number generator used in Case 2 is utilized to produce noise samples. **Figure 5.15** shows the

generated noise samples which randomly vary between -20 and +20 micro-strain. The strong linearity of the simulation samples against the standard normal distribution, as shown in **Figure 5.16**, demonstrates the validity of the generated noise data. **Figure 5.17** illustrates the strain response data with 10% noise corrupted.

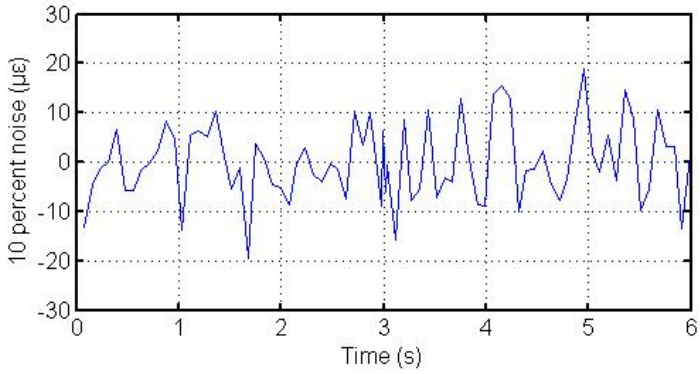

Figure 5.15 Generated Gaussian white noise sequence (10% noise)

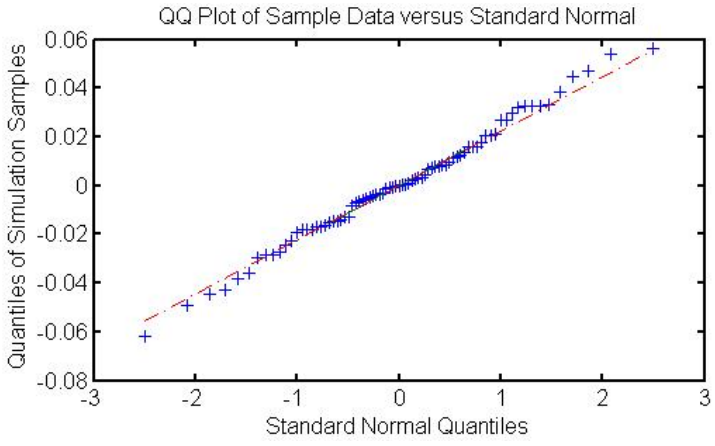

Figure 5.16 Q-Q plot of sample data versus standard normal distribution (10% noise)

As shown in **Figure 5.18**, the variation of the estimation results of neutral-axis position by the direct method ranges from 0.2 to 0.8 in Case 3. It is also observed in **Figure 5.18** that the direct method performs worse when the signal-noise ratio is low (at the beginning or ending of the data sequence). As expected, the KF estimator significantly improves the estimation accuracy.

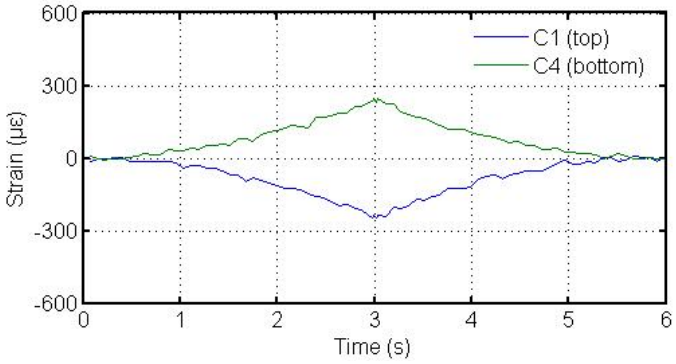

Figure 5.17 Simulated strain responses at top and bottom of section C (10% noise)

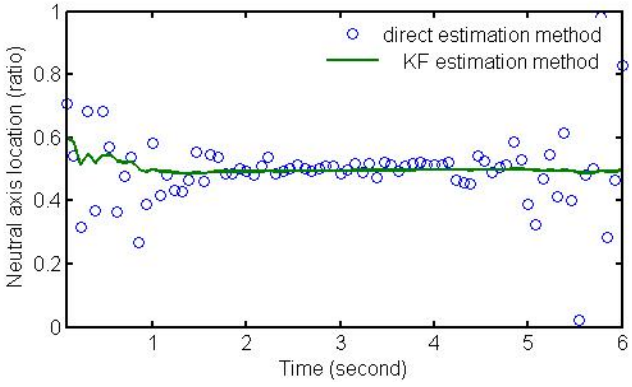

Figure 5.18 Comparison between direct and KF estimation methods (10% noise)

Residual errors in the process of KF estimation are illustrated in **Figure 5.19**, which randomly disperse around zero. The Q-Q plot shows a strong linearity of the residual errors against the standard normal distribution, as illustrated in **Figure 5.20**. **Figure 5.21** illustrates the convergence of the Kalman gain in Case 3. It shows that the Kalman gain descends quickly at the first 10 steps of iteration. Subsequently the descending speed decreases drastically when the estimate approaches to the true value.

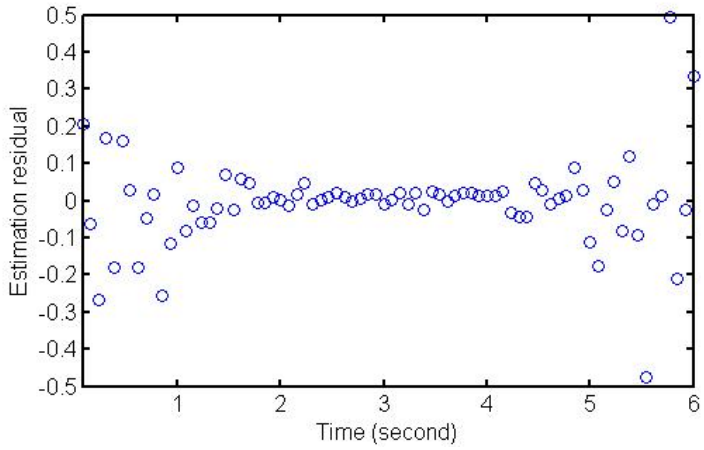

Figure 5.19 Residual errors (10% noise)

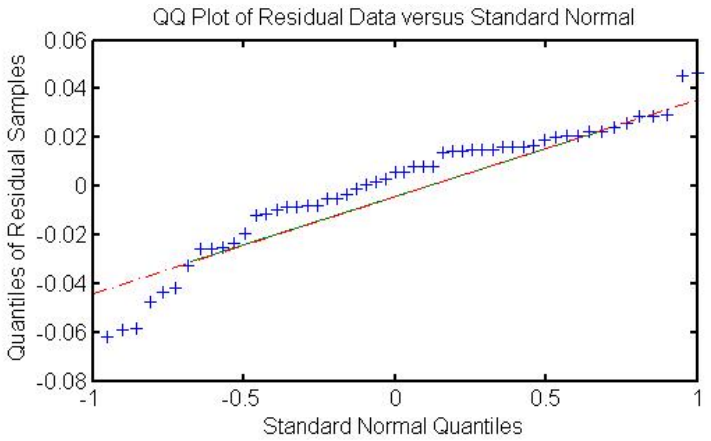

Figure 5.20 Q-Q plot of residual errors versus standard normal distribution (10% noise)

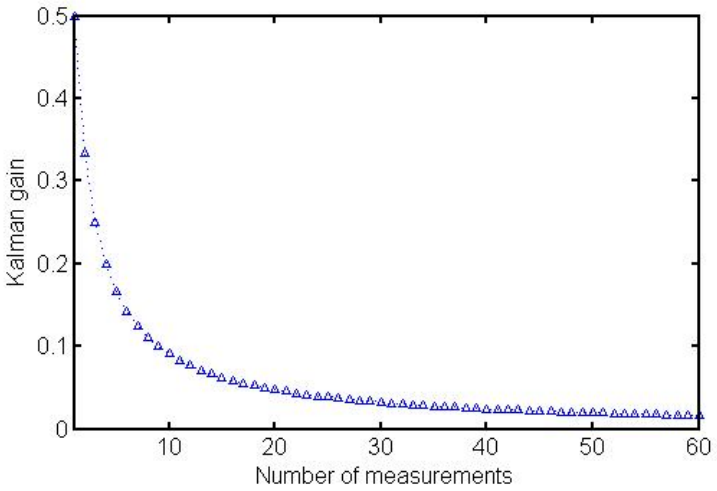

Figure 5.21 Kalman gain evolution in Case 3 (10% noise)

5.3.3.4 Analysis of results

In this section, the performance of the direct and KF estimation methods is evaluated. As illustrated in **Figure 5.22**, when there is no noise contamination, the KF estimator has a perfect performance. With 5% noise being corrupted, the performance of the KF estimator degrades at the beginning but after a while the estimation converges to the true value. As to the more noisy case with 10% noise contamination, the fluctuation becomes more serious at the beginning of the estimation process. But with the iteration going further, convergence is achieved as expected. A comparison of the results from the three cases is provided in **Table 5.1**. In Case 1, the direct and KF estimation methods both reach almost the true value of 0.5. Their relative errors are 0.0313% and 0.0308%, respectively. The standard deviation of the direct

estimation results is as small as 5.78 E-04, demonstrating its efficiency when there is no noise. However, with the increase of noise level, the estimation results by the direct method deteriorates seriously such that the relative error goes to 0.1038% and -0.3056% in Case 2 and Case 3, respectively. The standard deviation increases obviously, indicating that the direct estimation results are not reliable.

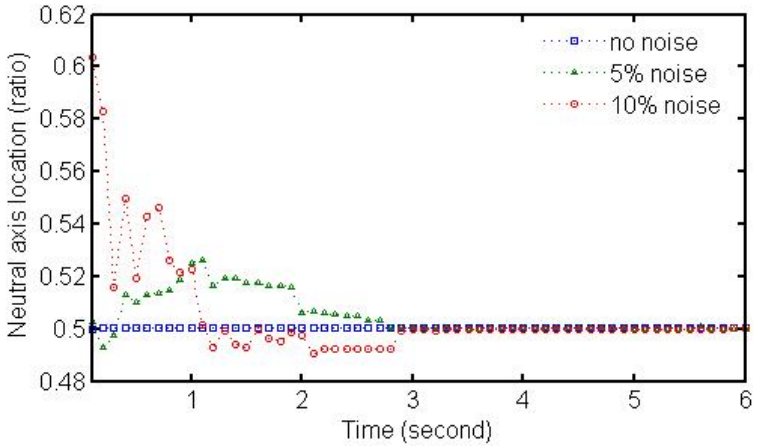

Figure 5.22 Performance assessment of KF estimator in different noise levels

Table 5.1 Performance analysis of KF estimator in simulation data

Simulation cases	Direct method		KF method
	mean	standard deviation	
Case 1	0.5001565	5.78E-04	0.5001539
Case 2	0.5005189	0.0258	0.5002154
Case 3	0.4984721	0.1156	0.4995412

Contrarily, the KF approach achieves improved estimates, evidenced by the relative

error of 0.0431% in Case 2 and -0.0918% in Case 3. These results demonstrate that the KF estimator has an excellent anti-disturbance ability in noise contamination.

5.4 Application to TMB Deck Assessment

As presented in Chapter 3, the extracted traffic-induced strain responses restore the flexural behavior very well either in highway or railway traffic. **Figure 5.23** illustrates the extracted traffic-induced strains experienced by a top chord and a bottom chord on the deck cross section CH24662.50 for a typical day. It is observed that the magnitude of the strain responses acquired at 2:00 to 5:00 am are relatively small since railway traffic ceases to operate during that period. This observation reveals that strain responses are sensitive to traffic load patterns.

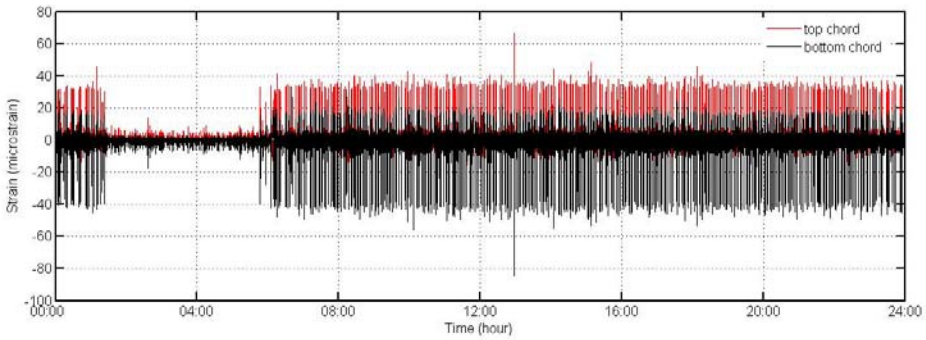

Figure 5.23 Traffic-induced strain time histories experienced by top and bottom chords on deck section CH24662.50 for a typical day

Theoretically, the neutral-axis position of the bridge deck cross section does not change under the varying traffic environment. It will be testified in this section. Four

typical load patterns are observed in **Figure 5.25** and grouped as follows: (1) 00:00~02:00; (2) 03:00~05:00; (3) 05:00~07:00; (4) 10:00~12:00. The KF approach to the neutral-axis position estimation is applied on these strain measurement data. **Figure 5.24** shows the extracted strain response data during the time period of 00:00~02:00, which include a transition of traffic pattern from having to not having railway traffic. Although this transition pattern is remarkably reflected in the strain responses, it does not affect the neutral-axis position estimated by the KF approach as shown in **Figure 5.25**.

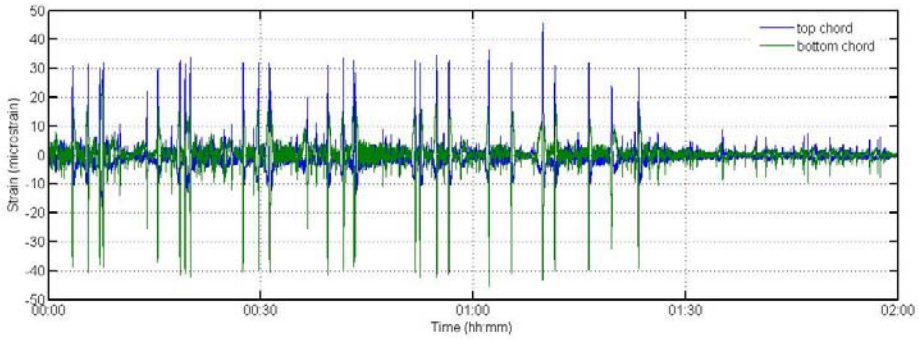

Figure 5.24 Traffic-induced strain time histories between 00:00 and 02:00

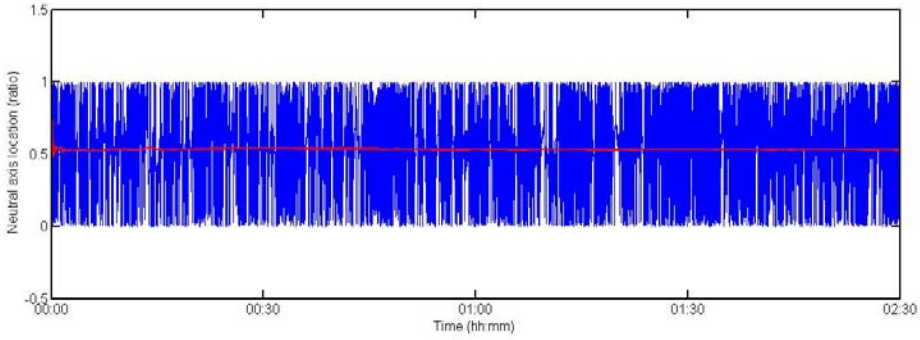

Figure 5.25 Estimated neutral-axis position from strain measurement (00:00 ~ 02:00)

Figure 5.26 illustrates the strain responses from 03:00 ~ 05:00 and there is no railway traffic effect in this time period. Magnitude of the strain responses is much lower than the case with railway traffic. The estimated neutral-axis position by the direct and KF methods in this scenario is shown in **Figure 5.27**.

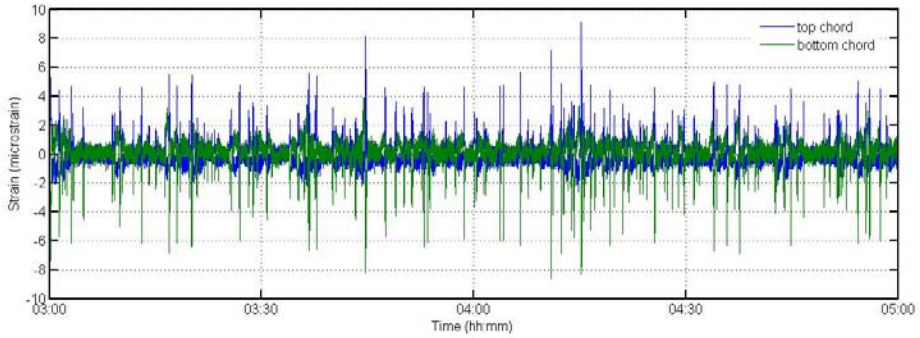

Figure 5.26 Traffic-induced strain time histories between 03:00 and 05:00

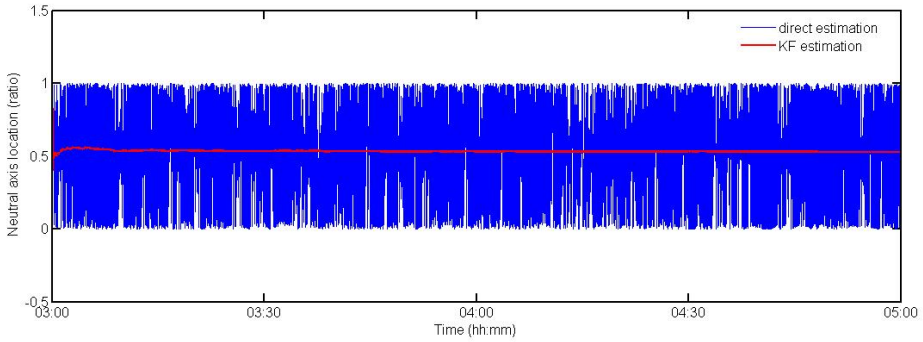

Figure 5.27 Estimated neutral-axis position from strain measurement (03:00 ~ 05:00)

In the time period of 05:00~07:00, there is a traffic pattern transition from not having to having railway traffic as shown in **Figure 5.28**. **Figure 5.29** illustrates the neutral-axis position estimated by the KF method during this time period, which is

not affected by the traffic pattern transition.

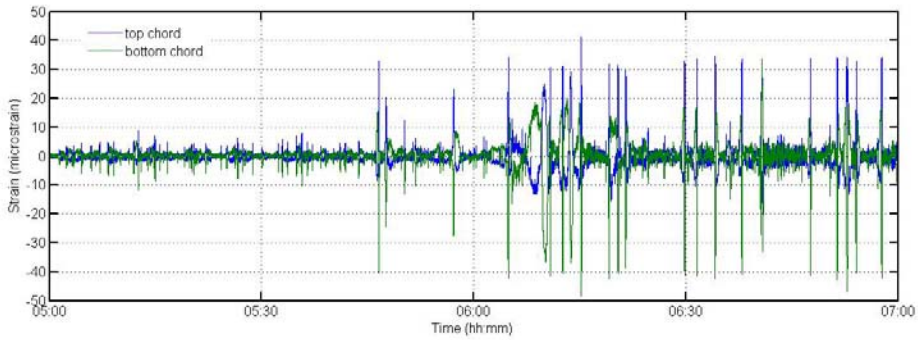

Figure 5.28 Traffic-induced strain time histories between 05:00 and 07:00

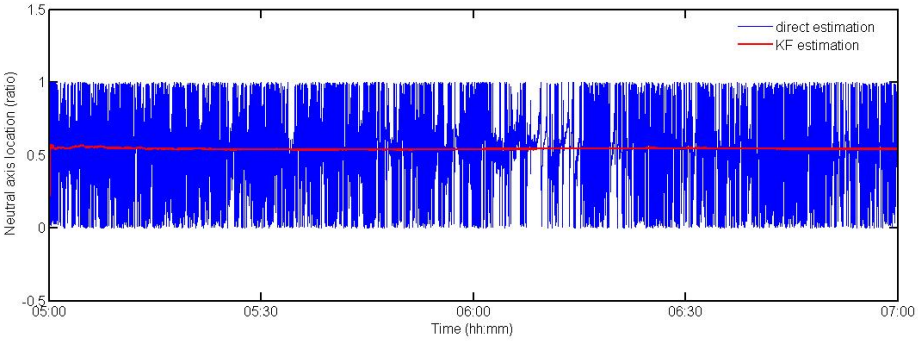

Figure 5.29 Estimated neutral-axis position from strain measurement (05:00 ~ 07:00)

For the last pattern of highway and railway traffic mixing together, the strain responses from 10:00 to 12:00 are illustrated in **Figure 5.30**. Estimation results of the neutral-axis position by the direct and KF methods are illustrated in **Figure 5.31**. No observable variation of the neutral-axis position estimated by the KF method is found.

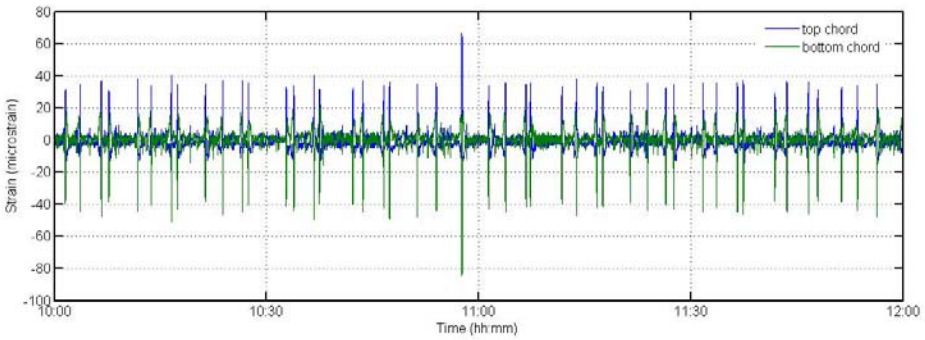

Figure 5.30 Traffic-induced strain time histories between 10:00 and 12:00

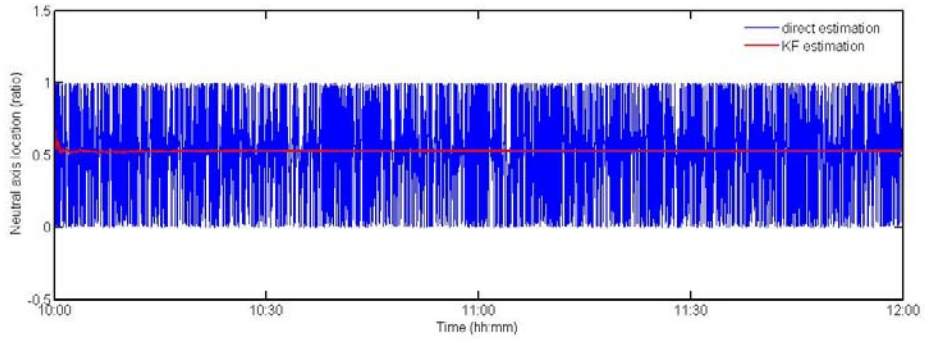

Figure 5.31 Estimated neutral-axis position from strain measurement (10:00 ~ 12:00)

The entire time histories of the neutral-axis position estimated by the direct and KF methods for a complete day (24 hours) are illustrated in **Figure 5.32**. It is shown that there are no remarkable transition patterns appearing in the time series of the estimated neutral-axis position although they do exist in the strain response time histories. Estimation results for different time periods are listed in **Table 5.2**. The variation range of the estimation mean by the direct method is between 0.5408021 and 0.5476296, but the standard deviation is remarkable. Contrarily the KF method

has a stable performance during the estimation process. The estimation results vary in the range of 0.5408047 to 0.5476295 for all the time periods. They fluctuate between -0.49% and 0.77% of their mean value.

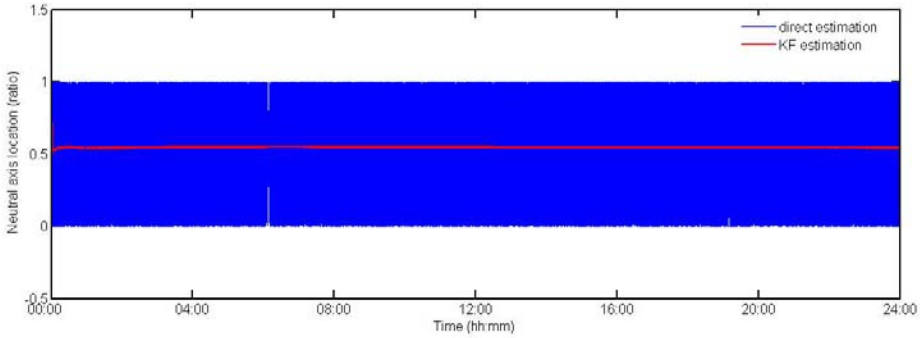

Figure 5.32 Estimated neutral-axis position from strain measurement (00:00 ~ 24:00)

Table 5.2 Comparison of estimated neutral-axis position in TMB deck under different load patterns

Time period	Direct method		Kalman Filter based method
	mean	standard deviation	
00:00 - 02:00	0.5423851	0.2127	0.5423849
03:00 - 05:00	0.5476296	0.2348	0.5476295
05:00 - 07:00	0.5425675	0.2071	0.5425693
10:00 - 12:00	0.5408021	0.2044	0.5408047
00:00 - 24:00	0.5438627	0.1968	0.5438627

5.5 Summary

In selection of damage indices for bridge deck assessment, their sensitivity to damage and robustness with respect to random traffic load patterns should be taken into consideration. Theoretically the neutral-axis position of a bridge deck cross section remains unchanged under the varying traffic environment. In addition, it has potential in improving the sensitivity to damage because it reflects the local cross-section property. In this chapter, the neutral-axis position is proposed as an indicator of damage for deck condition assessment. TMB bridge deck performs like a flexural beam, i.e., the deck top compresses and the deck bottom tensions concurrently, or vice versa. Based on the bending behavior, a KF estimator of locating the neutral-axis position from the strain measurement is formulated. Its capability of anti-disturbance in noise contamination has been testified by numerical studies.

Three extents of noise contamination (0%, 5% and 10%) in sensor readings are considered in the simulation. In Case 1, the direct and KF estimation methods almost reach the true value. Their relative errors are 0.0313% and 0.0308%, respectively. The standard deviation of the direct estimation results is as low as 5.78 E-04, demonstrating its efficiency when there is no noise. However, with the increase of noise extents, the estimation results by the direct method deteriorate seriously such that the relative error goes to 0.1038% in Case 2 and -0.3056% in Case 3 respectively.

The standard deviation increases obviously, implying that the direct estimation results are not reliable. Contrarily the KF approach improves the estimation accuracy significantly, with the relative error being 0.0431% and -0.0918% for Case 2 and Case 3, respectively. It can be concluded that the proposed KF estimator has an excellent anti-disturbance ability in noise contamination.

Moreover, the proposed KF estimator has been applied to the strain measurement data acquired from the TMB deck. The direct and KF estimation results of the neutral-axis position under different load patterns are obtained and compared. The variation range of the estimation mean by the direct method is between 0.5408021 and 0.5476296, but the standard deviation is remarkable. In contrast, the KF method has a stable performance under different load patterns and the estimation results vary in the range of 0.5408047 to 0.5476295. They fluctuate between -0.49% and 0.77% of their mean value. It is therefore concluded that the neutral-axis position of the bridge deck cross section does not change under the varying traffic environment.

CHAPTER 6

NEUTRAL-AXIS POSITION BASED DAMAGE DETECTION OF BRIDGE DECK USING STRAIN MEASUREMENT: EXPERIMENTAL VERIFICATION

6.1 Introduction

Structural damage is usually viewed as any deviation from original condition or status, which leads to the weakening of structural safety and serviceability. Early damage is desired to be detected by the practice of SHM. Significant attention has been devoted to finding damage-sensitive indices from global or local measurements. In recognizing that acceleration data can be conveniently acquired and the noise on them is relatively low, vibration based global damage detection methods have been extensively explored. Principally these methods are grounded on the assumption that changes in physical properties (such as mass, stiffness and boundary conditions) give rise to changes in dynamic characteristics (such as modal frequency, modal shape, or their derivations). Early work of such methodologies focused on the natural frequency (Cawley and Adams 1979) and modal shape information (Pandey *et al*. 1991; Chance *et al*. 1994; Dong *et al*. 1994). Some derivatives of modal shapes, such

as Modal Assurance Criteria (MAC) (West 1984), Coordinate Modal Assurance Criterion (COMAC) (Lieven and Ewins 1988), and Multiple Damage Location Assurance Criterion (MDLAC) (Lu *et al*. 2002), were also formulated for damage localization.

Although the underlying philosophy of vibration based damage detection appears intuitive, assessing structural damage in large-scale bridges remains still a challenging task. The main pitfalls limiting the practical applicability of vibration based damage detection methods include the insensitivity of modal properties to local damage in bridge structures, uncertainty and incompleteness in measurement data, modal variability arising from varying operational and environmental conditions, and modeling errors in the analytical model. Abdel Wahab and De Roeck (1997) showed that changes in modal properties resulting from changes in environmental conditions (such as temperature variation and random traffic effect) can be as significant as the changes caused by damage. Besides measurement noise can also significantly affect the success of vibration based damage detection. For example, changes of modal shape curvature, although sensitive to damage, could be masked by the derivative operation on the noisy data (Chance *et al*. 1994). An experimental verification of vibration based damage detection algorithms on a large-scale bridge was carried out by Frishwell and Penny (1997) and they concluded that modal characteristics might be insensitive to local damage.

In recognizing that damage is an intrinsically local phenomenon, the use of local measurement may have potential to improve the performance of damage detection methods. Jenkins *et al*. (1997) showed by an experiment that strain responses are more locally sensitive than the acceleration. However, strain responses are also sensitive to the loading environment and temperature variation, which cannot be related to damage. Therefore, in developing strain-related damage indicators, their insensitivity to loading and environmental variation should be taken into consideration. When using strain measurements for damage detection, strain components due to different mechanisms should be separated and processed individually. Because an indicator specially designed for a certain structural behavior may be seriously distorted by other source effects, and misjudgment of damage might happen. As described in Chapter 1, this study focuses on the development of a strain-related damage indicator for bridge deck assessment. Aiming at this purpose, Chapter 5 has proposed the neutral-axis position as a damage index for bridge deck assessment. A KF estimator has been formulated to locate the neutral-axis position based on the strain measurement. This Chapter is to testify the feasibility of neutral-axis position based damage detection by an elaborately designed experiment.

For the experimental verification, a flexible steel beam subject to moving bogies is used as the test structure to simulate the structural behavior of bridge deck under traffic effect. And cutting on a selected cross section is to simulate crack damage. Experimental setup including design and fabrication of the test model, sensor

instrumentation, testing load and damage simulation will be described. Then by establishing a multi-scale FEM (finite element method) model, numerical simulation based damage detection of the test model will be carried out for static and moving load cases, respectively. Physical experiment on damage detection of the test structure will be conducted eventually.

6.2 Experimental Setup

In the physical experiment, bridge deck is simplified as a flexural beam and traffic loading is modeled by a moving bogie with adjustable weight and speed. The crack damage is simulated by a reduction of stiffness properties of the cross section. Damage detection under static and moving load cases is experimentally explored.

6.2.1 Design and Fabrication of Test Model

As shown in **Figure 6.1**, the experimental model consists of two steel beams with a span of 6 m which are simply supported and fixed on two abutment pieces, respectively. Each steel beam is composed of three welded plates, namely left flange, web plate, and right flange. Its section parameters is HB 150×75×5×7mm as shown in **Figure 6.1(b)**. Two support conditions (shown in **Figure 6.2**) are designated in the experiment to testify whether the neutral-axis position of a cross section is affected by different boundary conditions.

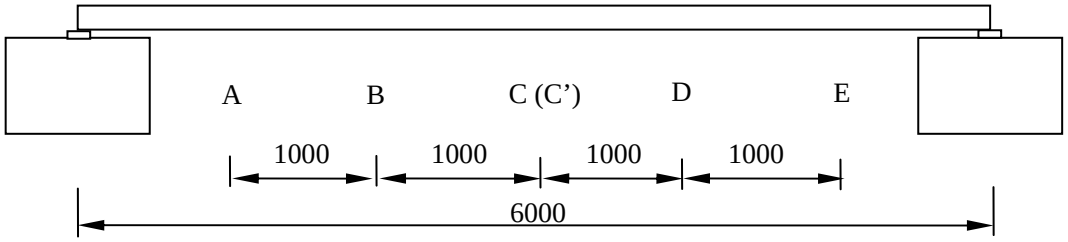

Elevation (Unit: mm)

(a) Elevation view

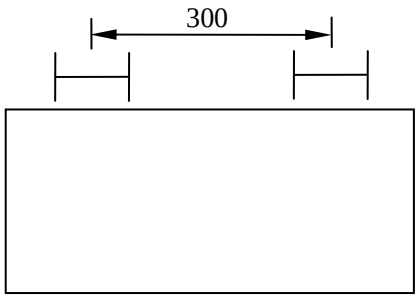

Side profile (Unit: mm)

(b) Cross section view

Figure 6.1 Schematic of experimental model

The material grade of the steel beam is BS4360-43A and its elastic modulus and yielding strength are 205GPa and 275MPa, respectively, and the Poisson's ratio are 0.3. The chemical compositions and mechanical properties are listed in **Table 6.1**.

6.2.2 Instrumentation

Table 6.1 Chemical compositions and mechanical properties

Material Grade	Chemical Compositions					Mechanical Properties		
	C	Mn	P	S	Si	Yield strength	Tensile strength	Elongation (%)
BS4360-4	0.25	1.60	0.05	0.05	0.50	275	430-58	22

(a) Simply supported case

(b) Fixed case

Figure 6.2 Two support conditions

The main experimental devices for the strain measurement are the ESG sensors (TML PFL-10-11) and data acquisition equipment (NI SCXI-1000), as shown in **Figure 6.3** and **Figure 6.4**. The maximum sampling rate of the ESG interrogator is 1000 Hz and the gauge length is 10 mm. The total number of the channels of the data acquisition system is 32, of which 12 channels are used for strain measurement. Totally 12 ESG sensors are installed on the three sections of the main beam (SB1) which are denoted by sections A, B, and C (shown in **Figure 6.1**). 4 ESG sensors are installed on the mid-span section (denoted as section C') of the reference beam (SB2). **Figure 6.5** shows the schematic of the sensor distribution on the mid-span section C, and **Figure 6.6** shows the photo of strain gauges deployed on the testing structure.

Figure 6.3 ESG gauges

Figure 6.4 ESG data acquisition equipment

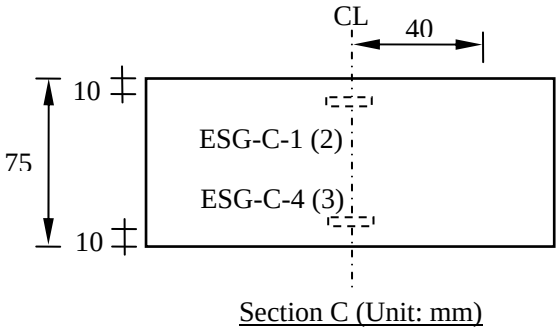

Figure 6.5 Deployment of strain sensors on section C

Figure 6.6 Photo of strain sensors deployed on section C

6.2.3 Description of Testing Load

In the experiment, traffic loading is simulated by a bogie with wheel axis length of 400 mm pulled by an automatic transmission equipment as shown in **Figure 6.7** and **Figure 6.8**. Four different load weights, namely 89 kg, 131 kg, 157 kg and 257 kg, are accounted for in the experiment for moving load simulation.

Figure 6.7 Automatic bogie transmission equipment

Figure 6.8 Bogie for moving vehicle simulation

6.2.4 Damage Simulation

Bending behavior dominates the response of bridge deck under traffic loading and hence bending cracks are prone to happen. An artificial cut on the cross section is introduced to simulate bending cracks induced by traffic loadings. In this experiment, two extents of damage are considered, respectively with 5 mm and 15 mm cuts on the mid-span section C of the main beam SB1, as shown in **Figure 6.9** and **Figure 6.10**.

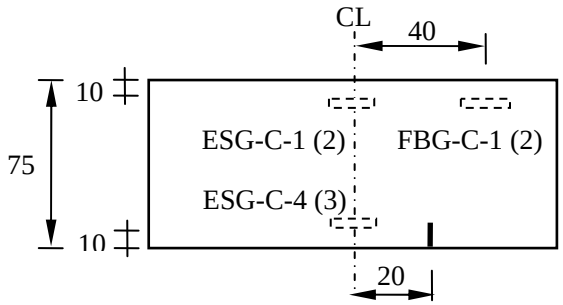

Section C (Unit: mm)

Figure 6.9 Schematic of cuts on cross section

6.2.5 Chart of Experiment

As illustrated in **Figure 6.11**, the model experiment includes two main parts: numerical simulation and physical testing. Numerical simulation for damage detection of the test structure is first conducted as a preparation of the physical testing. Undamaged, damaged_5mm, and damaged_15mm are considered in the static and moving load cases. The moving load simulation is to verify whether

(a) 5 mm

(b) 15 mm

Figure 6.10 Two extents of damage produced

the neutral-axis position is insensitive to the moving load weight and speed. Calibration of the neutral-axis position under different boundary conditions will be conducted before the physical testing.

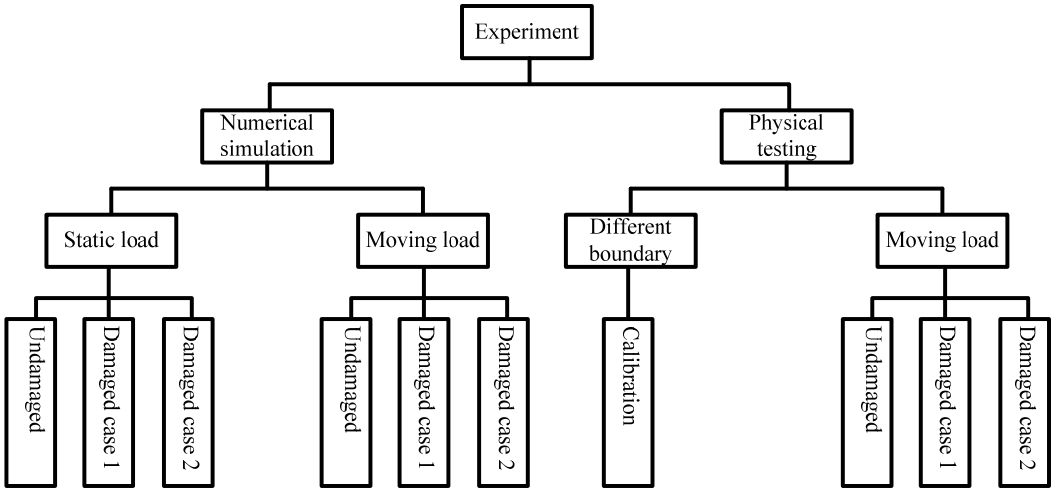

Figure 6.11 Chart of experiment

6.3 Neutral-Axis Position Based Damage Detection of Test Model: Numerical Simulation

6.3.1 Multi-Scale FEM Model

As strain and stress responses are required for the damage detection simulation, 3D solid elements are adopted to establish FEM model. When using a full 3D model, the computational time will become a big hurdle. In order to achieve a compromise between the computation precision and efficiency, the multi-scale finite element method (MsFEM) is applied in this study. It can efficiently capture the large scale behavior without resolving all the small-scale features. By using the commercial FEM software of ANSYS, the global model of the test structure is established as shown in **Figure 6.12**. Local FEM model at the damage region is illustrated in

Figure 6.13, where a smaller mesh size is used.

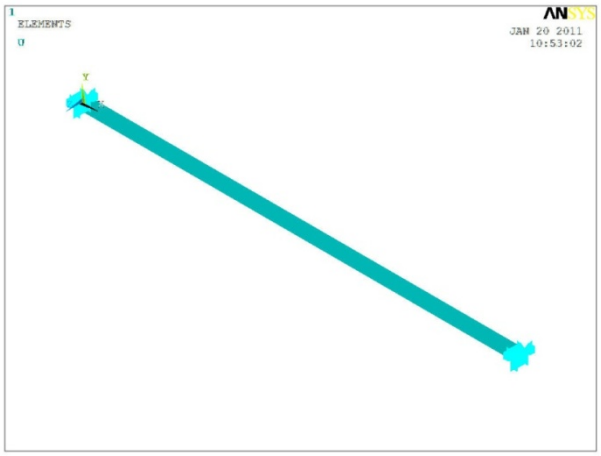

Figure 6.12 Global FEM model of test structure

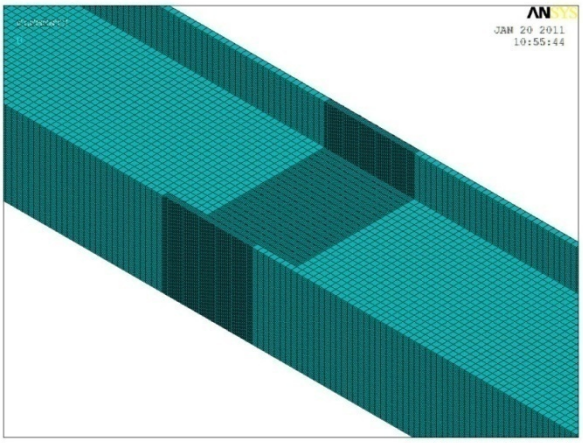

Figure 6.13 Local FEM model at damage region

As described in Chapter 5, under traffic loading environment, bending cracks are prone to arise in beam-like deck. For the crack damage simulation, an artificial deletion of the elements from the undamaged FEM model is used. **Figure 6.14** is for

the damage extent of 5 mm depth cut at the bottom of the selected cross section and **Figure 6.15** is for the damage extent of 15 mm depth cut at the same section.

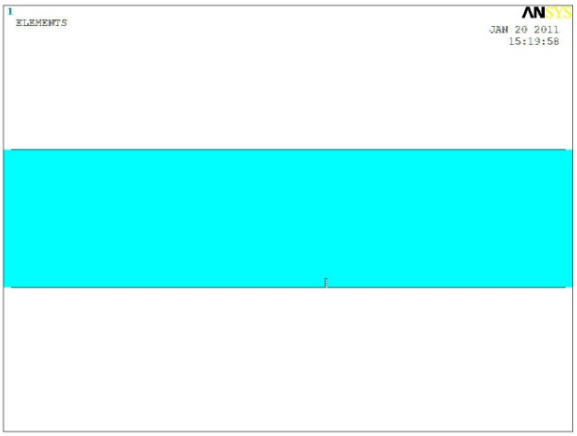

Figure 6.14 Damage simulation (Extent 1: cut with 5 mm depth)

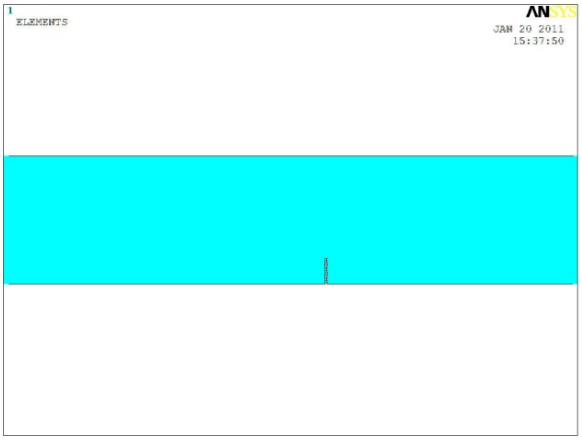

Figure 6.15 Damage simulation (Extent 2: cut with 15 mm depth)

6.3.2 Static Load Cases

In the static load simulation, a concentrated force is applied on the FEM model as

shown in **Figure 6.16**. The calculated strain distribution along the beam is illustrated in **Figure 6.17** and the strain distribution on the cross section C is shown in **Figure 6.18**. Based on the simulated strain responses at the top and bottom of the designated cross sections (refer to **Figure 6.1**), the neutral-axis positions for the undamaged case are obtained and listed in **Table 6.2**. And those for 5 mm and 15 mm damage are also obtained as shown in **Table 6.3** and **Table 6.4**, respectively.

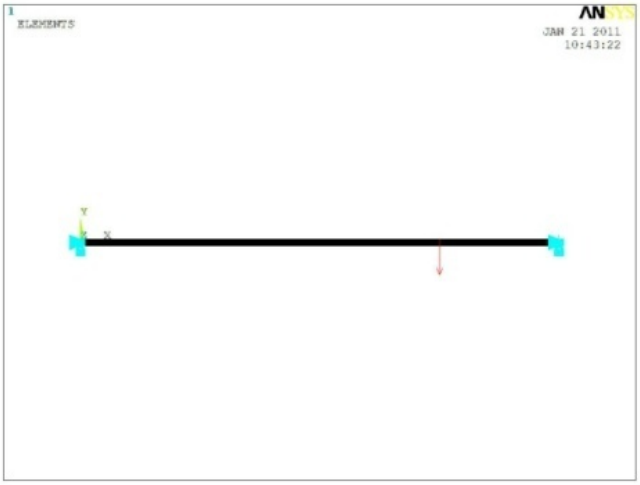

Figure 6.16 Static load simulation

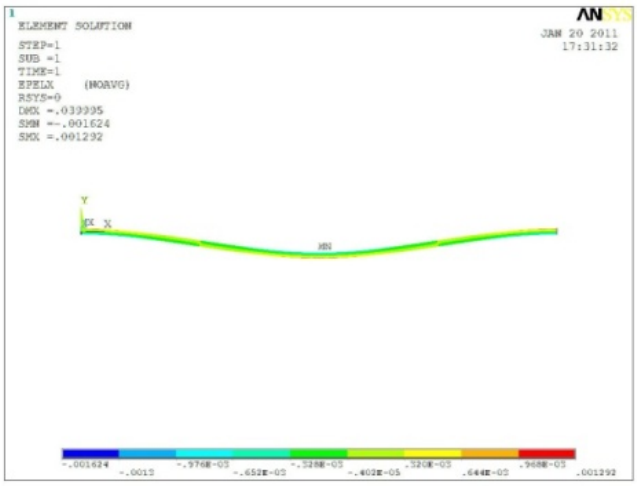

Figure 6.17 Strain distribution along beam structure

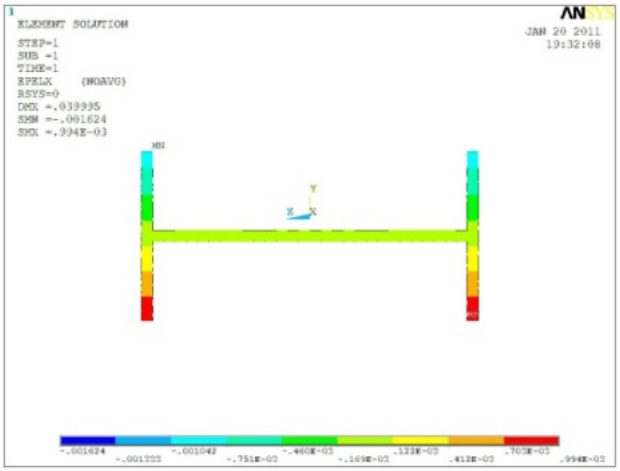

Figure 6.18 Strain distribution on cross section C

Table 6.2 Neutral-axis position obtained by simulation data (static load case 1: undamaged)

Strain at sensor locations	Beam cross sections		
	Section A	Section B	Section C
Top_1	0.12291 e-3	-0.29674 e-4	-0.18286 e-3
Bottom_4	-0.12294 e-3	0.29642 e-4	0.18283 e-3
Neutral-axis position (ratio)			
	0.50006	0.50003	0.50004

A comparison of the results obtained for the three damage cases is provided in **Table 6.5**. It is shown that shifts of the neutral-axis position of sections A, B and C are 0.38%, 0.96% and 3.19% for the 5 mm damage extent. In the case of 15 mm extent, they are 1.84%, 2.98% and 12.00%, respectively.

Table 6.3 Neutral-axis position obtained by simulation data (static load case 2: damage with 5 mm cut)

Strain at sensor locations	Beam cross sections		
	Section A	Section B	Section C
Top_1	0.84044 e-3	-0.20218 e-3	-0.12805e-2
Bottom_4	-0.83434 e-3	0.19837 e-3	0.12015 e-2
Neutral-axis position (ratio)			
	0.49818	0.49524	0.48409

Table 6.4 Neutral-axis position obtained by simulation data (static load case 3: damage with 15 mm cut)

Strain at sensor locations	Beam cross sections		
	Section A	Section B	Section C
Top_1	0.84435 e-3	-0.19824 e-3	-0.14773 e-2
Bottom_4	-0.81407 e-3	0.18679 e-3	0.11607 e-2
Neutral-axis position (ratio)			
	0.49087	0.48514	0.4400

Table 6.5 Comparison of neutral-axis position for three damage cases

Damage condition	Neutral-axis position (ratio)		
	Section A	Section B	Section C
Undamaged	0.50006	0.50003	0.50004
Damaged_5mm	0.49818	0.49524	0.48409
Damaged_15mm	0.49087	0.48514	0.4400
Scenario 1: Damaged_5mm			
	0.38%	0.96%	3.19%
Scenario 2: Damaged_15mm			
	1.84%	2.98%	12.00%

6.3.3 Moving Load Cases

In the moving load cases, strain responses at top and bottom of the designated sections A, B, and C are simulated and illustrated in **Figure 6.19** for the undamaged case. The moving speed is specified as 1 m/s. The simulation results show that bending behavior dominates the structural response of the test structure.

To testify whether the neutral-axis position is insensitive to load patterns, different load weights and moving speeds are simulated on the undamaged model. **Figure 6.20** shows the simulated strain responses at the top of section C for the load weights of 100 KN, 200 KN, and 300 KN. Based on the simulated strain response data, the KF estimation of neutral-axis position of at the three sections is obtained and given in **Table 6.6**. It is observed that the neutral-axis position remains almost unchanged

with varying load weight.

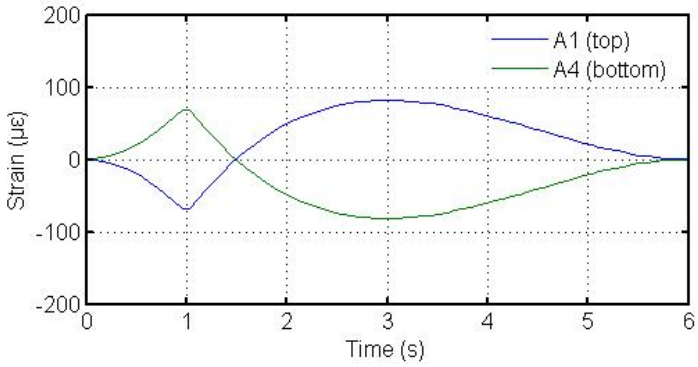

(a) Section A

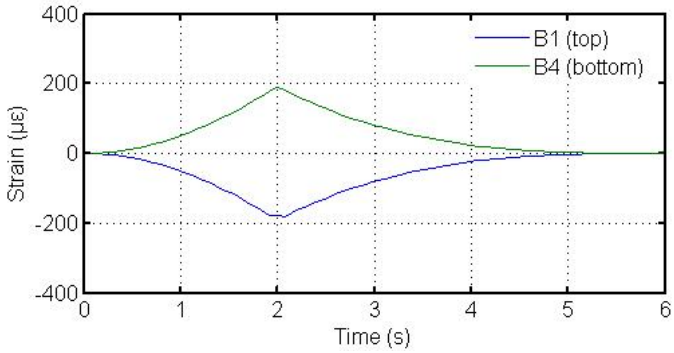

(b) Section B

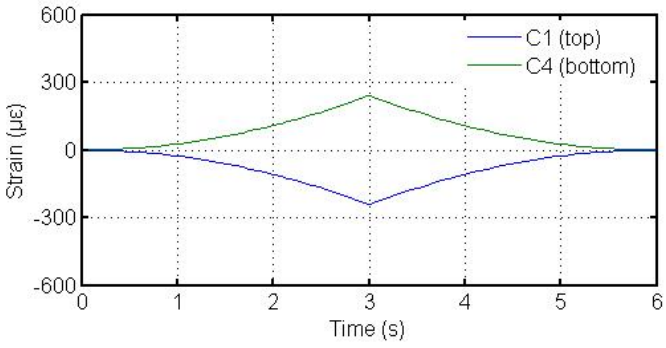

(c) Section C

Figure 6.19 Simulated strain responses at top and bottom of designated sections (moving speed: 1 m/s; undamaged)

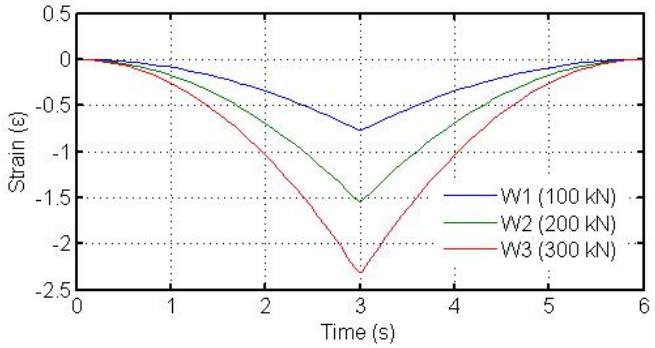

Figure 6.20 Simulated strain responses at top of section C under different load weights (moving speed: 1 m/s; undamaged)

Table 6.6 Neutral-axis position of designated sections under different load weights (moving speed: 1 m/s)

Load weight	Neutral-axis position (ratio)		
	Section A	Section B	Section C
W1 (100 kN)	0.5002	0.5004	0.5003
W2 (200 kN)	0.5008	0.5007	0.5004
W3 (300 kN)	0.5005	0.5001	0.5006

FEM simulation of strain responses under different moving speeds is conducted as well. **Figure 6.21** illustrates the obtained strain responses at the top of section C. As shown in **Table 6.7**, different moving speeds have no influence on the estimation of neutral-axis position.

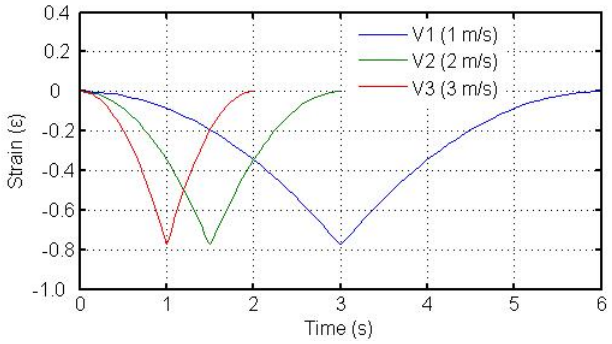

Figure 6.21 Simulated strain responses at top of section C under different moving speeds

Table 6.7 Neutral-axis position of designated sections under different moving speeds

Moving speed	Neutral-axis position (ratio)		
	Section A	Section B	Section C
V1 (1 m/s)	0.5006	0.5007	0.5002
V2 (2 m/s)	0.5003	0.5005	0.5009
V3 (3 m/s)	0.5008	0.5002	0.5004

After verifying the independence of neutral-axis position on moving load patterns, damage detection simulation based on the FEM model is conducted. Strain responses at top and bottom of the designated sections A, B, and C are illustrated in **Figure 6.22** for the damage case of 5 mm depth cut. **Figure 6.23** is for the damage case of 15 mm depth cut.

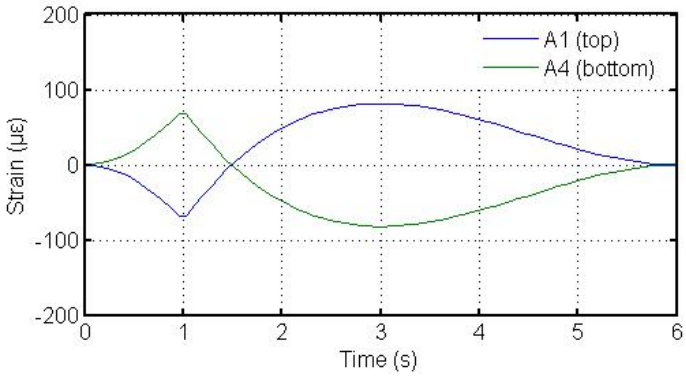

(a) Section A

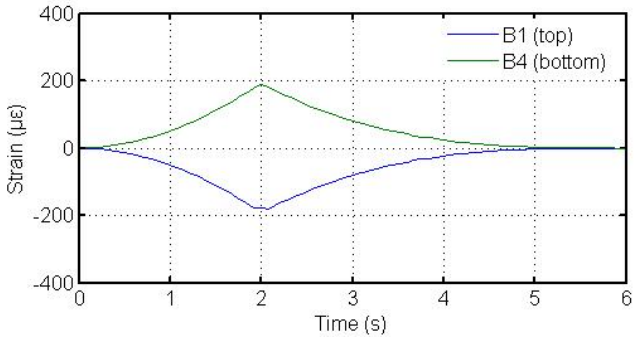

(b) Section B

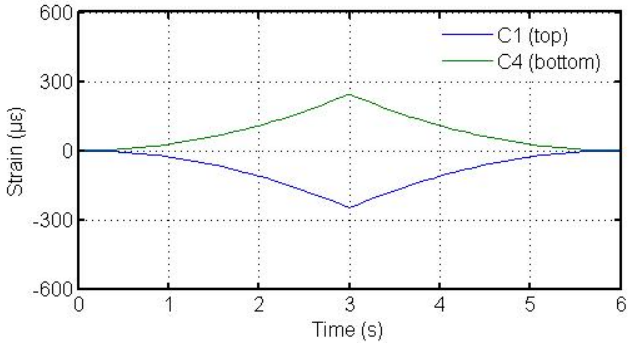

(c) Section C

Figure 6.22 Simulated strain responses at top and bottom of designated sections (moving speed: 1 m/s; damage case: 5 mm cut)

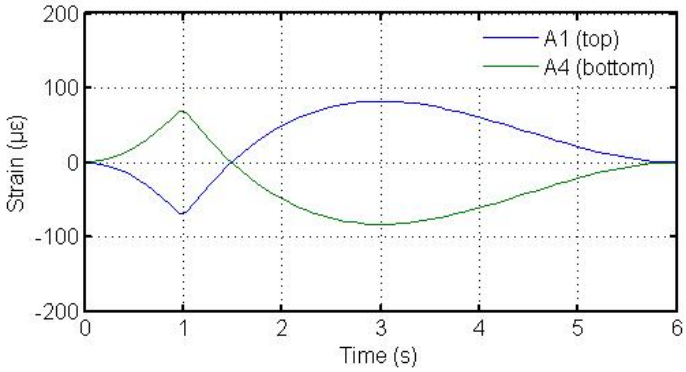

(a) Section A

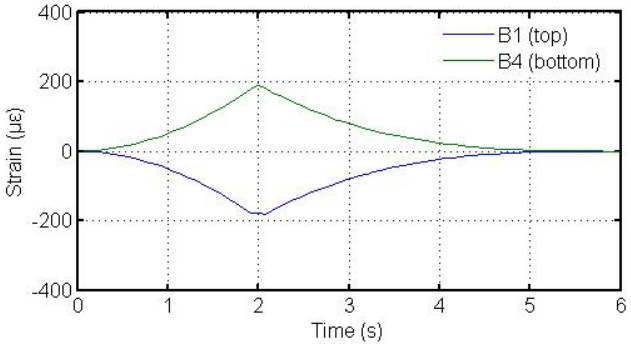

(b) Section B

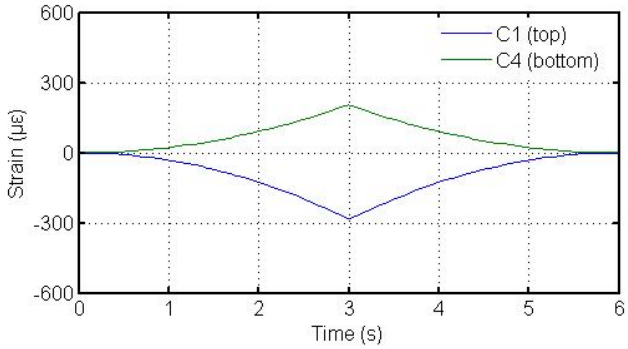

(c) Section C

Figure 6.23 Simulated strain responses at top and bottom of designated sections (moving speed: 1 m/s; damage case: 15 mm cut)

For the three damage cases, KF estimation of the neutral-axis position of the designated sections is obtained as shown in **Table 6.8**. It is shown that shifts of the neutral-axis position of sections A, B and C are 0.48%, 0.80% and 3.36% for the 5 mm damage case. And for the 15 mm damage case, the changing rate is 2.06%, 3.22% and 13.83%, respectively.

Table 6.8 Comparison of neutral-axis position for three damage cases (moving load simulation)

Damage condition	Neutral-axis position (ratio)		
	Section A	Section B	Section C
Undamaged	0.5006	0.5003	0.5004
Damaged_5mm	0.4982	0.4963	0.4836
Damaged_15mm	0.4903	0.4842	0.4312
Scenario 1: Damaged_5mm			
	0.48%	0.80%	3.36%
Scenario 2: Damaged_15mm			
	2.06%	3.22%	13.83%

6.4 Neutral-Axis Position Based Damage Detection of Test Model: Experiment and Data Analysis

6.4.1 Calibration of Neutral-Axis Position

Before the physical testing for damage detection, calibration of neutral-axis position with respect to different boundary condition is conducted. **Figure 6.24(a)** shows the

measured strain responses at the top and bottom of section C when the test beam is simply supported, while **Figure 6.24(b)** is for the fixed boundary condition. As shown in **Figure 6.24**, the testing data coincide favorably with the simulation data. And it is clearly observed that noise is present in the sensor readings.

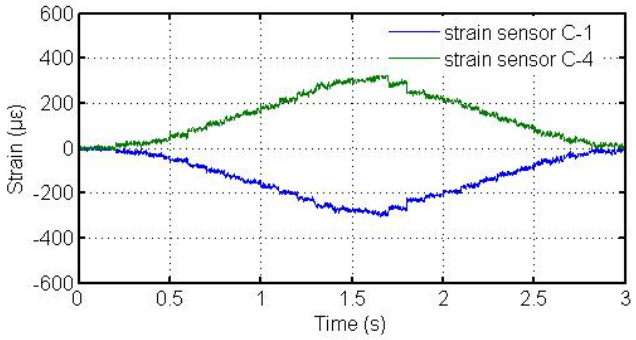

(a) Simply supported

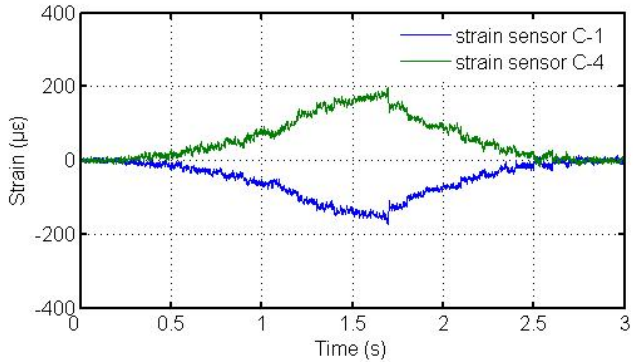

(b) Fixed supported

Figure 6.24 Measured strain responses at top and bottom of section C (different boundary conditions)

Direct and KF estimations of the neutral-axis position are illustrated in **Figure 6.25** for both support conditions. The results of neutral-axis position obtained by the KF

method are 0.5034 and 0.5046, respectively for the two boundary conditions. The difference is only 0.23%, which means different boundary conditions have little effect on the estimation of neutral-axis position.

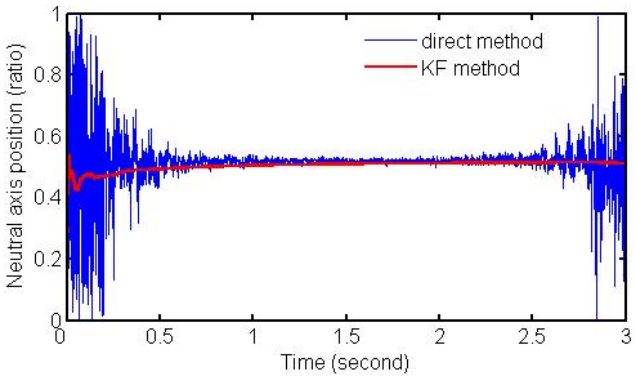

(a) Simply supported

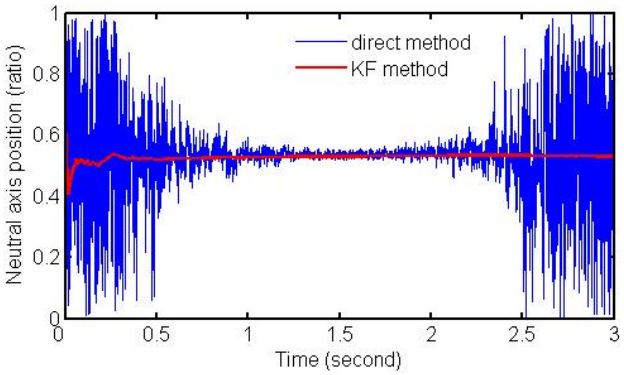

(b) Fixed supported

Figure 6.25 Estimated neutral-axis position based on measured strain responses (different boundary conditions)

6.4.2 Moving Load Testing

In the physical testing, strain responses at top and bottom of the designated sections

are measured and fed into the KF estimator to obtain the neutral-axis position. **Figure 6.26** shows strain responses measured at the top and bottom of sections A, B

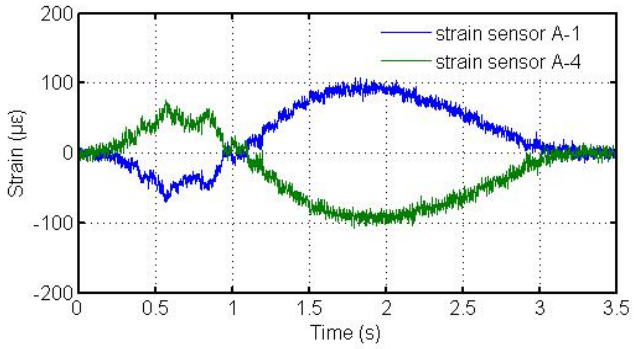

(a) Section A

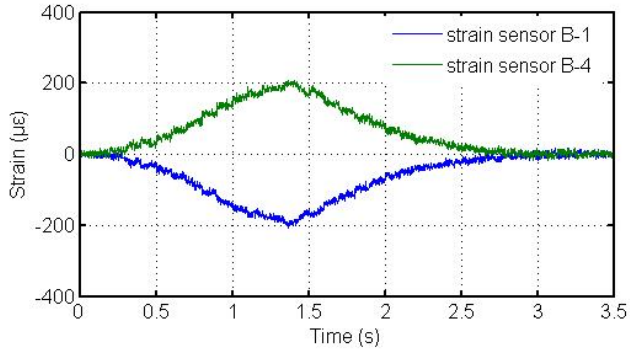

(b) Section B

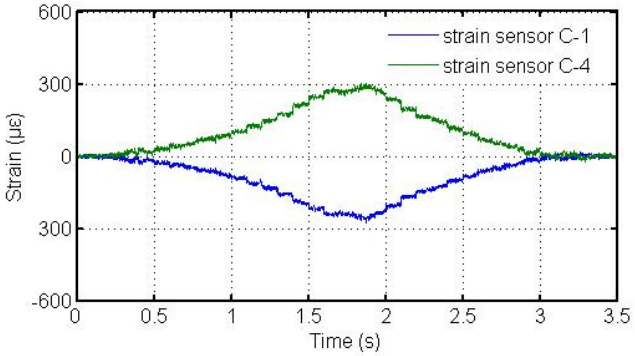

(c) Section C

Figure 6.26 Measured strain responses at top and bottom of designated sections (fixed boundary condition)

and C for the fixed boundary condition. By comparison with Figure 6.19, it is observed that the measured strain responses coincide favorably with the simulation results. Strain responses of the test structure under moving bogies are measured for all three damage cases, as shown in Figure 6.27(a). Figure 6.27(b) shows the estimated neutral-axis position by the direct and KF methods. It is observed that the neutral-axis position by the KF approach effectively reflects the damage conditions of the test structure.

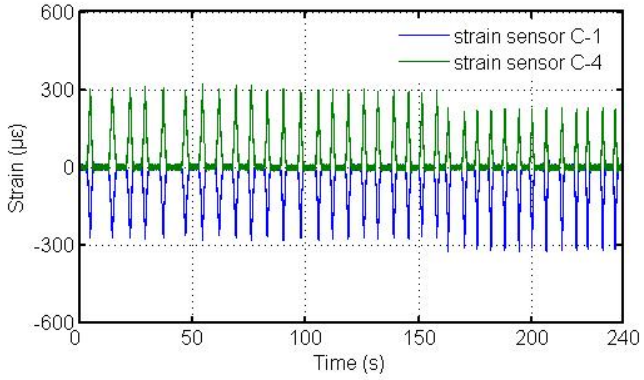

(a) Strain measurements

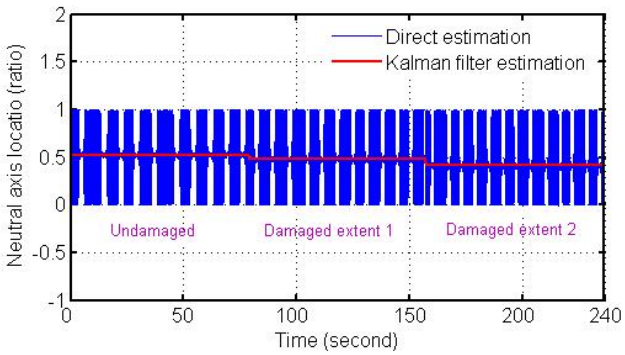

(b) Estimated neutral-axis position

Figure 6.27 Damage detection of test structure under three damage conditions by KF estimator

Sensitivity analysis of the neutral-axis position at the three instrumented sections A, B and C is conducted, of which the results are listed in **Table 6.9**. In the damage case 1, change rates of neutral-axis position at the three sections are 0.43%, 0.92% and 3.58%, respectively. For the 15 mm damage case, they are 2.15%, 2.14% and 10.96%. These results validate that neutral-axis position is sensitive enough for damage detection. Besides, **Table 6.9** indicates that the sensitivity of neutral-axis position decreases substantially as it is away from the damaged section. Therefore the neutral-axis position can also serve as an indicator of damage location. With the development of distributed sensing technology (such as distributed Brillouin optical fiber sensor), the limitation of spatial resolution in strain measuring can be overcome in the near future.

Table 6.9 Comparison of neutral-axis position for three damage cases (moving load testing)

Damage condition	Neutral-axis position (ratio)		
	Section A	Section B	Section C
Undamaged	0.5061	0.5092	0.5054
Damaged_5mm	0.5039	0.5045	0.4873
Damaged_15mm	0.4952	0.4983	0.4500
Scenario 1: Damaged_5mm			
	0.43%	0.92%	3.58%
Scenario 2: Damaged_15mm			
	2.15%	2.14%	10.96%

6.5 Summary

Small structural defects could be often discerned from the variation in strain or its derivatives rather than in acceleration. Strain based identification methods for structural damage detection have received increasing attention. But strain responses are also sensitive to the loading environment and temperature variation, which cannot be related to damage. In developing strain-related damage indicators, their insensitivity to loading and environmental variation is a big concern. Theoretically the neutral-axis position of bridge deck cross section should remain unchanged under the varying traffic environment, and it may have a better damage sensitivity because it reflects the local cross-section property. Because of these advantages, Chapter 5 has proposed the neutral-axis position as a damage index for bridge deck assessment. A KF estimator has been formulated to locate the neutral-axis position from the strain measurement. The feasibility of neutral-axis position based damage detection is testified by an elaborately designed experiment in this Chapter. The experiment includes two parts: numerical simulation and physical testing.

Numerical simulation based damage detection of the test model was conducted for static and moving load cases, respectively. In the static load simulation, it is shown that shifts of the neutral-axis position of sections A, B and C are 0.38%, 0.96% and 3.19%, respectively for the 5 mm damage case. For the 15 mm damage case, they are 1.84%, 2.98% and 12.00%, respectively. As to the moving load case, shifts of the

neutral-axis position of sections A, B and C are 0.48%, 0.80% and 3.36%, respectively for 5 mm damage case. They are 2.06%, 3.22% and 13.83% for the 15 mm damage case. It is observed that the results from the static load case agree favorably with those from the moving load case. The neutral-axis position obtained in the two cases can capture the damage happening on the test model. In addition, it is validated that the neutral-axis position is insensitive to different moving load weights and speeds.

Calibration of the neutral-axis position with respect to two different boundary conditions is conducted before the physical testing. The difference between simply and fixed support cases is only 0.23%, which means different boundary conditions have little effect on the estimation of neutral-axis position. In the physical testing, change rates of the neutral-axis position at the three sections are identified as 0.43%, 0.92% and 3.58% for the 5 mm damage case. They are 2.15%, 2.14% and 10.96% for the 15 mm damage case. The experimental results validate that neutral-axis position is sensitive enough for detecting local damage. Neutral-axis position can also serve as an indicator of damage location. The recent development of distributed sensing technology can bring a promise in overcoming the limitation of spatial resolution faced by the traditional strain measuring technologies.

CHAPTER 7

CONCLUSIONS AND RECOMMENDATIONS

7.1 Conclusions

The research described in this dissertation chiefly contributes to the development of a systematic framework for condition assessment of existing bridge structures making use of long-term monitoring data of strain response. This approach involves multi-component analysis of strain monitoring data, mixture distribution model based reliability assessment, KF based optimal estimation of neutral-axis position, and experimental verification of neutral-axis position based damage detection. Following this approach, objective and quantitative condition assessment of in-service bridge structures is realized.

(1) Development of a method for source separation of strain monitoring data according to physical mechanisms

As demonstrated by the monitoring data, strain responses of bridge structures under in-service conditions are a combination of live-load and environmental effects. Multi-component data structures have been found in the long-term strain monitoring

data. A logical way to efficiently interpolate the multi-component measurement data is to decompose them into mono-components. In this way distinct structural behaviors under different loading scenarios and environmental conditions are revealed for condition assessment or damage detection. With specialized PR filter banks, DWT based decomposition possesses advantages of parsimonious representation, energy decomposition, and effective de-correlation. However, there is no guarantee that the decomposed components by DWT transform have exactly the same waveforms as the source signals. To restore the desired source signal, component extraction needs to be conducted in the wavelet decomposition domain.

Correlation coefficients of the level component of wavelet transform with a reference signal are introduced to determine the DWT decomposition resolution and establish the selection criterion for physical component extraction. Based on the selection criterion, physical source separation of the multi-component data is realized. With the application of the proposed method to TMB, the following observations have been made:

(i) DWT can effectively separate a multi-component strain data into a set of narrow band components which satisfying the perfect reconstruction requirement. By scaling and shifting a mother wavelet, DWT decomposes strain data into various resolution scales: the data with coarse resolution contain the information about low-frequency components and the data with fine resolution contain the information about high-frequency components.

Each level component carries a single frequency content of the original signal; and

(ii) The extracted temperature-induced strain component in along-bridge direction coincides well with the displacement time history measured at the expansion joint. Under temperature effect, the bridge deck behaves mainly as expanding or contracting along the longitudinal direction and the expansion joint moves forward or backward accordingly. A strong correlation between the temperature-caused strain and the longitudinal displacement at the expansion joint has been demonstrated; and

(iii) The extracted traffic-induced strains at the top and bottom chords of the same deck cross section evolve with time in almost same amplitudes but opposite directions. Under traffic loading, the bridge deck performs like a flexural beam, i.e., the deck top compresses and the deck bottom extends concurrently, or vice versa. The extracted strain component due to traffic effect reveals the bending behavior of the bridge deck under traffic loading favorably.

(2) Establishment of mixture distribution model based reliability assessment of in-service bridge deck

When using the strain response data due to live load effect for reliability assessment, a problem arises in the inference of probability distribution from observation data. Collected under in-service environment, strain response due to live load effect is a result of multi-load effect such as traffic (highway, railway, or both of them) and

wind (monsoon or typhoon). It cannot be characterized by a standard probability density function adequately. Weibull mixture models are therefore developed and applied to characterize the statistical properties of peak-stress data. With the application of the proposed method to TMB, the following observations have been made:

(i) The PDF of peak stresses has a very complicated shape due to multi-load effect. Mixture distributions are clearly displayed in the histogram analysis of the peak-stress data for different load conditions. It is concluded that multiple engendering effects with distinct statistical characteristics create the mixture distribution phenomenon; and

(ii) In distribution modeling Weibull mixtures have advantages of less component number and lower AIC values in comparison with normal and log-normal mixtures. Weibull family is demonstrated to have a capability of extensive adaptation through various shape and scale parameters. Advantages of Weibull mixtures in modeling measurement data has been exhibited in the PDF inference of peak stresses; and

(iii) The EM algorithm is a suitable tool for Weibull mixture parameter estimation with fast convergence and excellent stability. Formulas of the EM algorithm for Weibull mixtures have been derived. That component parameters converge almost simultaneously demonstrates the efficiency of EM algorithm in the Weibull mixture modeling; and

(iv) By reliability analysis based on the estimated PDFs, it is found that all the

deck truss members are in a good safety condition so no maintenance action is needed. Among the three load scenarios (HL + NW, HL + RL + NW, and HL + RL + TW), the HL + RL + TW case is the most dangerous.

(3) Development of a KF estimation method to locate neutral-axis position of bridge deck from traffic-induced strain response

Bending behavior dominates the response of bridge deck under traffic loading. Based on the structural behavior, direct and KF methods of locating the neutral-axis position from the strain measurement data are formulated. Numerical studies on their capability of anti-disturbance in noise contamination have been conducted and some conclusions are drawn as follows:

(i) The efficiency of the direct estimation method can only be ensured on the condition that measurement data are without noise contamination. When the simulation data are free of noise, the direct method reaches the true value. With the increase of noise levels, the estimates by the direct method deteriorate seriously. Standard deviation of the estimation results increases remarkably, indicating that the direct estimation results are not reliable under noisy environment; and

(ii) In comparison to the direct method, the KF estimator achieves a better estimation, and particularly has an excellent performance when the signal-noise ratio is low. It is demonstrated that the KF estimator is superior to the direct method which uses the measurement alone.

The verified KF estimator is further applied to the strain measurement data acquired from the TMB deck. Estimates of the neutral-axis position for different load patterns are obtained. The direct and KF methods obtain a consistent result of 0.5408~0.5476, which fluctuate between -0.49% and 0.77% of their mean value. It is therefore concluded that the neutral-axis position of the bridge deck cross section remains almost unchanged under the varying traffic environment. Hence it can serve as a good indicator for deck condition assessment.

(4) Experimental verification of neutral-axis position based damage detection of bridge deck under traffic loading

The neutral-axis position is independent of traffic load patterns and it shifts in the occurrence of damage. An experimental verification of neutral-axis position based damage detection of bridge deck has been conducted in this study. The experiment includes two parts: numerical simulation and physical testing.

(i) Numerical simulation shows that the neutral-axis position is insensitive to moving load weights and speeds. The sensitivity of neutral-axis position to damage under static load cases agree favorably with that of moving load cases; and

(ii) Calibration of the neutral-axis position with respect to two different support conditions has been conducted before damage testing. The difference of estimation results between simply and fixed support cases is 0.23%, implying

that different support conditions have little effect on the neutral-axis position.

(iii) In the damage detection testing, change rates of the neutral-axis position are effectively identified from the strain measurement data. Testing results show that neutral-axis position is sensitive enough for local damage detection and can also serve as an indicator of damage location.

7.2 Recommendations

The established methods for condition assessment of in-service bridge structures using strain measurements are still preliminary and in its infancy. More thorough research is expected to improve the proposed methods for better benefiting bridge maintenance and management. The recommendations for future exploration are as follows.

(1) Development of Wiener-filter based component extraction method in wavelet decomposition domain

As demonstrated in this project, wavelet multi-resolution decomposition satisfies the mathematical principle of source separation quite well with the specialized PR filter banks. Component extraction in the wavelet decomposition domain according to physical mechanisms is realized by establishing a correlation-based selection criterion. The proposed method handles the extraction problem at different-resolution levels where components with a correlation coefficient higher or lower than a

threshold will be retained or discarded. Dropping a certain level-component entirely could incur a loss of useful information because the desired source signal may disperse on various levels as fractals. As to the fractal extraction, Wiener filter in the wavelet domain could perform better than the thresholding methods because correlation based selection might be carried out on each subband individually. Therefore, wavelet based Wiener filter approach to signal source separation can be expected to extract whole segments in different level components of wavelet decomposition.

(2) Establishment of a time-dependent mixture distribution model by using long-term monitoring data and Bayesian theory

In this study, hybrid mixture estimation including model selection and parameter estimation has been explored and a structure of Weibull mixture model has been proposed for PDF inference of peak-stress values counted from the derived stress time histories. As more and more strain monitoring data acquired by the SHM system become available, a more accurate probabilistic model of live load effect can be formulated with the aid of the Bayesian updating method.

Bayesian theory is a powerful and feasible tool to improve the model and parameter estimation as new data are coming into (Yuen 2010). It offers the possibility to combine existing knowledge with subsequent available information to update the pre-established probabilistic model and parameters. By integrating the updated live

load effect model into the reliability based condition assessment procedure, time-dependent failure probability or reliability index for a structural component in a bridge can be calculated. With the obtained time-dependent reliability indices and rating factors, the bridge inspection and maintenance activities could be planned in accordance with the variation of reliability index and rating factor profiles at the in-service stage.

(3) Investigation of distributed optical fiber sensing technology in integration with neutral-axis position based damage detection method

The use of strain measurement may have potential to improve the performance of damage detection methods in recognition of the trait of local damage phenomenon. This study has demonstrated that neutral-axis position derived from strain measurements is sensitive enough to damage and insensitive to different moving load weights and speeds. Therefore, the neutral-axis position can serve as a damage indicator for bridge deck assessment. But the neutral-axis position based damage detection method will confront the problem of locality that the influence of damage on neutral-axis position cannot be reflected effectively unless the area where the strain sensors are deployed could cover the damage region.

The recent development of distributed Brillouin optical fiber sensing (BOFS) technology can provide the measurement availability of strain field and, in a sense, can solve the spatial resolution problem. Fiber optical strain gauges (FOSGs) have

the ability to multiplex many sensors using only one optical fiber, providing a very low-cost mechanism for densely instrumenting large-scale structures. Investigation of distributed optical fiber sensing technology can be expected to extend the applicability of the proposed damage detection method.

REFERENCES

AASHTO, *Manual for Maintenance Inspection of Bridges*, American Association of State Highway and Transportation Officials, Washington D.C., USA, 1989.

Abarbanel, H.D.I., *Analysis of Observed Chaotic Data*, Springer, New York, 1996.

Abdel Wahab, M., and De Roeck, G. (1997), "Effect of temperature on dynamic system parameters of a highway bridge", *Journal of Structural Engineering*, Vol. 4, 266–270.

Abdel Wahab, M.M., and De Roeck, G. (1999), "Damage detection in bridges using modal curvatures: application to a real damage scenario", *Journal of Sound and Vibration*, Vol. 226, 217–235.

Abe, M., Fujino, Y., Yanagihara, M., and Sato, M. (2000), "Monitoring of Hakucho Suspension Bridge by ambient vibration measurement", *Proceedings of SPIE*, Vol. 3995, 237–244.

Adewuyi, A.P., Wu, Z., and Serker, N. (2009), "Assessment of vibration-based damage identification methods using displacement and distributed strain measurement", *Structural Health Monitoring*, Vol. 8, 443–461.

Akaike, H. (1973), "Information theory and an extension of the maximum likelihood principle", *Second international symposium on information theory*, 267–281.

Aktan, A.E., Farhey, D.N., Brown, D.L., Dalal, V., Helmicki, A.J., Hunt, V.J., and Shelley, S.J. (1996), “Condition assessment for bridge management”, *Journal of Infrastructure Systems*, ASCE, Vol. 2, 108–117.

Aktan, A.E., Farhey, D.N., Helmicki, A.J., Brown, D.L., Hunt, H.J., Lee, K.L., and Levi, A. (1997), “Structural identification for condition assessment: experimental arts”, *Journal of Structural Engineering*, ASCE, Vol. 123, 1674–1684.

Aktan, A.E., Catbas, F.N., Grimmelsman, K.A., and Tsikos, C.J. (2000) “Issues in infrastructure health monitoring for management”, *Journal of Engineering Mechanics*, ASCE, Vol. 126, 711–724.

Andersen, E.Y., and Pedersen, L. (1994), “Structural monitoring of the Great Belt East Bridge”, *Strait Crossings 94*, Krokeborg, J. (editor), A.A. Balkema, Rotterdam, 189–195.

Banerjee, A., Dhillon, I.S., Ghosh, J., and Sra, S. (2005), “Clustering on the unit hypesphere using von Mises-Fisher distributions”, *Journal of Machine Learning Research*, Vol. 6, 1345–1382.

Bao, X., DeMerchant, M., Brown, A., and Bremner, T. (2001), “Tensile and compressive strain measurement in the lab and field with the distributed Brillouin scattering sensor”, *Journal of Lightwave Technologies*, Vol. 19, 1698–1704.

Barr, P.J., Eberhard, M.O., and Shanton, J.F. (2001), “Live-load distribution factors in prestressed concrete girder bridges”, *Journal of Bridge Engineering*, Vol.

6, 298–306.

Barrish, R.A., Grimmelsman, K.A., and Aktan, A.E. (2000), “Instrumented monitoring of the Commodore Barry Bridge”, *Nondestructive Evaluation of Highways, Utilities, and Pipelines IV*, Aktan, A.E., and Gosselin, S.R. (editors), The International Society for Optical Engineering, Bellingham, Vol. 3995, 112–126.

Begueret, J.B., Benbrahin, M.R., Li, A.Q., Rodes, F., and Dom, J.P. (1997), “Converters dedicated to long-term monitoring of strain gauge transducers”, *IEEE Journal of Solid-State Circuits*, Vol. 32, 349–356.

Beran, J., *Statistics for Long-Memory Process*, London: Chapman & Hall, 1994.

Bergmeister, K., and Santa, U. (2000), “Global mentoring concepts for bridges”, *Nondestructive Evaluation of Highways, Utilities, and Pipelines IV*, SPIE, Bellingham, WA, Vol. 3995, 4–25.

Bernard, K.J., Culmo, M.P., and DeWolf, J.T. (1997), “Strain monitoring to evaluate steel bridge connections”, *Structures Congress XV*, ASCE, Portland, Oregon, 919–923.

Bernini, R., Fraldi, M., Minardo, A., Minutolo, V., Carannante, F., Nunziante, L., and Zeni, L. (2006), “Identification of defects and strain error estimation for bending steel beams using time domain Brillouin distributed optical fiber sensors”, *Smart Materials and Structures*, Vol. 15, 612–622.

Bhattacharya, B., Li, D., and Chajes, M. (2008), “Bridge rating using in-service data in the presence of strength deterioration and correlation in load processes”,

Structure and Infrastructure Engineering, Vol. 4, 237–249.

Biernacki, C., Celeux, G., and Govaert, G. (1999), "An improvement of the NEC criterion for assessing the number of clusters in a mixture model", *Pattern Recognition Letters*, Vol. 20, 267–272.

Biernacki, C., Celeux, G., and Gold, E.M. (2000), "Assessing a mixture model for clustering with the integrated completed likelihood", *IEEE Transactions on Pattern Analysis and Machine Intelligence*, Vol. 22, 719–725.

Bishop, C.M., *Neural Networks for Pattern Recognition*, Oxford: Clarendon Press, 1995.

Brown, R.G., and Hwang, P.Y.C., *Introduction to Random Signals and Applied Kalman Filtering*, Second Edition, John Wiley & Sons, Inc., 1992.

Bucar, T., and Nagode, M. (2004), "Reliability approximation using finite Weibull mixture distributions", *Reliability Engineering & System Safety*, Vol. 84, 241–251.

Burrus, C.S., Gopinath, R.A., and Guo, H., *Introduction to Wavelets and Wavelet Transforms: A Primer*, Prentice Hall, Englewood Cliffs, N.J., 1997.

Cardini, A.J., and DeWolf, J.T. (2009), "Long-term structural health monitoring of a multi-girder steel composite bridge using strain data", *Structural Health Monitoring*, Vol. 8, 47–58.

Catbas, F.N. and Aktan, A.E. (2002), "Condition and damage assessment: issues and some promising indices", *Journal of Structural Engineering*, Vol. 128, 1026–1036.

Catbas, F.N., Susoy, M., and Frangopol, D.M. (2008), “Structural health monitoring and reliability estimation: long span truss bridge application with environmental monitoring data”, *Engineering Structures*, Vol. 30, 2347–2359.

Cawley, P., and Adams, R.D. (1979), “The location of defects in structures from measurements of natural frequencies”, *Journal of Strain Analysis for Engineering Design*, Vol. 14, 49–57.

Chajes, M.J., and Shenton, H.W. (2005), “Using diagnostic load test for accurate load rating of typical bridges”, *Proceedings of the 2005 Structures Congress and the 2005 Forensic Engineering Symposium*, New York, USA.

Chakraborty, S., and DeWolf, J.T. (2005), “Development and Implementation of a Continuous Monitoring System on a Multi-Girder Composite Steel Bridge in Connecticut”, *Proceedings of the 4th International Workshop on Structural Health Monitoring*, Stanford, California, USA.

Chance, J., Thomlinson, G.R., and Worden, K. (1994), “A simplified approach to the numerical and experimental modeling of the synamics of a cracked beam”, *Proceedings of the 12th International Modal Analysis Conference*, Honolulu, USA, 778–785.

Chang, F.K. (2001), “Structural health monitoring: The demands and challenges”, *Proceedings of 3rd International Workshop on Structural Health Monitoring*, Stanford, California, September 11-14, Technomic Publishing Co. Inc., Lancaster, P.A..

Chen, S.E., Venkatappa, S., Moody, J., Petro, S., and GangaRao, H. (2000), “A novel damage detection technique using scanning laser vibrometry and a strain energy distribution method”, *Materials Evaluation*, Vol. 58, 1389–1394.

Chen, G., Mu, H.M., Pommerenke, D., and Drewniak, J.L. (2004), “Damage detection of reinforced concrete beams with novel distributed crack/strain sensors”, *Structural Health Monitoring*, Vol. 3, 225–243.

Cheung, M.S., Tadros, G.S., Brown, T., Dilger, W.H., Ghali, A., and Lau, D.T. (1997), “Field monitoring and research on performance of the Confederation Bridge”, *Canadian Journal of Civil Engineering*, Vol. 24, 951–962.

Choi, H.I., and Williams, W.J. (1989), “Improved time frequency representation of multicomponent signals using exponential kernels”, *IEEE Transmission Signal Processing*, Vol. 37, 862–871.

Choi, S., Park, S., Bolton, R., Stubbs, N., and Sikorsky, C. (2004), “Periodic monitoring of physical property changes in a concrete box girder bridge”, *Journal of Sound and Vibration*, Vol. 278, 365–381.

Classen, T.A.C.M., and Mecklenbrauker, W.F.G. (1980), “The Wigner distribution: a tool for time-frequency signal analysis part I: Continuous-time signals”, *Philips Journal of Research*, Vol. 35, 217–250.

Cohen, A.C. (1967), “Estimation in mixtures of two normal distributions”, *Technometrics*, Vol. 9, 15–28.

Cohen, L. (1989), “Time-Frequency Distributions: A Review”, *Proceedings of the IEEE*, Vol. 77, 941–981.

Cornwell, P., Doebling, S.W. and Farrar, C.R. (1999), “Application of the strain energy damage detection method to plate-like structures”, *Journal of Sound and Vibration*, Vol. 224, 359–374.

Daubechies, I. (1988), “Orthonormal basis of compactly supported wavelets”, *Communications on Pure and Applied Mathematics*, Vol. 41, 909–996.

DelGrego, M.R., Culmo, M.P., and DeWolf, J.T. (2004), “Monitoring of century-old railroad truss bridges”, *Annual Meeting of Transportation Research Board*, Washington, D.C., USA.

DelGrego, M.R., Culmo, M.P., and DeWolf, J.T. (2008), “Performance evaluation through field testing of century-old railroad truss bridge”, *Journal of Bridge Engineering*, ASCE, Vol. 13, 132–138.

DeMerchant, M., Brown, A., Bao, X., and Bremner, T. (1999), “Structural monitoring by use of a Brillouin distributed sensor”, *Applied Optics*, Vol. 38, 2755–2759.

DeMerchant M., Brown, A., Smith, J., Bao, X., and Bremner, T. (2000), “Distributed strain sensing for structural monitoring applications”, *Canadian Journal of Civil Engineering*, Vol. 27, 873–877.

Dempster, A.P, Laird, N.M., and Rubin, D.B. (1977), “Maximum likelihood from incomplete data via the EM algorithm”, *Journal of Royal Statistical Society*, Vol. 39, 1–38.

DeWolf, J.T., Culmo, M.P., and Lauzon, R.G. (1998), “Connecticut’s bridge infrastructure monitoring program for assessment”, *Journal of*

Infrastructural Systems, Vol. 4, 86–90.

DeWolf, J.T., Olund, J.K., Liu, C., and Cardini, A.J. (2006), "The long-term structural health monitoring of bridges in the state of connecticut", *In: Proceedings of the Third European Workshop on Structural Health Monitoring*, Granada, Spain, pp. 372–378.

Doebling, S.W., Farrar, C.R., Prime, M.B., and Shevitz, D.W. (1996), "Damage identification and health monitoring of structural and mechanical systems from changes in their vibration characteristics: a literature review", *Technical Report LA-13070-MS*, Los Alamos National Laboratory, Los Alamos.

Doebling, S.W., Hemez, F.M., Peterson, L.D., and Farhat, C. (1997), "Improved damage location accuracy using strain energy-based mode selection criteria", *Journal of AIAA*, Vol. 35, 693–699.

Doebling, S.W., Farrar, C.R., and Prime, M.B. (1998), "A summary review of vibration-based damage identification methods", *The Shock and Vibration Digest*, Vol. 30, 91–105.

Dong, C., Zhang, P.Q., Feng, W.Q., and Huang, T. C. (1994), "The sensitivity study of the modal parameters of a cracked beam", *Proceedings of the 12th International Modal Analysis Conference*, Honolulu, Hawaii, 98–104.

Ebeling, C.E., *An Introduction to Reliability and Maintainability Engineering*, McGraw-Hill, New York, 1997.

Ellingwood, B.R. (1996), "Reliability-based condition assessment and LFRD for

existing structures", *Structural Safety*, Vol. 18, 67–80.

Everitt, B.S., Hand, D.J., *Finite Mixture Distributions*, Chapman and Hall, London, 1981.

Farrar, C.R., and Jauregui, D.A. (1998), "Comparative study of damage identification algorithms applied to a bridge: I. Experiment", *Smart Materials and Structures*, Vol. 7, 704–719.

Feng, M.Q., and Kim, D.K. (2001), "Long-term structural performance monitoring of two highway bridges", *Technical Report of the California Department of Transportation*, University of California, Irvine.

Feng M.R. (2008), "Construction of bridges and roads to bring benefit to people's livelihood", *Journal of Highway and Transportation Research and Development*, Vol. 12, 1–5.

FHWA (1977), *Economic Impact of Highway Snow and Ice Control*, Federal Highway Administration, FHWA-RD-77-95.

FHWA (2001), *Bridge Scour and Stream Instability Countermeasure Experience, Selection, and Design Guidance*, Second Edition, Federal Highway Administration, FHWA-NHI-01-003.

Fox, R., and Taqqu, M.S. (1986), "Large sample properties of parameter estimates for strongly dependent stationary Gaussian time series", *Annals of Statistics*, Vol. 14, 517–532.

Frangopol, D.M., Estes, A.C. (1997), "Bridge maintenance strategies based on system reliability", *Structural Engineering International*, IABSE, Zurich,

Switzerland, Vol. 7, 193–198.

Frangopol, D.M., Kong, J.S., and Gharaibeh, E.S. (2001), “Riliability-based life-cycle management of highway bridges”, *Journal of Computing in Civil Engineering*, ASCE, Vol. 15, 27–34.

Frangopol, D.M., Strauss, A., and Kim, S.Y. (2008), “Bridge reliability assessment based on monitoring”, *Journal of Bridge Engineering*, ASCE, Vol. 13, 258–270.

Friswell, M.I., and Penny, J.E.T. (1997), “Is damage location using vibration measurements practical?”, *Structural Damage Assessment Using Advanced Signal Processing Procedures, Proceedings of DAMAS ’97*, University of Sheffield, UK, Sheffield Academic Press Ltd., 351–362.

Frýba, L., *Dynamics of Railway Bridges*, Thomas Telford, New York, NY 10017-2398, 1996.

Fryer, J.G., and Robertson, C.A. (1972), “A comparison of some methods for estimating mixed normal distributions”, *Biometrika*, Vol. 59, 639–648.

Gandomi, A.H., Sahab, M.G., Rahaei, A., and Gorji, M.S. (2008), “Development in mode shape-based structural fault identification technique”, *World Applied Sciences Journal*, Vol. 5, 29–38.

Gao, J., Shi, B., Zhang, W., and Zhu, H. (2006), “Monitoring the stress of the post-tensioning cable using fiber optic distributed strain sensor”, *Measurement*, Vol. 39, 420–428.

Grosso, A.D., Inaudi, D., and Pardi, L. (2002), “Overview of European activities in the

health monitoring of bridges", *First International Conference on Bridge Maintenance, Safety and Management*, IABMAS'02, CIMNE, Barcellona.

Hoerst, B.C., and Ratcliffe, C.P. (1997), "Damage detection in beams using Laplacian operators on experimental modal data", *The 15th International Modal Analysis Conference*, Orlando, USA, 1305–1311.

Imai, K., and Frangopol, D.M. (2001), "Reliability-based assessment of suspension bridges: application to the Innoshima Bridge" *Journal of Bridge Engineering*, ASCE, Vol. 6, 398–411.

Jenkins, C.H., Kjerengtroen, L. and Oestensen, H. (1997) "Sensitivity of parameter changes in structural damage detection", *Journal of Shock and Vibration*, Vol. 4, 23–37.

Johnson, T.J., Brown, R.L., Adams, D.E., and Schiefer, M. (2004), "Distributed structural health monitoring with a smart sensor array", *Mechanical Systems and Signal Processing*, Vol. 18, 555–572.

KahI, K., and Sirkis, J.S. (1996), "Damage detection in beam structures using subspace rotation algorithm with strain data", *Journal of AIAA*, Vol. 34, 2609–2614.

Kalman, R.E. (1960), "A new approach to linear filtering and prediction problems", *Journal of Basic Engineering*, ASME, Vol. 82, 35–45.

Kang, I.P., Schulz, M.J., Kim, J.H., Shanov, V., and Shi, D.L. (2006), "A carbon nanotube strain sensor for structural health monitoring", *Smart Materials and Structures*, Vol. 15, 737–748.

Kantz, H., and Schreiber, T., *Nonlinear Time Series Analysis*, Cambridge University Press, New York, 1997.

Katsikeros, C.E., and Labeas, G.N. (2009), "Development and validation of a strain-based structural health monitoring system", *Mechanical Systems and Signal Processing*, Vol. 23, 372–383.

Kesavan, A., John, S., and Herszberg, I. (2008), "Strain-based structural health monitoring of complex composite structures", *Structural Health Monitoring*, Vol. 7, 203–213.

Kim, S., Lee, J., and Kwon, I. (2002), "Structural monitoring of a bending beam using Brillouin distributed optical fiber sensors", *Smart Material Structures*, Vol. 11, 396–403.

Kim, S., and Nowak, A.S. (1997), "Load distribution and impact factors for I-girder bridges", *Journal of Bridge Engineering*, ASCE, Vol. 2, 97–104.

Kim, S.K. (2003), "Experimental investigation of local damage detection on a 1/15 scale model of a suspension bridge deck", *Journal of Civil Engineering*, KSCE, Vol. 7, 461–468.

Ko, J.M., and Ni, Y.Q. (2005), "Technology developments in structural health monitoring of large-scale bridges", *Engineering Structures*, Vol. 27, 1715–1725.

Ko, J.M., Ni, Y.Q., Zhou, H.F., Wang, J.Y., and Zhou, X.T. (2009), "Investigation concerning structural health monitoring of an instrumented cable-stayed bridge", *Structure and Infrastructure Engineering*, Vol. 5, 497–513.

Koh, H.M., Choo, J.F., Kim, S.K., and Kim, C.Y. (2003), “Recent application and development of structural health monitoring systems and intelligent structures in Korea”, *Structural Health Monitoring and Intelligent Infrastructure*, Wu, Z. S., and Abe, M. (editors), A.A. Balkema, Lisse, 99–111.

Koshiba, A., Abe, M., Sunaga, T., and Ishii, H. (2001), “Bridge inspection in steel road bridge based on real measurement”, *Current and Future Trends in Bridge Design, Construction and Maintenance 2: Safety, Economy, Suitability and Aesthetics*, Thomas Telford, London, 268–273.

Lark, R.J., Flaig, K.D. (2005), “The use of reliability analysis to aid bridge management”, *The Structural Engineer*, Vol. 83, 27–31.

Lee, J.J., Lee, J.W., Yi, J.H., Yun, C.B., and Jung, H.Y. (2005), “Neural networks-based damage detection for bridges considering errors in baseline finite element models”, *Journal of Sound and Vibration*, Vol. 280, 555–578.

Lee, J.W., Choi, K.H., and Huh, Y.C. (2010), “Damage detection method for large structures using static and dynamic strain data from distributed fiber optic sensor”, *International Journal of Steel Structures*, Vol. 10, 91–97.

Lee, J.W., Kim, J.D., Yun, C.B., Yi, J.H., and Shim, J.M. (2002), “Health-monitoring method for bridges under ordinary traffic loadings”, *Journal of Sound and Vibration*, Vol. 257, 247–264.

Lee, J.W., Kirikera, G.R., Kang, I., Schulz, M.J., and Shanov, V.N. (2006), “Structural

health monitoring using continuous sensors and neural network analysis", *Smart Materials and Structures*, Vol. 15, 1266–1274.

Li, J., and Zha, H. (2006), "Two-way Poisson mixture models for simultaneous document classification and word clustering", *Computational Statistics and Data Analysis*, Vol. 50, 163–180.

Li, Y., Cichocki, A., and Amari, S. (2004), "Analysis of sparse representation and blind source separation", *Neural Computation*, Vol. 16, 1193–1234.

Liang, Y.C., and Hwu, C. (2001), "On-line identification of holes/cracks in composite structures", *Smart Materials and Structures*, Vol. 10, 599–609.

Lieven, N.A.J., and Ewins, D.J. (1988), "Spatial correlation of mode shapes, the Coordinate Modal Assurance Criterion (COMAC)", *Proceedings of the 6th International Modal Analysis Conference*, Vol. 1, 690–695.

Liu, P.L, and Lin, H.T. (1996), "Direct identification of non-uniform beams using static strains", *International Journal of Solids and Structures*, Vol. 33, 2775–2787.

Lu, Q., Ren, G., and Zhao, Y. (2002), "Multiple damage location with flexibility curvature and relative frequency change for beam structures", *Journal of Sound and Vibration*, Vol. 253, 1101–1114.

Mallat, S., *A Wavelet Tour of Signal Processing*, Second Edition, Academic Press, 1999.

Matthiessen, C.W. (2000), "Bridging the Öresund: potential regional dynamics", *Journal of Transport Geography*, Vol. 8, 171–180.

McLachlan, G.J., and Basford, K.E., *Mixture Models: Inference and Applications to Clustering*, New York: Dekker, USA, 1988.

McLachlan, G., and Peel, D., *Finite Mixture Models*, John Wiley and Sons Inc., New York, USA, 2000.

Messervey, T.B., and Frangopol, D.M. (2008), "Innovative treatment of monitoring data for reliability-based code-compliant structural assessment with the incorporation of error", *Proceedings of 4th International Conference in Bridge Maintenance, Safety, and Management*, IABMAS'08 (CD-ROM), Koh, H.M., and Frangopol, D.M. (editors), CRC/Balkema, Taylor & Francis Group, London, 1466–1474.

Mufti, A.A. (2002), "Structural health monitoring of innovative Canadian civil engineering structures", *International Journal of Structural Health Monitoring*, 1, 89–103.

Mufti, A.A., and Bakht, B. (2002), "The benefits of structural health monitoring", *Proceedings of 1st International Conference on Bridge Maintenance, Safety and Management*, Barcelona, Spain, July 14–17, CIMNE.

Ndambi, J.M., Vantomme, J., and Harri, K. (2002), "Damage assessment in reinforced concrete beams using eigen-frequencies and mode shape derivatives", *Engineering Structures*, Vol. 24, 501–515.

Newcomb, S. (1886), "A generalized theory of the combination of observations so as to obtain the best result", *American Journal of Mathematics*, Vol. 8, 343–366.

Oh, B.H., and Jung, B.S. (1998), “Structural damage assessment with combined data of static and modal tests”, *Journal of Structural Engineering*, ASCE, Vol. 124, 956–965.

Olund, J.K. (2006) “Long-term structural health monitoring of Connecticut’s bridge infrastructure with a focus on a composite steel tub-girder bridge”, *Master of Science Thesis*, University of Connecticut.

Ou, J.P., and Li, H. (2005), “The state-of-the-art and practice of structural health monitoring for civil infrastructures in the mainland of china”, *Structural Health Monitoring and Intelligent Infrastructure*, Ou, J.P., Li, H., and Duan, Z.D. (editors), Taylor & Francis, London, 69–93.

Pan, W., and Shen, X. (2006), “Penalized model-based clustering with application to variable selection”, *Journal of Machine Learning Research*, Vol. 8, 1145–1164.

Pandey, A.K., Biswas, M., and Samman, M.M. (1991), “Damage detection from changes in curvature mode shapes”, *Journal of Sound and Vibration*, Vol. 145, 321–332.

Park, H.J., Koo, K.Y., and Yun, C.B. (2007), “Modal flexibility-based damage detection technique of steel beam by dynamic strain measurements using FBG sensors”, *International Journal of Steel Structures*, Vol. 7, 11–18.

Pearson, K. (1894), “Contribution to the mathematical theory of evolution”, *Philosophical Transactions of the Royal Society*, Vol. 185, 71–110.

Ponnuswamy, S., *Bridge Engineering*, Second Edition, McGraw-Hill, New York,

USA, 2008.

Ratay, R.T., *Structural Condition Assessment*, Wiley Publishing Co., 2005.

Ratay, R.T. (2006), "Structural condition assessment – an introduction", *Proceedings of the 2006 Structures Congress*, Structural Engineering and Public Safety, 1–2.

Ratcliffe, C.P., and Bagaria, W.J. (1998), "Vibration technique for locating delamination in a composite beam", *Journal of AIAA*, Vol. 36, 1074–1077.

Ray, L.R., Koh, B.H., and Tian, L. (2000), "Damage detection and vibration control in smart plates: towards multifunction smart structures", *Journal of Intelligent Material Systems and Structures*, Vol. 11, 725–739.

Ray, S., and Lindsay, B. (2008), "Model selection in high dimensions: a quadratic-risk-based approach", *Journal of the Royal Statistical Society (B)*, Vol. 70, 95–118.

Robertson, I.N., Johnson, G.P., and Wang, S.J. (2005), "Instrumentation performance during long-term bridge monitoring", *Sensing Issues in Civil Structural Health Monitoring*, Ansari, F. (editor), 331–340.

Sahin, M., and Shenoi, R.A. (2003), "Quantification and localization of damage in beam-like structures by using artificial neural networks with experimental validation", *Engineering Structures*, Vol. 25, 1785–1802.

Salawu, O.S. (1997), "Detection of structural damage through changes in frequency: a review", *Engineering Structures*, Vol. 19, 718–723.

Sartor, R.R. (1995), "Strain monitoring of highway bridge structures", *Master of*

Science Thesis, University of Connecticut, USA.

Sartor, R.R., Culmo, M.P., and DeWolf, J.T. (1999), "A short-term monitoring of bridge structures", *Journal of Bridge Engineering*, ASCE, Vol. 4, 157–164.

Schwarz, G. (1978), "Estimating the dimensions of a model", *Annals of Statistics*, Vol. 6, 461–464.

Shepherd, R., and Frost, J.D., *Failures in Civil Engineering: Structural, Foundation, and Geo-environmental Case Studies*, ASCE, New York, USA, 1995.

Shkarayev, S., Krashantisa, R., and Tessler, A. (2001), "An inverse interpolation method utilizing in-flight strain measurements for determining loads and structural response of aerospace vehicles", *Proceedings of the 3rd International Workshop on Structural Health Monitoring*, Stanford, California, 336–343.

Smith, J., Brown, A., DeMerchant, M., and Bao, X. (1999) "Simultaneous strain and temperature measurement using a Brillouin scatting based distributed sensor", *SPIE Sensory Phenomena and Measurement Instrumentation for Smart Structures and Materials*, Vol. 3670, 366–372.

Sohn, H., Czarnecki, J.A., and Farrar, C.R. (2000), "Structural health monitoring using statistical process control", *Journal of Structural Engineering*, ASCE, Vol. 126, 1356–1363.

Sohn, H., Charles, R.F., Francois M.H., Devin, D.S., Daniel, W.S., Brett, R.N., and Jerry, J.C. (2003), "A review of structural health monitoring literature:

1996-2001", *LANL Report*, LA-13976-MS.

Sorenson, H.W. (1970), "Least-squares estimation: from Gauss to Kalman", *IEEE Spectrum*, Vol. 7, 63–68.

Stubbs, N., Kim, J.T., and Topole, K. (1992), "An efficient and robust algorithm for damage localization in offshore structures", *Proceedings of 10th Structures Congress*, ASCE, 543–546.

Stubbs, N., Farrar, C.R. (1995), "Field verification of a nondestructive damage localization and severity estimation algorithm", *Proceedings of 13th IMAC*, Nashville, Tennessee.

Sumitro, S., Matsui, Y., Kono, M., Okamoto, T., and Fujii, K. (2001), "Long-span bridge health monitoring system in Japan", *Health Monitoring and Management of Civil Infrastructure Systems*, Chase, S.B., and Aktan, A.E. (editors), The International Society for Optical Engineering, Bellingham, 517–524.

Tan, W.Y., and Chang, W.C. (1972), "Some comparisons of the method of moments and the method of maximum likelihood in estimating parameters of a mixture of two normal densities", *Journal of the American Statistical Association*, Vol. 67, 702–708.

Titterington, D.M., Smith, A.F.M., and Makov, V.E., *Statistical Analysis of Finite Mixture Distributions*, John Wiley and Sons Inc., New York, 1985.

Tonias, D.E., and Zhao, J.J., *Bridge Engineering*, Second Edition, McGraw-Hill, New York, USA, 2007.

Trung, N.L., Belouchrani, A., Abed Meraim, K., and Boashash, B. (2005), “Separating more sources than sensors using time-frequency distributions”, *EURASIP Journal on Applied Signal Processing*, Vol. 2005, 2818–2847.

Vardi, Y., Shepp, L.A., and Kaufman, L.A. (1985), “A statistical model for positron emission tomography”, *Journal of the American Statistical Association*, Vol. 80, 8–37.

Vetterli, M., and Herly, C. (1992), “Wavelets and Filter Banks: Theory and Design”, *IEEE Transactions on Signal Processing*, Vol. 40, 1057–1071.

Wang, C.H., Chen, W.Z., and Chen, A.R. (2002), “Damage safety assessment and maintenance management strategy of bridges”, *Journal of Traffic and Transportation Engineering*, Vol. 2, 21–28 (in Chinese).

Wang, C.Y., Wang, H.L., Wu, C.Y., and Chen, C.H. (2003), “Development of bridge health monitoring systems in Taiwan”, *Structural Health Monitoring and Intelligent Infrastructure*, Wu, Z. S., and Abe, M. (editors), A.A. Balkema, Lisse, 1067–1072.

Wang, J.Y. (2003), “Construction of data management system based on one-year monitoring data from WASHMS”, *Research Report*, Department of Civil and Structural Engineering, The Hong Kong Polytechnic University, Hong Kong.

Wang, M.L. (2005), “Damage assessment and monitoring of long-span bridges”, *Structural Health Monitoring 2005: Advancements and Challenges for Implementation*, Chang, F. K. (editor), DEStech Publications, Lancaster,

Pennsylvania, 61–79.

Wang, T.L., Liu, C., Huang, D., and Shahawy, M. (2005), “Truck loading and fatigue damage analysis for girder bridges based on weigh-in-motion data”, *Journal of Bridge Engineering*, ASCE, Vol. 10, 12–20.

Weinstein, E., Feder, M., and Oppenheim, A.V. (1993), “Multi-channel signal separation by decorrelation”, *IEEE Transactions on Speech and Audio Processing*, Vol. 1, 405–413.

West, W.M. (1984), “Illustration of the use of modal assurance criterion to detect structural changes in an orbiter test specimen”, *Proceedings of the Air Force Conference on Aircraft Structural Integrity*, 1–6.

Wildy, S.J., Kotousov, A.G., and Codrington, J.D. (2008), “A new passive defect detection technique based on the principle of strain compatibility”, *Smart Materials and Structures*, Vol. 17, 1–8.

Windham, M.P., and Cutler, A. (1992), “Information ratios for validating mixture analyses”, *Journal of the American Statistical Association*, Vol. 87, 1188–1192.

Wong, K.Y., and Ni, Y.Q. (2009), “Structural health monitoring of cable-supported bridges in Hong Kong”, *Structural Health Monitoring of Civil Infrastructure Systems*, Karbhari, V.M., and Ansari, F. (editors), Woodhead Publishing, Cambridge, UK, 371–411.

Wong, K.Y. (2004), “Instrumentation and health monitoring of cable-supported bridges”, *Structural Control and Health Monitoring*, Vol. 11, 91–124.

Wong, K.Y. (2007), "Stress and traffic loads monitoring of Tsing Ma Bridge", *Proceedings of China Bridge Congress 2007*, Chongqing, China (CR-ROM).

Wu Z.S., Xu, B., and Harada, T. (2003), "Review on structural health monitoring for infrastructures", *Journal of Applied Mechanics*, JSCE, Vol. 6, 1043–1054.

Wu, Z., Xu, B., Hayashi, K., and Machida, A. (2006), "Distributed optic fiber sensing for a full-scale PC girder strengthened with prestressed PBO sheets", *Engineering Structures*, Vol. 28, 1049–1059.

Wu, Z.S., and Li, S.Z. (2007), "Two-level damage detection strategy based on modal parameters from distributed dynamic macro-strain measurements", *Journal of Intelligent Material Systems and Structures*, Vol. 18, 667–676.

Xiang, H.F., *Major Bridges in China*, China Communications Press, Beijing, China, 2003.

Yakel, A.J., and Azizinamini, A. (2005), "Improved moment strength prediction of composite steel plate girders in positive bending", *Journal of Bridge Engineering*, ASCE, Vol. 10, 28–38.

Yam, L.H., Leung, T.P., Li, D.B., and Xue, K.Z. (1996), "Theoretical and experimental study of modal strain analysis", *Journal of Sound and Vibration*, Vol. 192, 251–260.

Yao, G.C., Chang, K.C., and Lee, G.C. (1992), "Damage diagnosis of steel frames using vibrational signature analysis", *Journal of Engineering Mechanics*,

Vol. 118, 1949–1961.

Yuen, K.V. (2010), “Recent developments of Bayesian model class selection and applications in civil engineering”, *Structural Safety*, Vol. 32, 338–346.

Zeng, X., Bao, X., Chhoa, C., Bremner, T., Brown, A., DeMerchant, M., Ferrier, G., Kalamkarov, A., and Georgiades, A. (2002), “Strain measurement in a concrete beam by use of the Brillouin-scattering-based distributed fiber sensor with single-mode fibers embedded in glass fiber reinforced polymer rods and bonded to steel reinforcing bars”, *Applied Optics*, Vol. 41, 5105–5110.

Zhang, W., Gao, J., Shi, B., Cui, H., and Zhu, H. (2006), “Health monitoring of rehabilitated concrete bridges using distributed optical fiber sensing”, *Computer-Aided Civil Infrastructural Engineering*, Vol. 21, 411–424.

Zhu, X.Q., and Law, S.S. (2006), “Wavelet-based crack identification of bridge beam from operational deflection time history”, *International Journal of Solids and Structures*, Vol. 43, 2299–2317.

Zonta, D., Lanaro, A., and Zanon, P. (2003), “A strain-flexibility-based approach to damage location”, *Key Engineering Materials*, Vols. 245–246, 87–94.